Supporting Information for:

Evaluating iron diimines: ion-pairing, lability and the reduced state

David Schilter[1]*, Umberto Terranova[2], Caden B. Summers[1†] and Rebecca R. Robinson[1,3]

[1]Department of Chemistry and Biochemistry, Texas State University, San Marcos, TX 78666, USA
[2]Faculty of Medicine and Health Sciences, The University of Buckingham, Buckingham, MK18 1EG, UK
[3]Department of Chemistry and Physics, Western Carolina University, Cullowhee, NC 28723, USA
[†]Present address: Department of Biochemistry and Biophysics, Texas A&M University, College Station, TX 77843, USA

Contents

Experimental methods

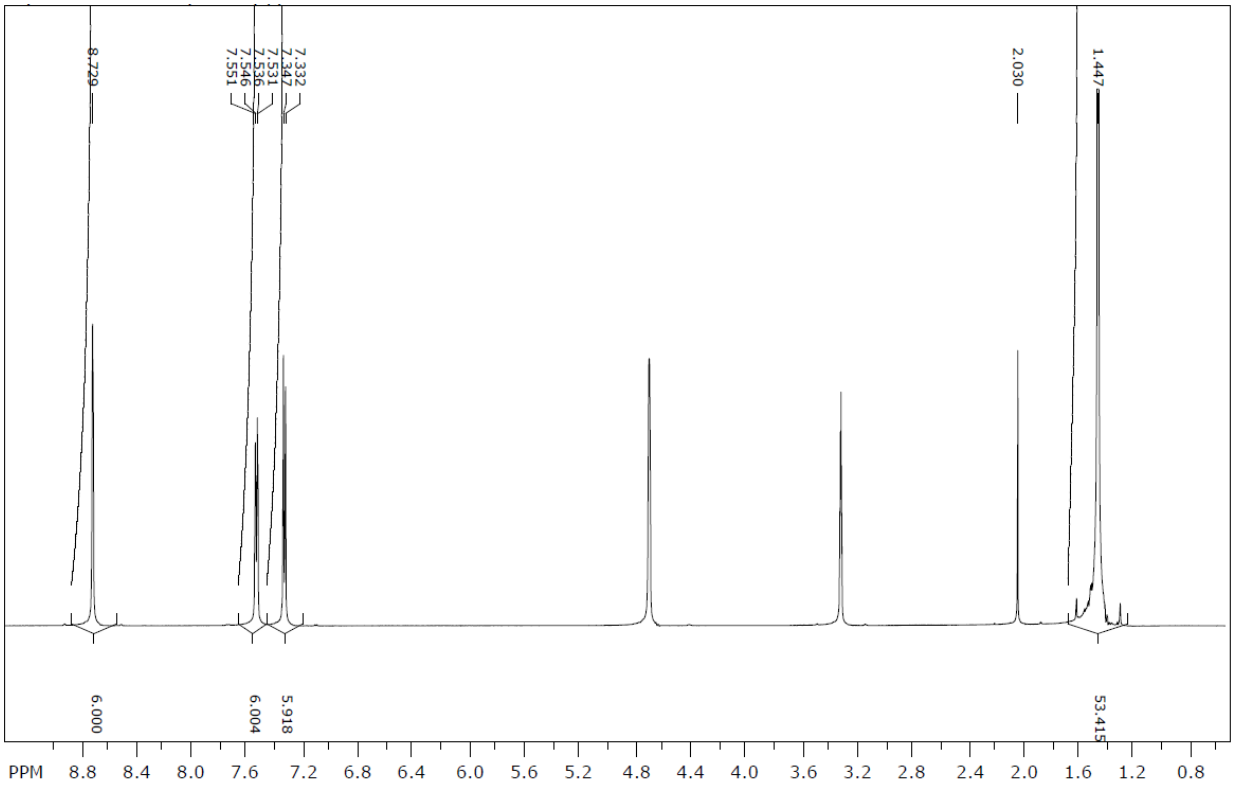

Figure S1. ^{1}H NMR spectrum (400 MHz) of $[Fe(bipy^{t\text{-}Bu})_3]Cl_2$. Signals at 4.7 (HOD), 3.31 (CHD_2OD) and 2.03 ppm (CH_3CN) are due to residual solvents.

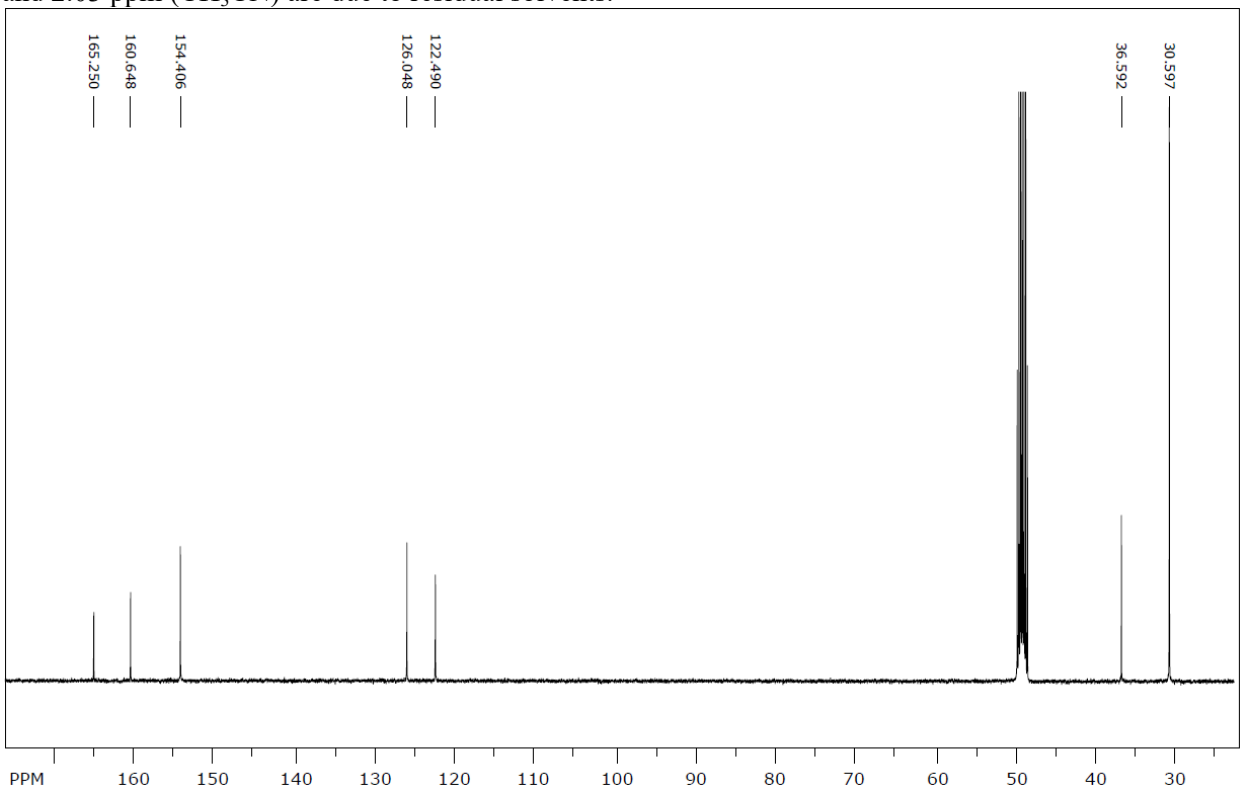

Figure S2. $^{13}C\{^1H\}$ NMR spectrum (100 MHz) of $[Fe(bipy^{t\text{-}Bu})_3]Cl_2$. The signal at 49 ppm is due to CD_3OD.

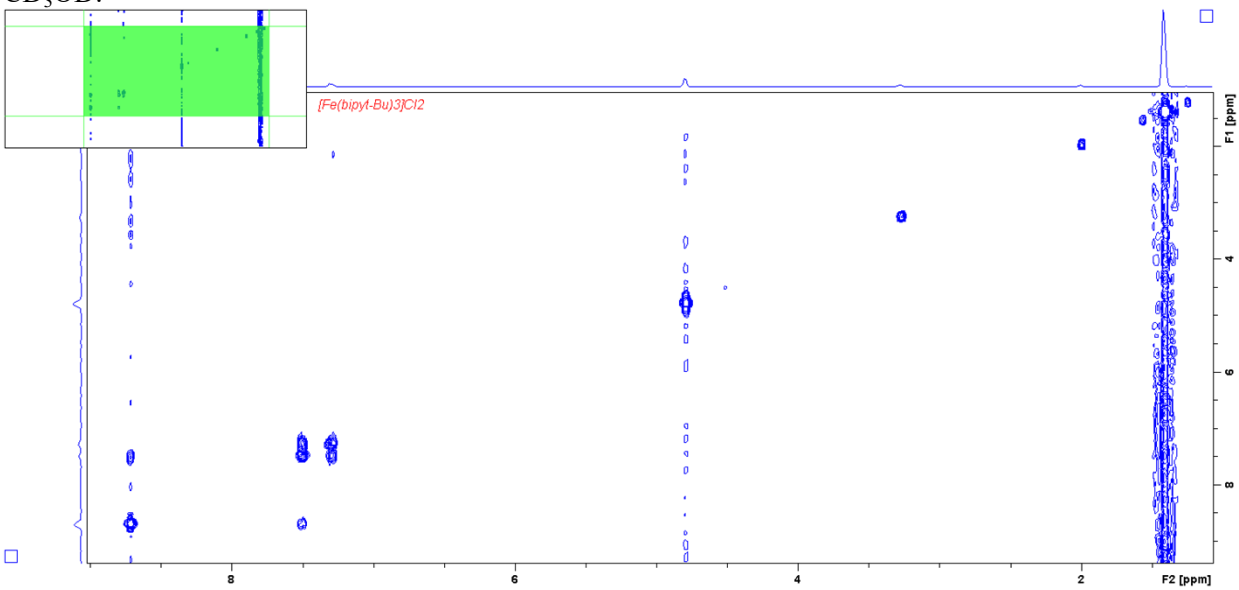

Figure S3. ^1H–^1H COSY NMR spectrum (400 MHz) of $[Fe(bipy^{t\text{-}Bu})_3]Cl_2$.

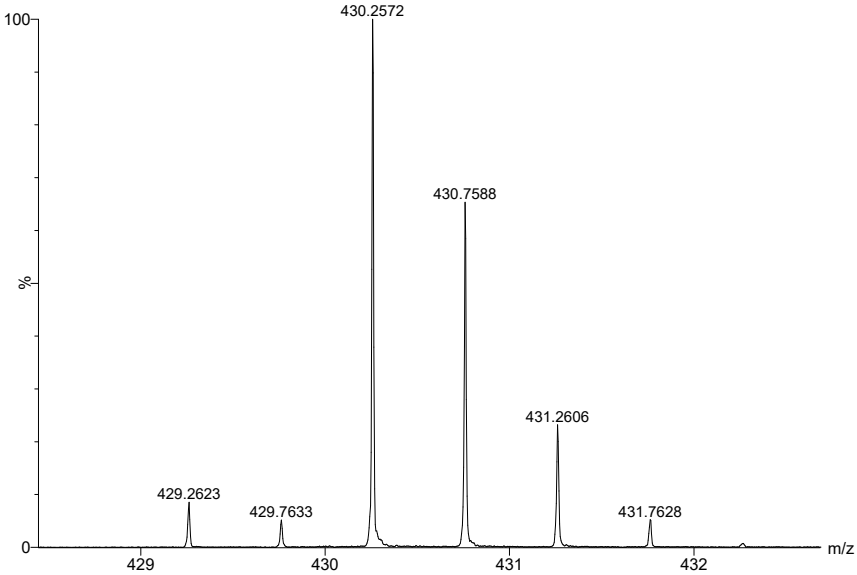

Figure S4. ESI-MS of $[Fe(bipy^{t\text{-}Bu})_3]Cl_2$ affords $[Fe(bipy^{t\text{-}Bu})_3]^{2+}$.

$[Fe(bipy^{Br})_3]Cl_2$

$FeCl_2$ (17.9 mg, 0.141 mmol) and $bipy^{Br}$ (137.5 mg, 438 mmol, 3.1 equivalents) were suspended in MeCN (2 mL) and stirred for 3 days. The suspension was cooled to −30 °C, and the blue-grey precipitate was isolated by filtration, washed with MeCN (2 mL) and dried to give the product as a blue-grey powder (138.9 mg, 0.1300 mmol, 92%).

^1H NMR: δ 9.08 (s, 6H, H3,3′), 7.75 (m, 6H, H6,6′), 7.37 ppm (m, 6H, H5,5′). $^{13}C\{^1H\}$ NMR: δ 160.39, 156.01, 137.70, 132.71, 129.78 ppm. ESI-MS: *m/z* calc. for $C_{30}H_{18}Br_6FeN_6^+$: 498.7989. Found: 498.8000.

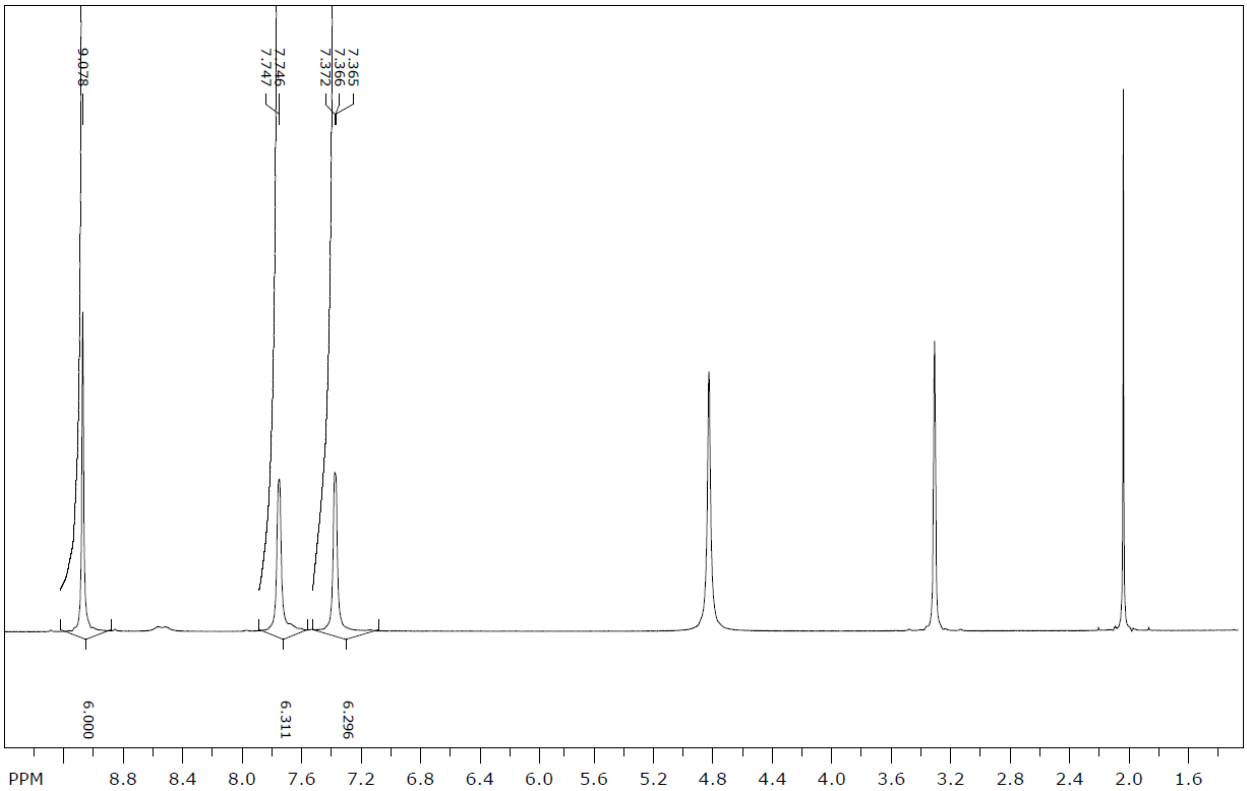

Figure S5. ^{1}H NMR spectrum (400 MHz) of $[Fe(bipy^{Br})_3]Cl_2$. Signals at 4.7 (HOD), 3.31 (CHD_2OD) and 2.03 ppm (CH_3CN) are due to residual solvents.

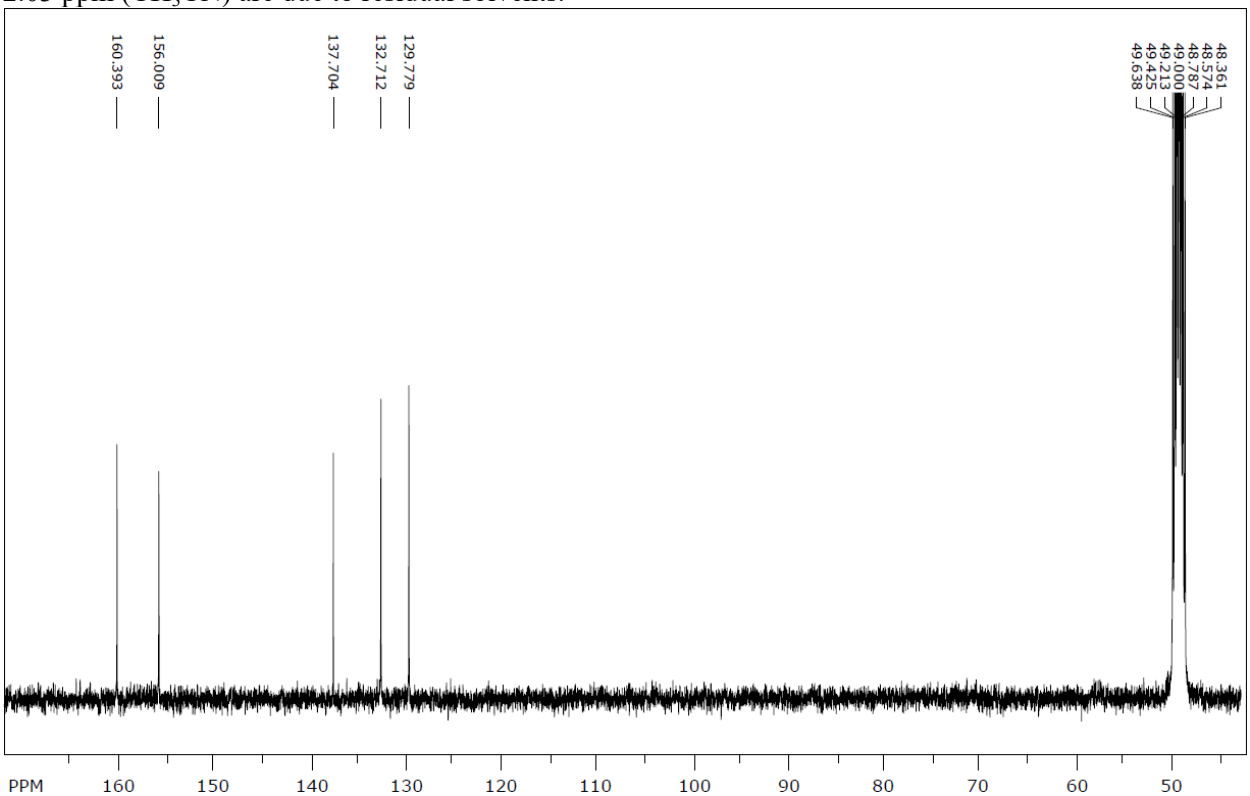

Figure S6. $^{13}C\{^{1}H\}$ NMR spectrum (100 MHz) of $[Fe(bipy^{Br})_3]Cl_2$. The signal at 49 ppm is due to CD_3OD.

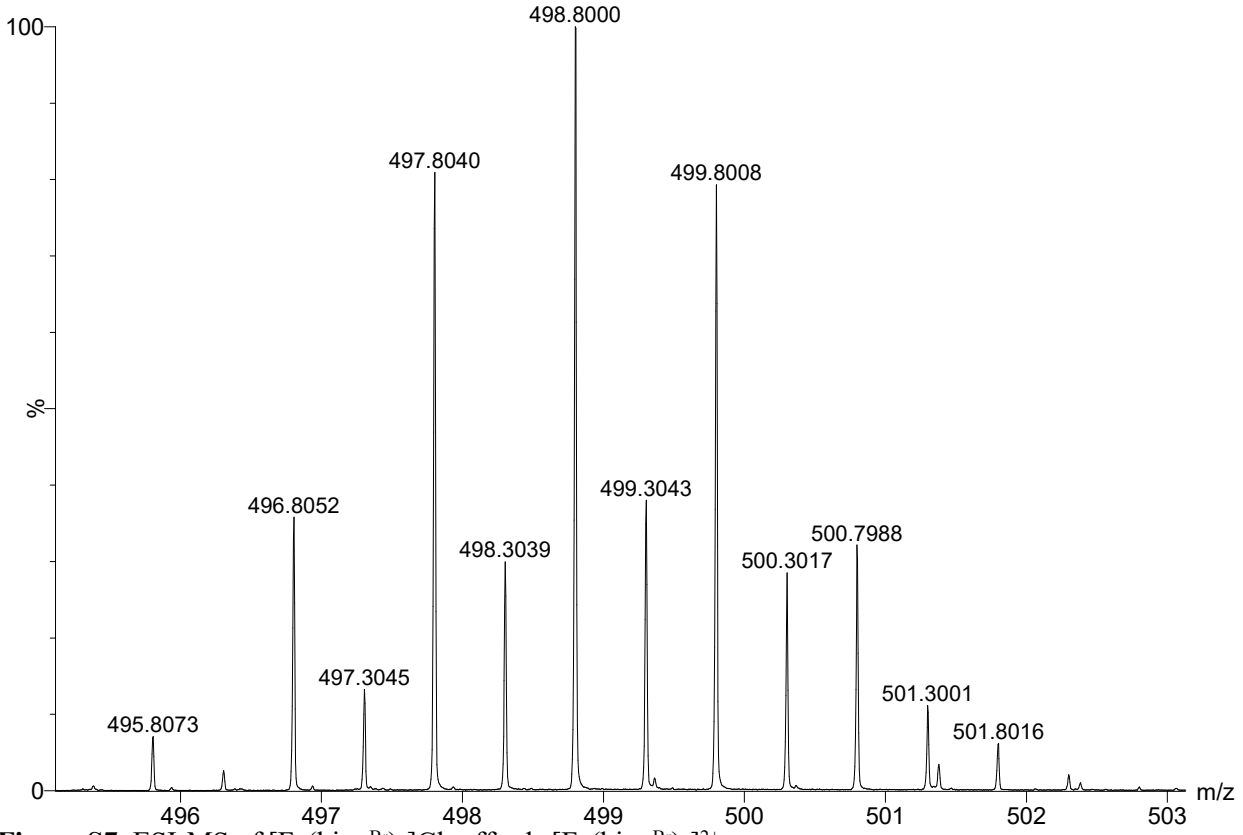

Figure S7. ESI-MS of $[Fe(bipy^{Br})_3]Cl_2$ affords $[Fe(bipy^{Br})_3]^{2+}$.

Mass Spectrometry

Stock solutions were prepared using HPLC-grade MeOH and deionized/millipore-filtered H_2O. $[Fe(bipy)_3]Cl_2$, $[Fe(phen)_3]Cl_2$, $[Fe(bipy^{Br})_3]Cl_2$, $[Fe(bipy^{t\text{-}Bu})_3]Cl_2$, $[Co(bipy)_3](PF_6)_2$, $^{n}Bu_4NOAc$, $NaBPh_4$ and $NaBAr^{F}_4$ solutions were prepared and stored in a refrigerator.

Solutions of the heteroleptic complexes were typically prepared by diluting stock solutions (0.25 mM in MeOH) of $[Fe(bipy)_3]Cl_2$ (10 μL) and $[Fe(phen)_3]Cl_2$ (10 μL) with MeOH (980 μL), such that that $[[Fe(N\hat{}N)_3]^{2+}] = 2.5$ μM. Higher concentration solutions were used in some cases. A syringe pump infused these solutions (10 $\mu L min^{-1}$) into a Waters Synapt XS ion-mobility mass spectrometer, equipped with a standard ESI probe and LockSpray II source. The generated ions encounter a resolving quadrupole, travelling-wave ion-mobility cell and then a time-of-flight analyzer. Data were acquired in High Resolution positive-ion mode with: cone 10 V, source offset 4.5, source 80 °C, and N_2 desolvation temperature 200 °C. MS data were acquired at a capillary voltage of ~1.51 kV. MS^2 data were acquired at a capillary voltage of 1.25 kV, acquiring scans at different transfer collision energies until virtually all parent ions dissociated in the Ar gas. The low-mass resolution of the quadrupole was typically ~4, whence most isotopologs of the parent ions were transmitted. If necessary, the resolution was increased to ensure the parent ion was pure. 10 MS scans were acquired at each capillary voltage and 10 MS^2 scans were acquired at each transfer collision energy. The spectra were combined and integrated in MassLynx v4.2. Breakdown curves were fitted with Boltzmann sigmoids to obtain $CE_{½}$ values.

Table S1. In each case, prior to ETD measurement the $[Fe(N^N)_3]^{2+}$ parent ion was measured in ESI-MS^2 mode using the settings below. This helped ensure the intensities of $[Fe(N^N)_3]^{2+}$ were comparable prior to interaction with DCB^-.

Salt	*C* /μM	LM resolution
$[Fe(bipy)_3]Cl_2$	2.5	17.0
$[Fe(bipy^{Br})_3]Cl_2$	20	17.0
$[Fe(phen)_3]Cl_2$	2.5	17.8
$[Fe(bipy^{t\text{-}Bu})_3]Cl_2$	10	20.0

For MS-IMS-MS, we used a capillary voltage of 1.00 kV and a low-mass resolution of 15 to select the most intense isotopologs of the parent ion envelope to enter the N_2-filled mobility cell. The final mobiligrams are of the most intense isotopolog. The traveling voltage wave velocity was 4.6 ms^{-1} and the wave height was 18.8 V. In each case, 294 scans were acquired and arrival times t_d visualized using DriftScope v3.0.

Solutions for ligand exchange experiments were held at 26 °C using a Thermo Scientific bath (88880029). The spectra presented are sums of 20 scans.

Mass spectrometric data

Ions derived from $[Fe(bipy)_3]^{2+}$

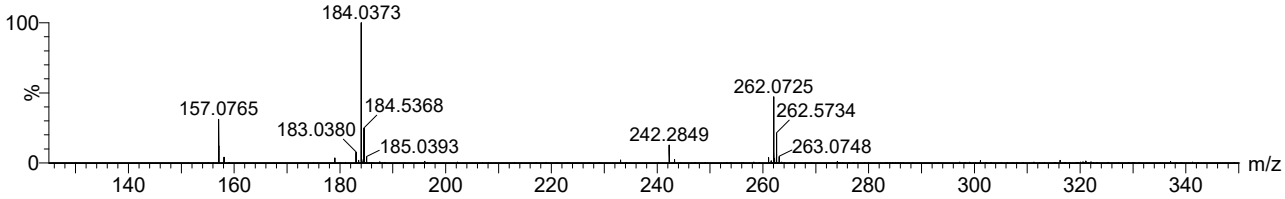

Figure S8. Positive-ion ESI-MS data for $[Fe(bipy)_3]Cl_2$ (2.5 μM) acquired at a capillary voltage of 1.52 kV. Major species: *m*/*z* 262 $[Fe(bipy)_3]^{2+}$ and 184 $[Fe(bipy)_2]^{2+}$. Note: *m*/*z* 242 $[^nBu_4N]^+$ and 157 $[bipyH]^+$.

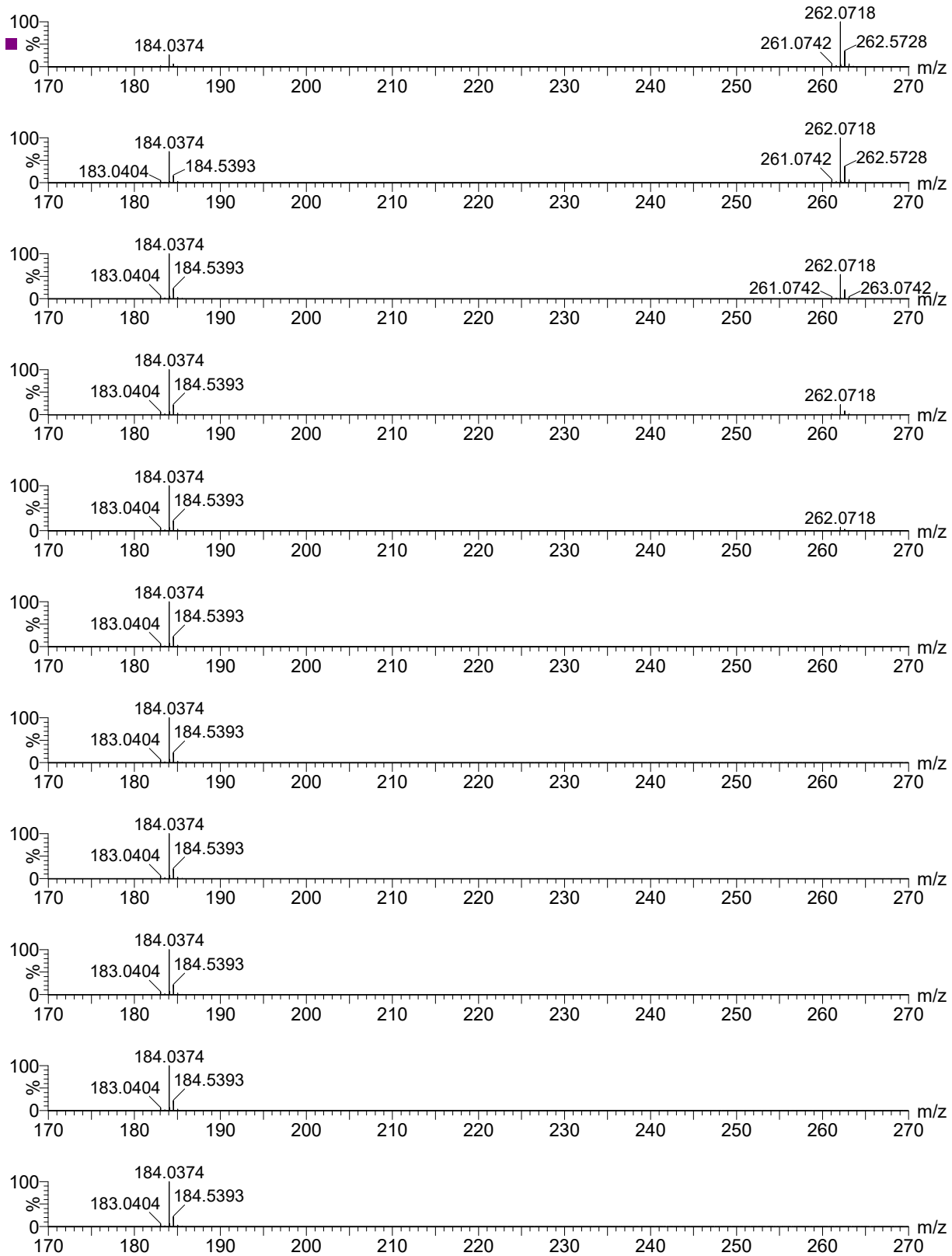

Figure S9. Positive-ion ESI-MS^2 data for the $[Fe(bipy)_3]^{2+}$ parent ion generated from $[Fe(bipy)_3]Cl_2$ (2.5 μM) acquired at low-mass resolution of 4.0 and transfer collision energies of 0, 2, 4, 6, 8, 10, 12, 14, 16, 18 and 20 eV (top to bottom). Major species: *m/z* 262 $[Fe(bipy)_3]^{2+}$ and 184 $[Fe(bipy)_2]^{2+}$.

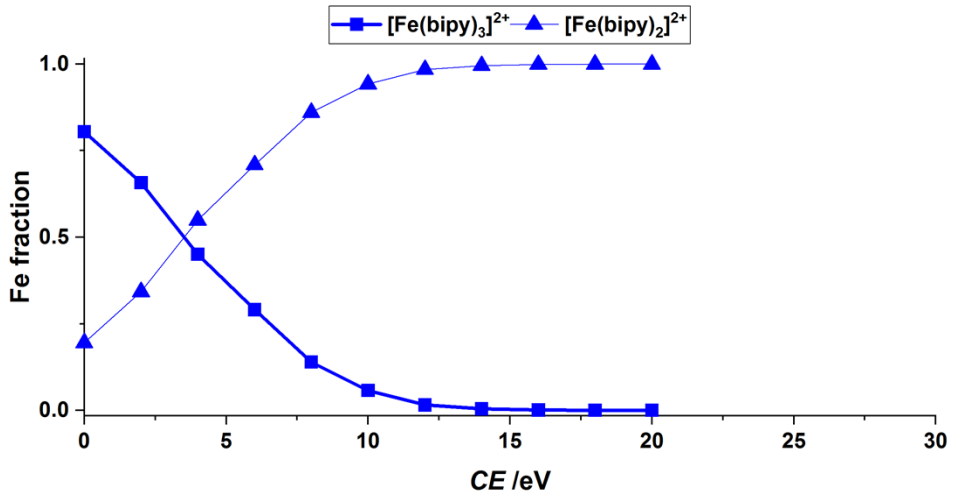

Figure S10. Breakdown curve for $[Fe(bipy)_3]^{2+}$.

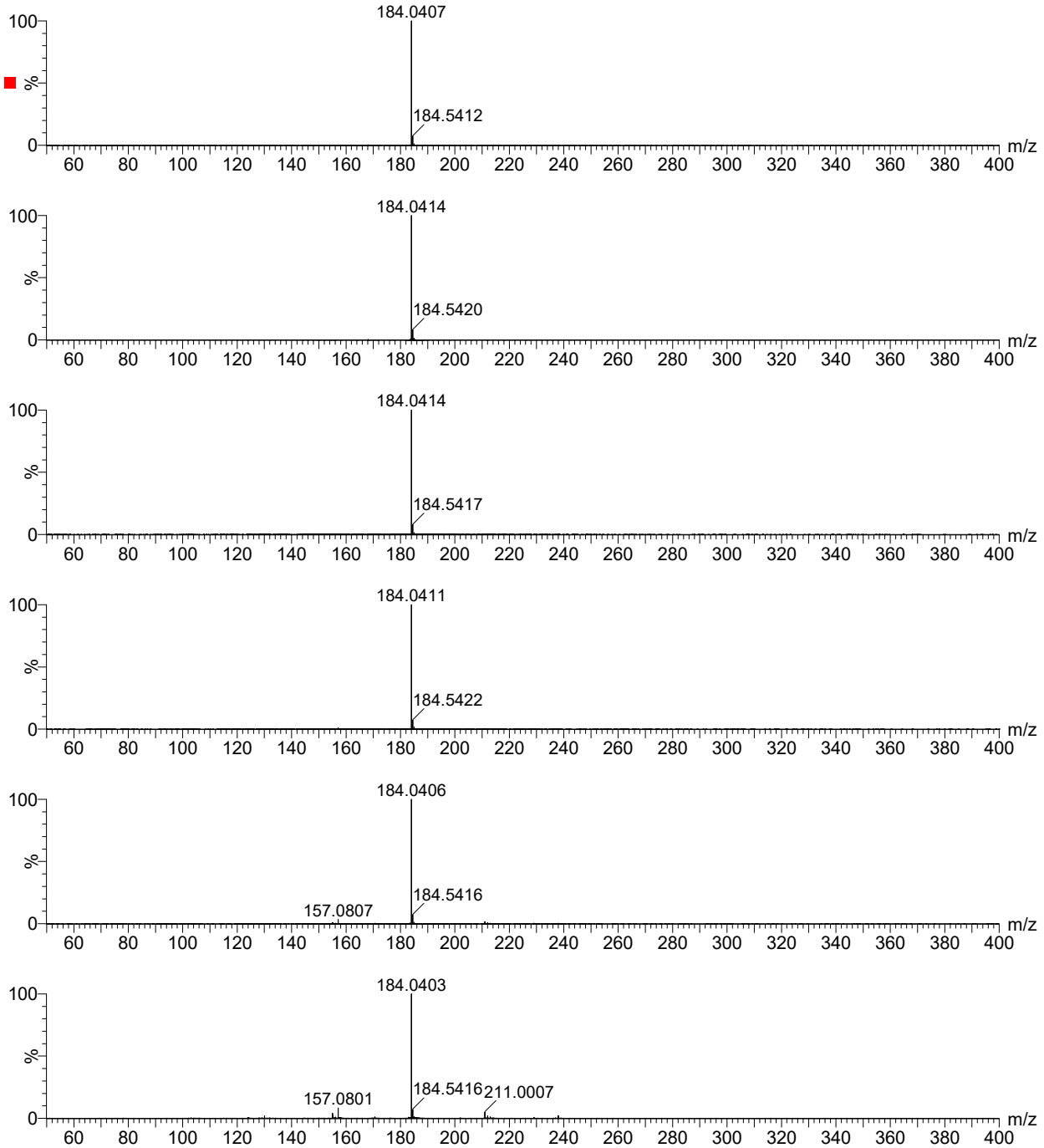

Figure S11. Positive-ion ESI-MS^2 data for the $[Fe(bipy)_2]^{2+}$ parent ion generated from $[Fe(bipy)_3]Cl_2$ (2.5 μM). Data were acquired at low-mass resolution of 15 and transfer collision energies of 0, 4, 8, 12, 16 and 20 eV (top to bottom). Major species: *m/z* 212 $[Fe(bipy)]^+$, 211 $[Fe(bipy-H)]^+$, 184 $[Fe(bipy)_2]^{2+}$, 157 $[bipyH]^+$ and 78 $[NC_6H_4]^+$.

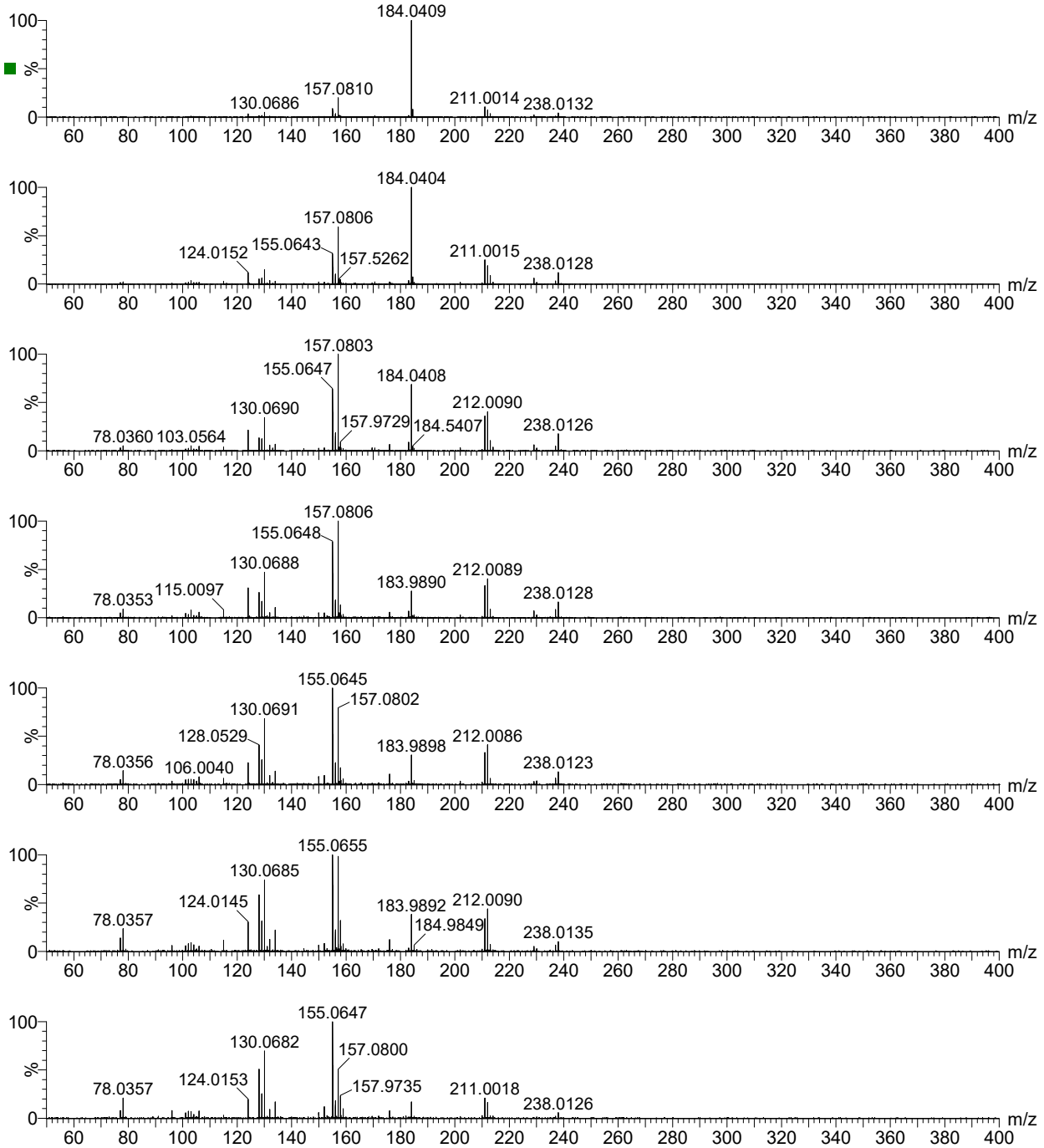

Figure S12. Positive-ion ESI-MS^2 data for the $[Fe(bipy)_2]^{2+}$ parent ion generated from $[Fe(bipy)_3]Cl_2$ (2.5 μM). Data were acquired at low-mass resolution of 15 and transfer collision energies of 24, 28, 32, 36, 40, 44 and 48 eV (top to bottom). Major species: *m*/*z* 212 $[Fe(bipy)]^+$, 211 $[Fe(bipy-H)]^+$, 184 $[Fe(bipy)_2]^{2+}$, 157 $[bipyH]^+$, 155 $[bipy-H]^+$ and 78 $[NC_6H_4]^+$.

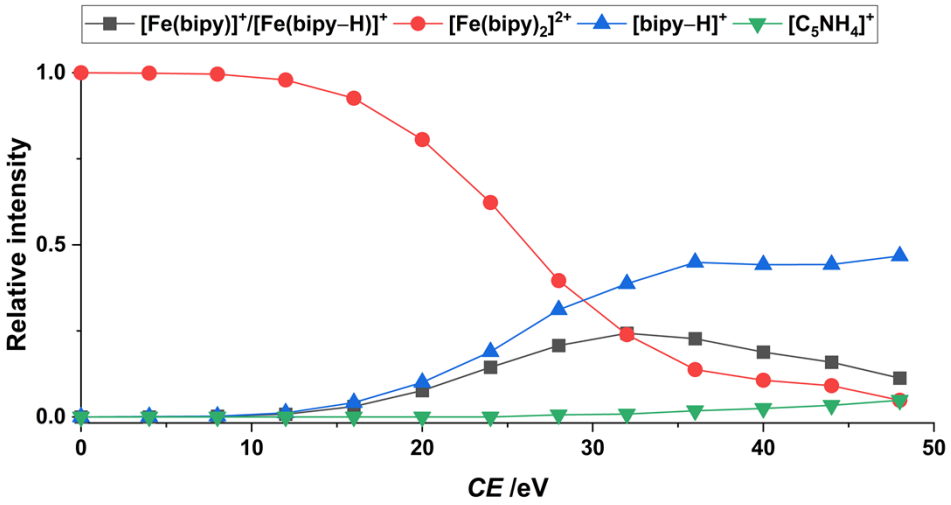

Figure S13. Breakdown curve for $[Fe(bipy)_2]^{2+}$.

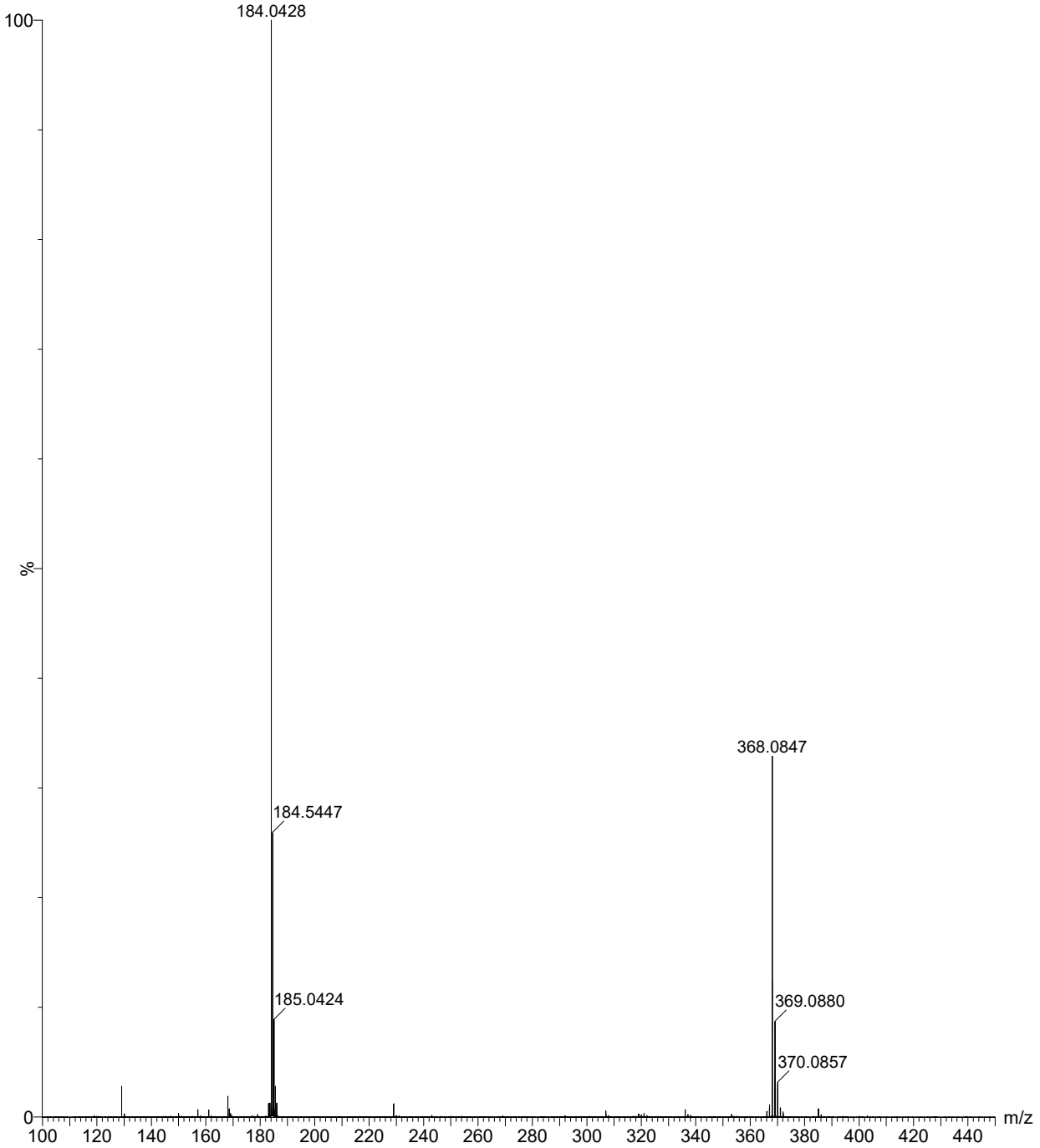

Figure S14. Positive-ion ESI-MS-ETD-MS data for the $[Fe(bipy)_2]^{2+}$ parent ion generated from $[Fe(bipy)_3]Cl_2$ (2.5 µM). Data (40 scans) were acquired at low-mass resolution of 5. Major species: *m*/*z* 368 $[Fe(bipy)_2]^{+}$ and 184 $[Fe(bipy)_2]^{2+}$. Peak integration suggested the extent of reduction was 40%.

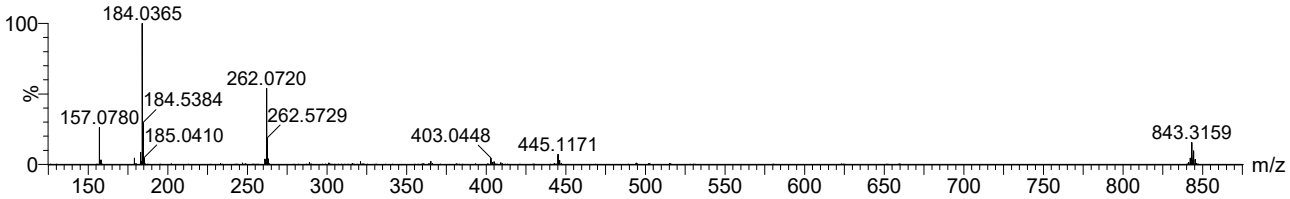

Figure S15. Positive-ion ESI-MS data for $[Fe(bipy)_3]Cl_2$ (50 μM) + $2NaBPh_4$ (100 μM) acquired at a capillary voltage of 1.52 kV. Major species: *m*/*z* 843 $\{[Fe(bipy)_3]BPh_4\}^+$, 445 $[Fe(bipy)_2(Ph)]^+$, 262 $[Fe(bipy)_3]^{2+}$ and 184 $[Fe(bipy)_2]^{2+}$. Note: *m*/*z* 157 $[bipyH]^+$.

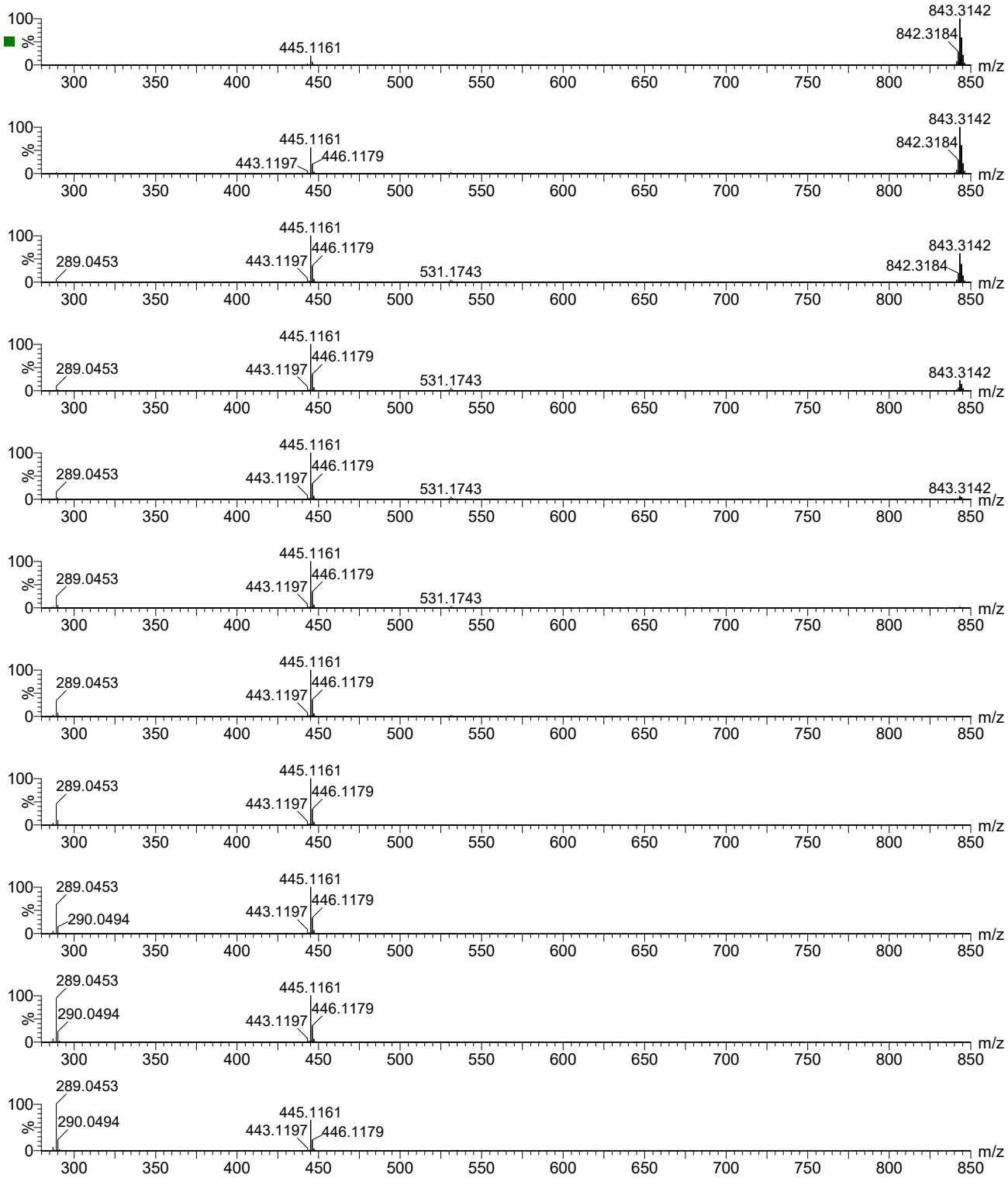

Figure S16. Positive-ion ESI-MS^2 data for the $\{[Fe(bipy)_3]BPh_4\}^+$ parent ion generated from $[Fe(bipy)_3]Cl_2$ (50 µM) and $2NaBPh_4$ (100 µM). Data were acquired at low-mass resolution of 4.0 and transfer collision energies of 0, 2, 4, 6, 8, 10, 12, 14, 16, 18 and 20 eV (top to bottom). Major species: *m*/*z* 843 $\{[Fe(bipy)_3]BPh_4\}^+$, 531 $[Fe(bipy)(BPh_4)]^+$, 445 $[Fe(bipy)_2(Ph)]^+$ and 289 $[Fe(bipy)(Ph)]^+$.

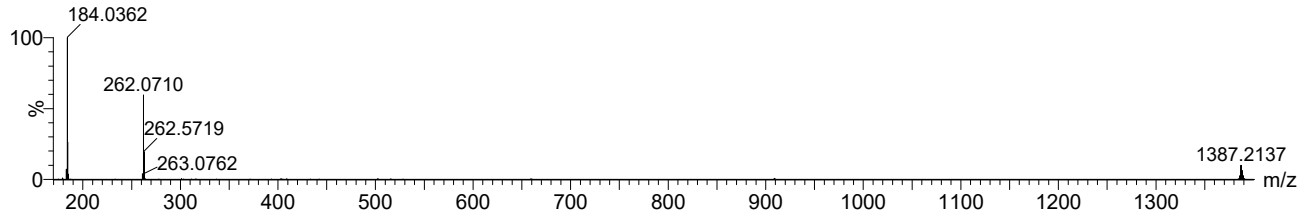

Figure S17. Positive-ion ESI-MS data for $[Fe(bipy)_3]Cl_2$ (50 μM) + $2NaBAr^F{}_4$ (100 μM) acquired at a capillary voltage of 1.52 kV. Major species: *m/z* 1387 $\{[Fe(bipy)_3]BAr^F{}_4\}^+$, 262 $[Fe(bipy)_3]^{2+}$ and 184 $[Fe(bipy)_2]^{2+}$.

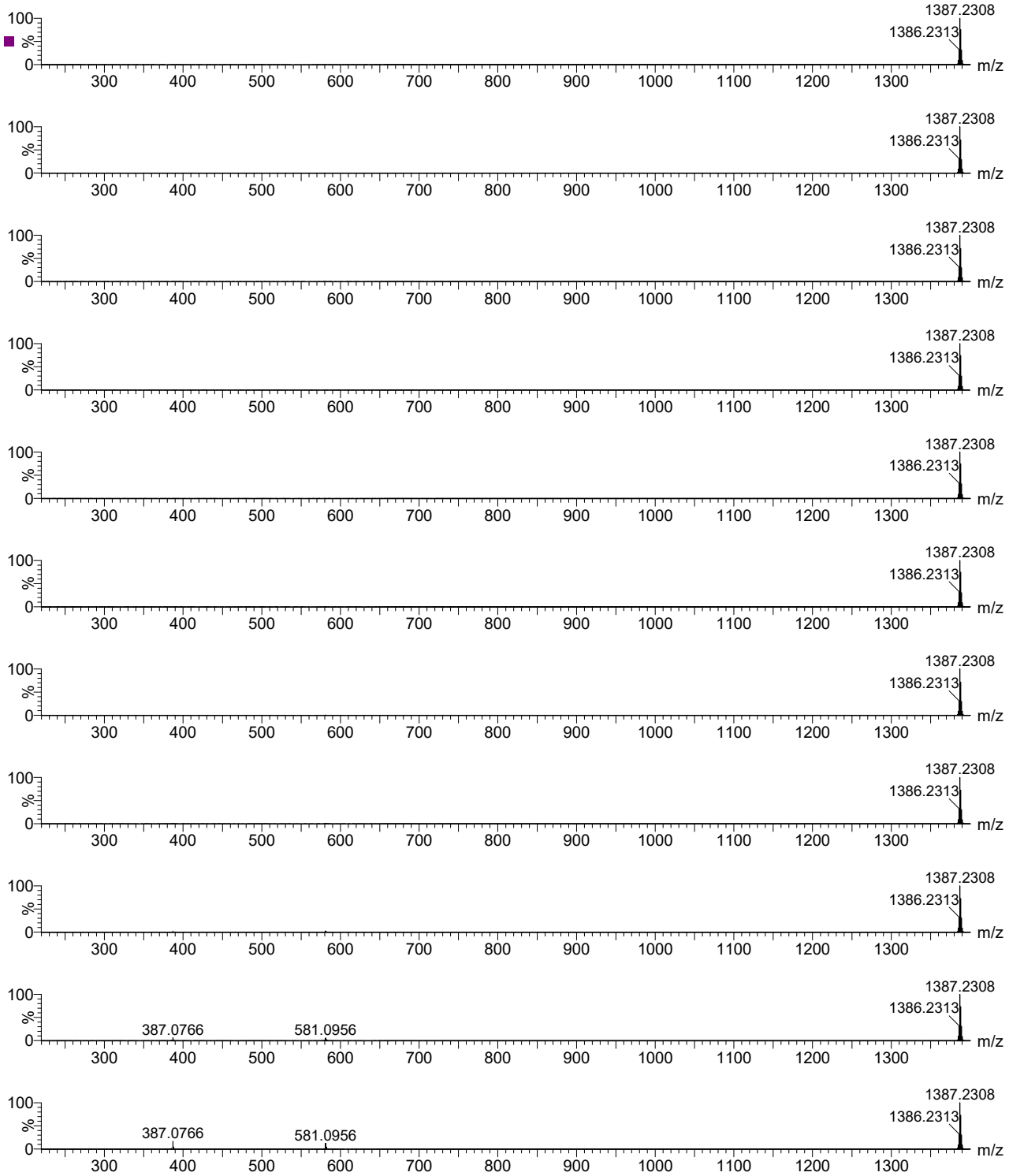

Figure S18. Positive-ion ESI-MS^2 data for the $\{[Fe(bipy)_3]BAr^F{}_4\}^+$ parent ion generated from $[Fe(bipy)_3]Cl_2$ (50 μM) and $NaBAr^F{}_4$ (100 μM). Data were acquired at low-mass resolution of 4.0 and transfer collision energies of 0, 2, 4, 6, 8, 10, 12, 14, 16, 18 and 20 eV (top to bottom). Major species: *m*/*z* 1387 $\{[Fe(bipy)_3]BAr^F{}_4\}^+$, 581 $[Fe(bipy)_2(Ar^F)]^+$, 387 $[Fe(bipy)_2F]^+$ and 231 $[Fe(bipy)F]^+$.

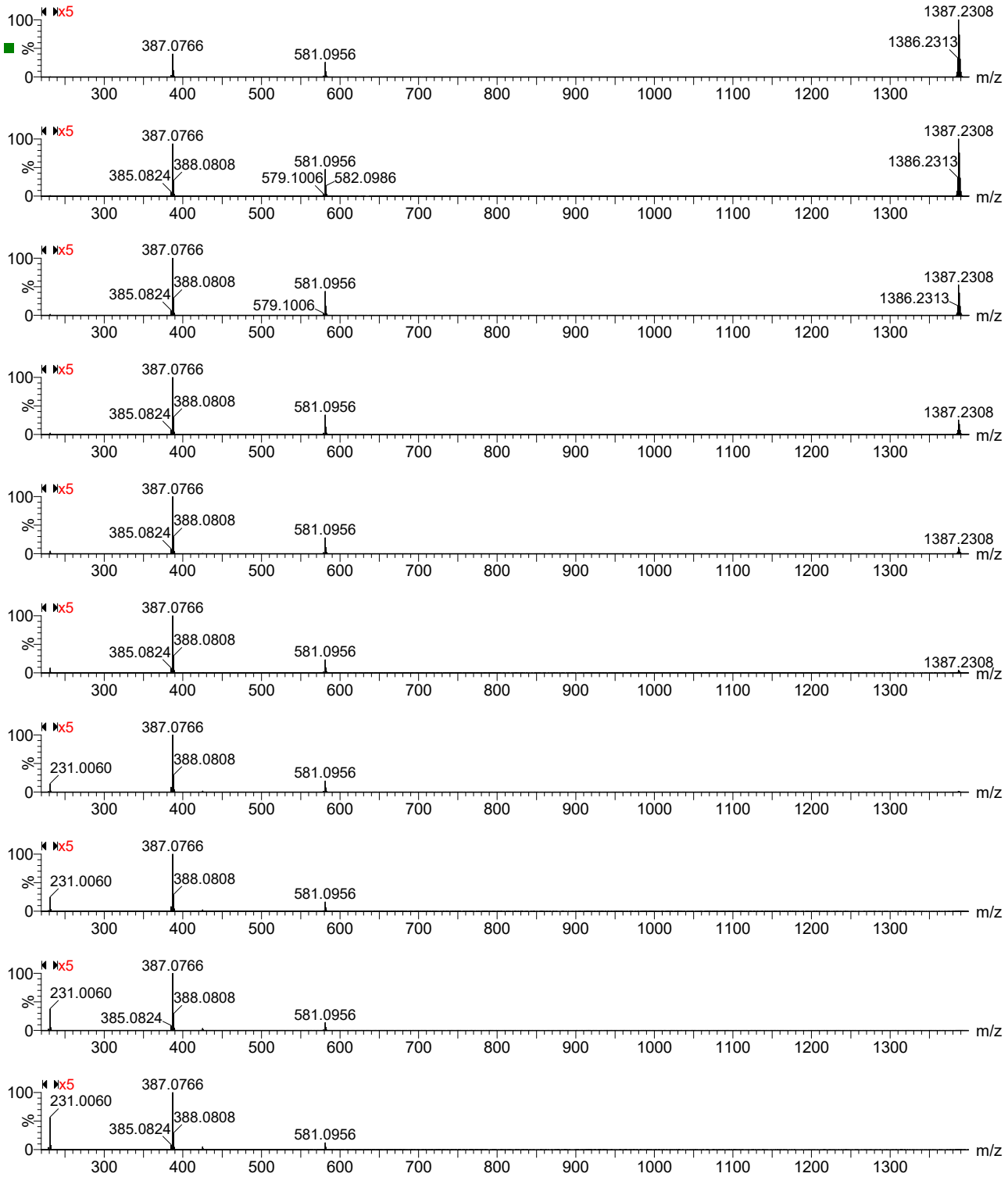

Figure S19. Positive-ion ESI-MS^2 data for the $\{[Fe(bipy)_3]BAr^F{}_4\}^+$ parent ion generated from $[Fe(bipy)_3]Cl_2$ (50 μM) and $NaBAr^F{}_4$ (100 μM). Data were acquired at low-mass resolution of 4.0 and transfer collision energies of 22, 24, 26, 28, 30, 32, 34, 36, 38 and 40 eV (top to bottom). Major species: *m/z* 1387 $\{[Fe(bipy)_3]BAr^F{}_4\}^+$, 581 $[Fe(bipy)_2(Ar^F)]^+$, 387 $[Fe(bipy)_2F]^+$ and 231 $[Fe(bipy)F]^+$.

Ions derived from $[Fe(phen)_3]^{2+}$

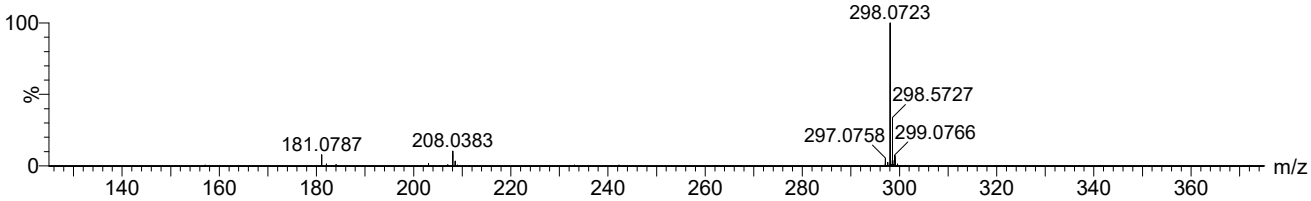

Figure S20. Positive-ion ESI-MS data for $[Fe(phen)_3]Cl_2$ (2.5 μM) acquired at a capillary voltage of 1.51 kV. Major species: *m*/*z* 298 $[Fe(phen)_3]^{2+}$ and 208 $[Fe(phen)_2]^{2+}$. Note: *m*/*z* 242 $[^nBu_4N]^+$.

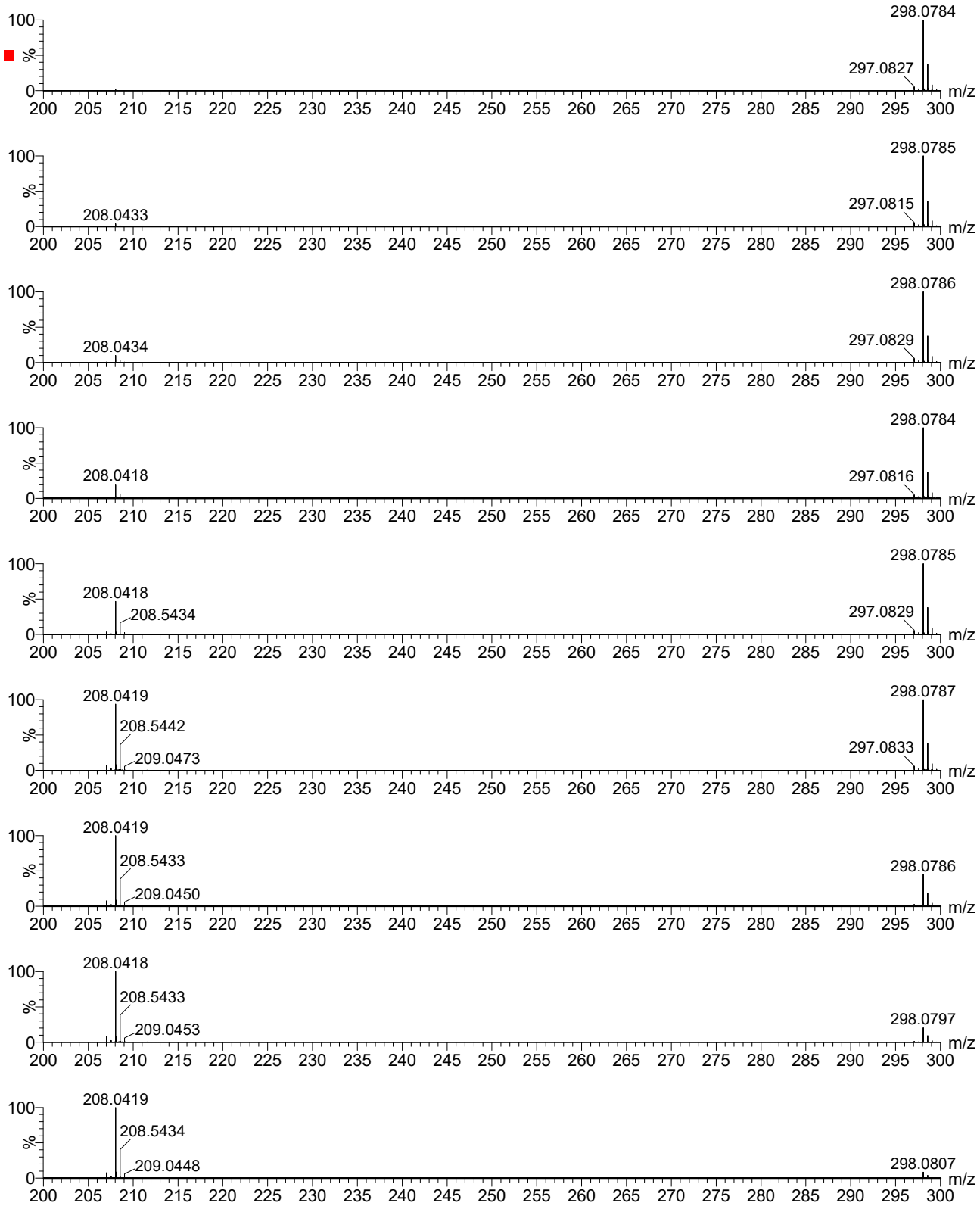

Figure S21. Positive-ion ESI-MS^2 data for the $[Fe(phen)_3]^{2+}$ parent ion generated from $[Fe(phen)_3]Cl_2$ (2.5 µM) acquired at low-mass resolution of 4.5 and transfer collision energies of 0, 2, 4, 6, 8, 10, 12, 14 and 16 eV (top to bottom). Major species: *m/z* 298 $[Fe(phen)_3]^{2+}$ and 208 $[Fe(phen)_2]^{2+}$.

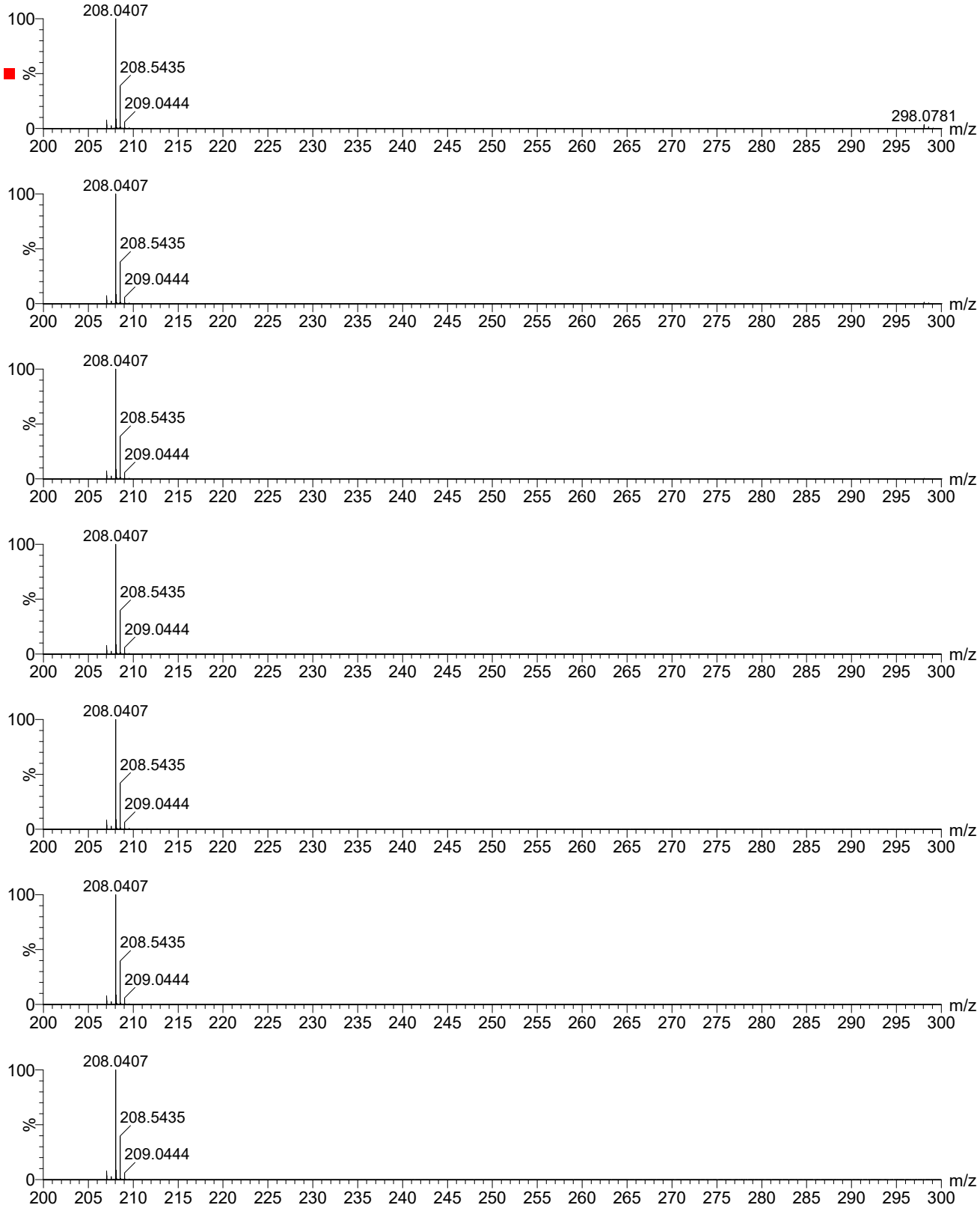

Figure S22. Positive-ion ESI-MS^2 data for the $[Fe(phen)_3]^{2+}$ (2.5 μM) parent ion generated from $[Fe(phen)_3]Cl_2$ (2.5 μM) acquired at low-mass resolution of 4.5 and transfer collision energies of 18, 20, 22, 24, 26, 28 and 30 eV (top to bottom). Major species: *m/z* 298 $[Fe(phen)_3]^{2+}$ and 208 $[Fe(phen)_2]^{2+}$.

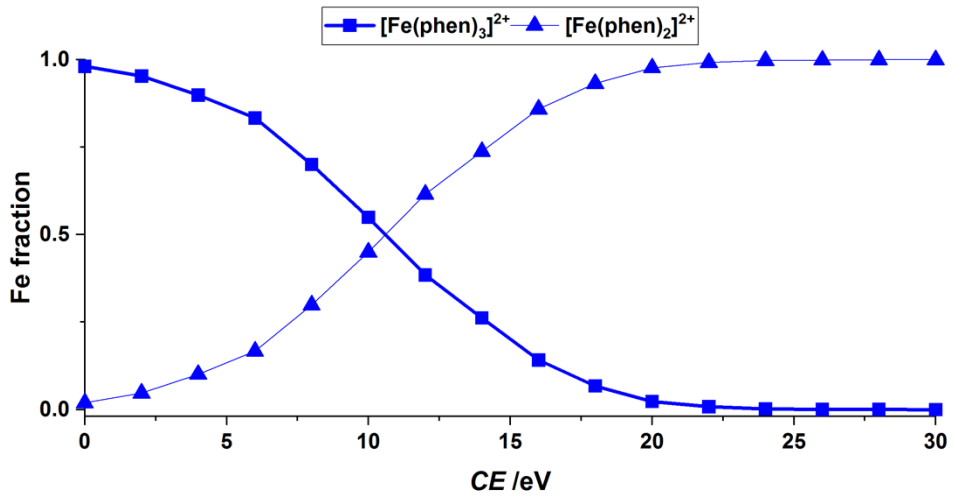

Figure S23. Breakdown curve for $[Fe(phen)_3]^{2+}$.

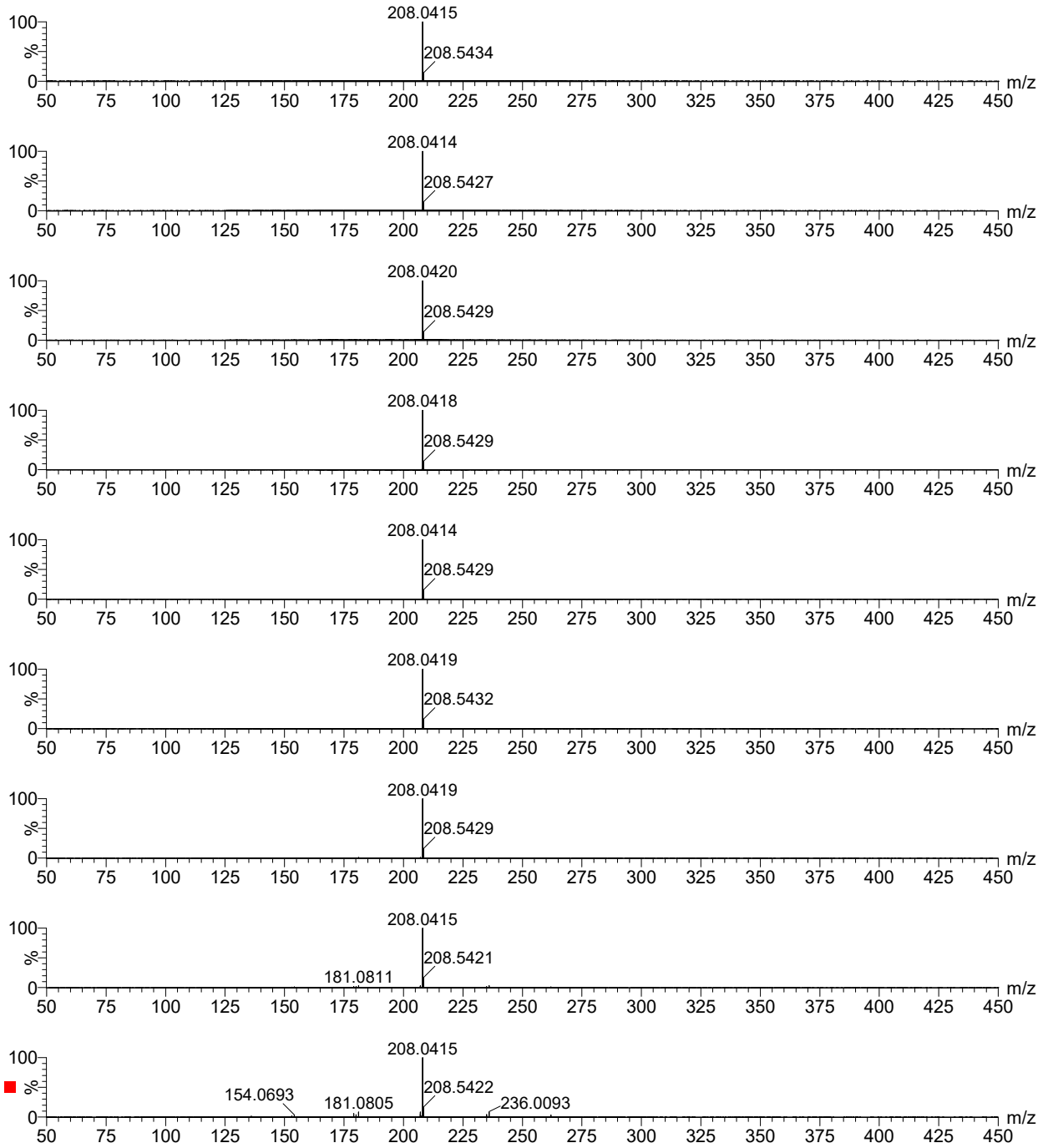

Figure S24. Positive-ion ESI-MS^2 data for the $[Fe(phen)_2]^{2+}$ parent ion generated from $[Fe(phen)_3]Cl_2$ (10 µM). Data were acquired at low-mass resolution of 15 and transfer collision energies of 0, 4, 8, 12, 16, 20, 24, 28 and 32 eV (top to bottom). Major species: *m/z* 262 $[Fe(phen)(N_2)]^+$, 252 $[Fe(phenO{-}H)]^+$, 236 $[Fe(phen)]^+$, 208 $[Fe(phen)_2]^{2+}$, 194 unknown fragment, 181 $[phenH]^+$, 153 $[bipy{-}H_3]^+$ and 128 $[bipy{-}NCH_2]^+$. The presence of bipy fragments does not indicate an impurity in the parent ion but instead the fragmentation of phen, for example through extrusion of C_2H_2.

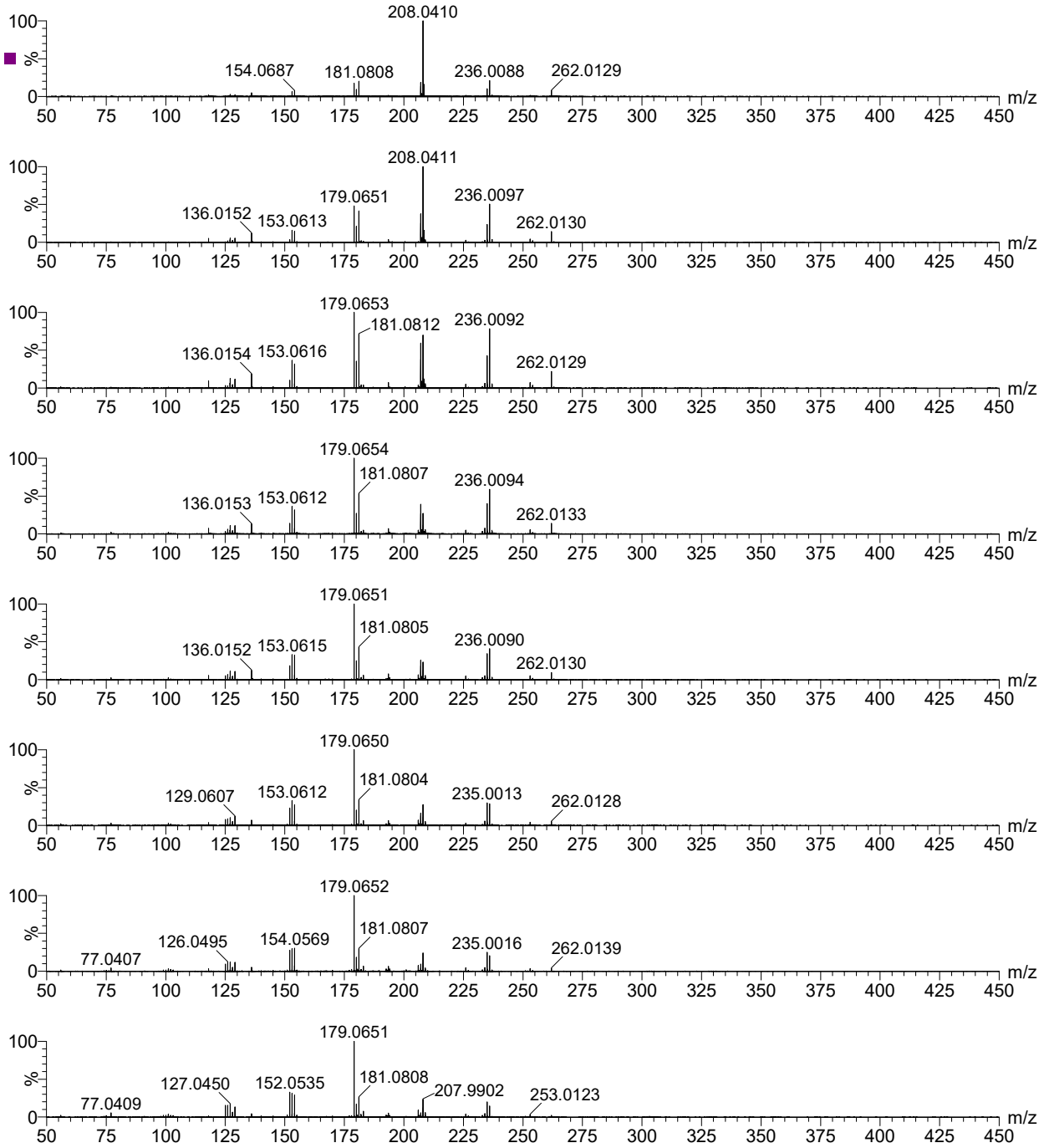

Figure S25. Positive-ion ESI-MS^2 data for the $[Fe(phen)_2]^{2+}$ parent ion generated from $[Fe(phen)_3]Cl_2$ (10 μM). Data were acquired at low-mass resolution of 15 and transfer collision energies of 36, 40, 44, 48, 52, 56, 60 and 64 eV (top to bottom). Major species: *m/z* 262 $[Fe(phen)(N_2)]^+$, 252 $[Fe(phenO{-}H)]^+$, 236 $[Fe(phen)]^+$, 208 $[Fe(phen)_2]^{2+}$, 194 unknown fragment, 181 $[phenH]^+$, 153 $[bipy{-}H_3]^+$ and 128 $[bipy{-}NCH_2]^+$.

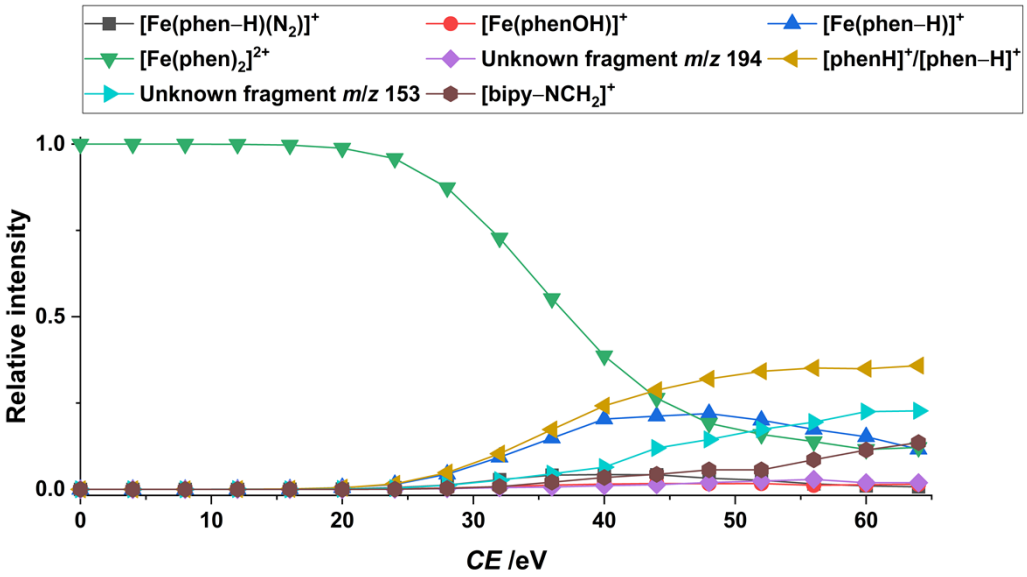

Figure S26. Breakdown curve for $[Fe(phen)_2]^{2+}$.

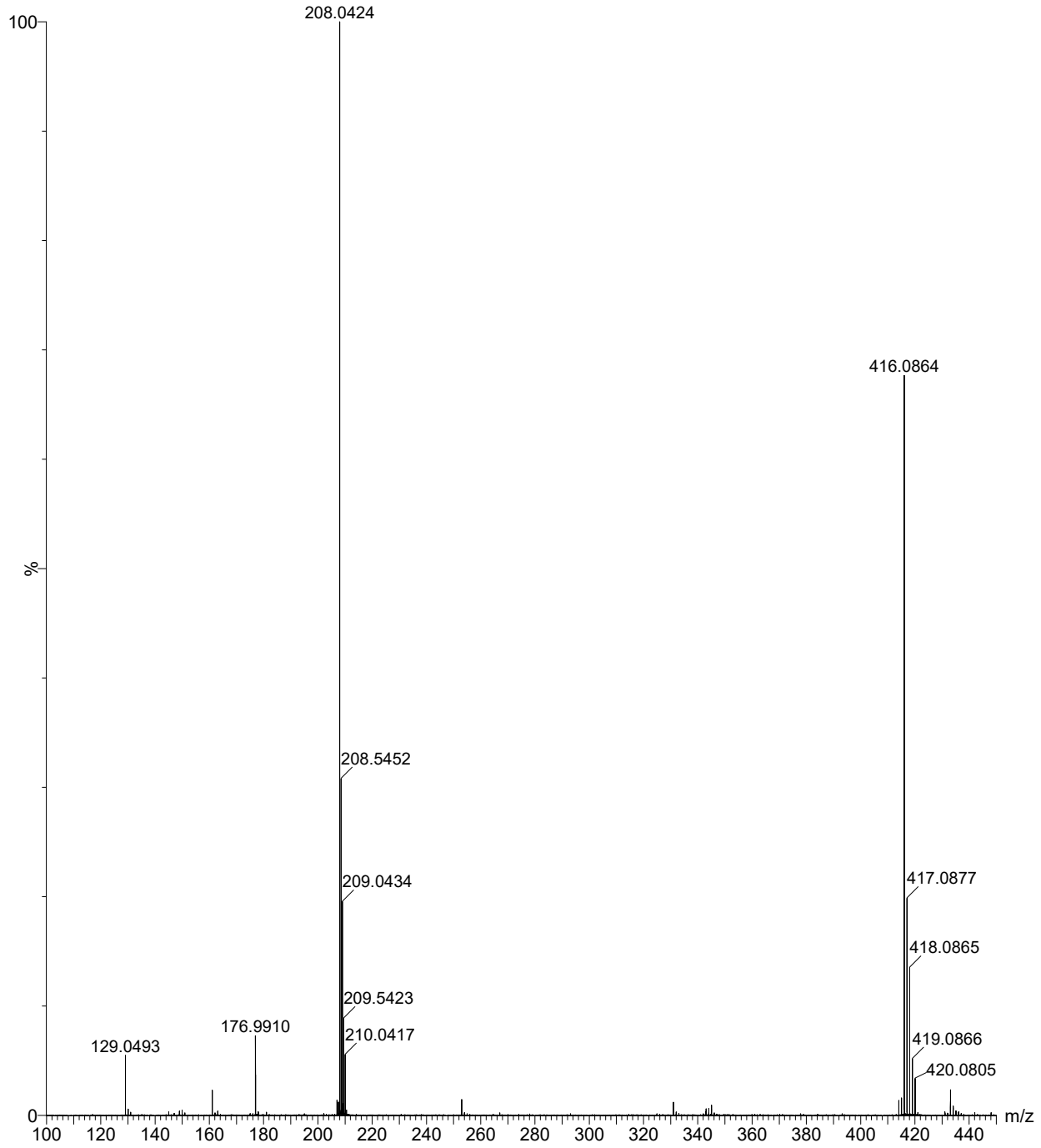

Figure S27. Positive-ion ESI-MS-ETD-MS data for the $[Fe(phen)_2]^{2+}$ parent ion generated from $[Fe(phen)_3]Cl_2$ (10 μM). Data (40 scans) were acquired at low-mass resolution of 5. Major species: *m*/*z* 416 $[Fe(phen)_2]^{+}$ and 208 $[Fe(phen)_2]^{2+}$. Peak integration suggested the extent of reduction was 57%.

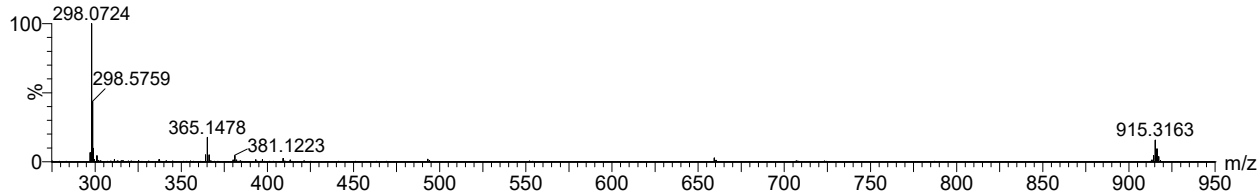

Figure S28. Positive-ion ESI-MS data for $[Fe(phen)_3]Cl_2$ (50 μM) + $2NaBPh_4$ (100 μM) acquired at a capillary voltage of 1.51 kV. Major species: *m*/*z* 915 $\{[Fe(phen)_3]BPh_4\}^+$, 298 $[Fe(phen)_3]^{2+}$. Note: *m*/*z* 365 $[Na_2BPh_4]^+$.

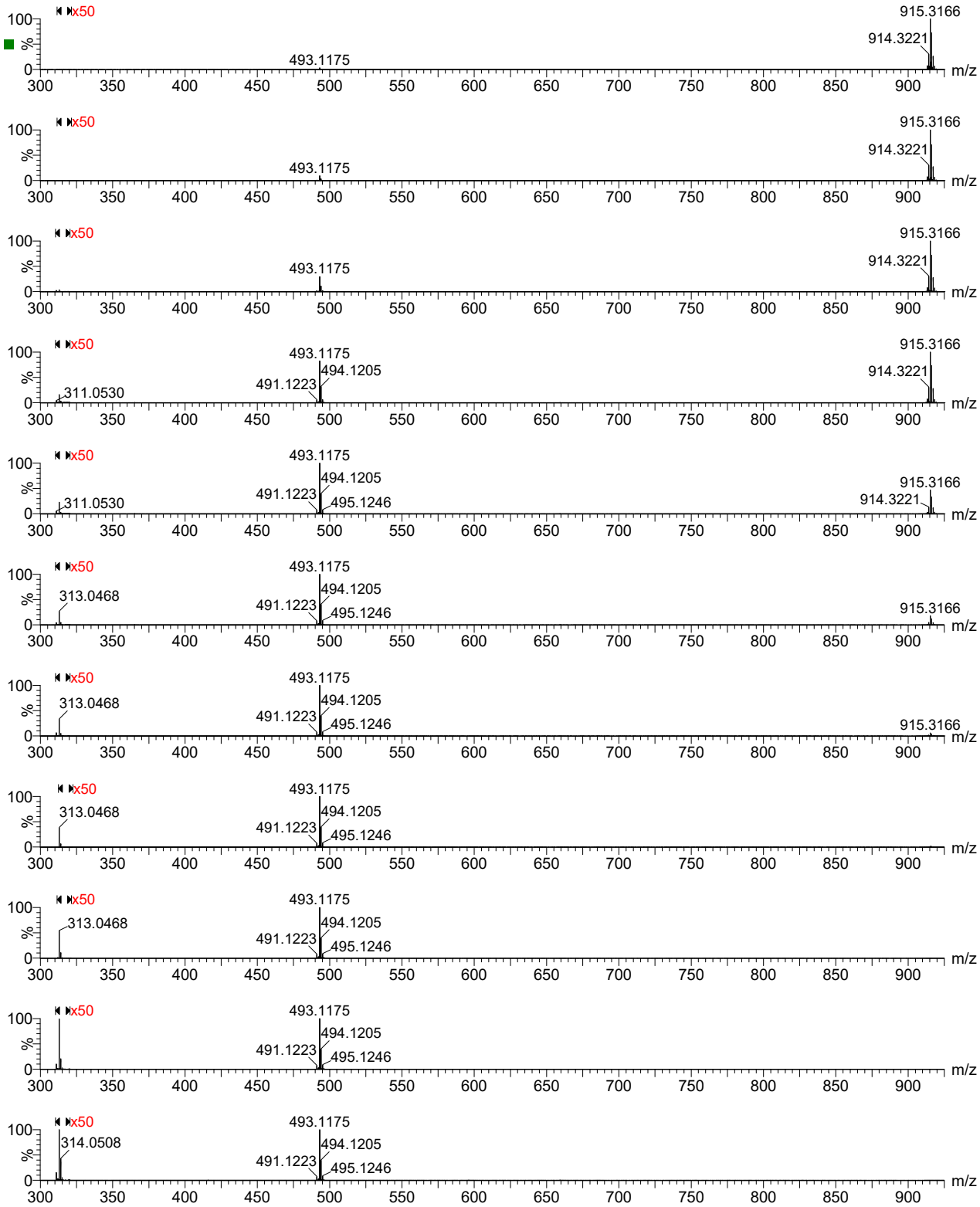

Figure S29. Positive-ion ESI-MS^2 data for the $\{[Fe(phen)_3]BPh_4\}^+$ parent ion generated from $[Fe(phen)_3]Cl_2$ (50 µM) and $2NaBPh_4$ (100 µM). Data were acquired at low-mass resolution of 4.4 and transfer collision energies of 0, 2, 4, 6, 8, 10, 12, 14, 16, 18 and 20 eV (top to bottom). Major species: *m*/*z* 915 $\{[Fe(phen)_3]BPh_4\}^+$, 493 $[Fe(phen)_2(Ph)]^+$ and 313 $[Fe(phen)(Ph)]^+$.

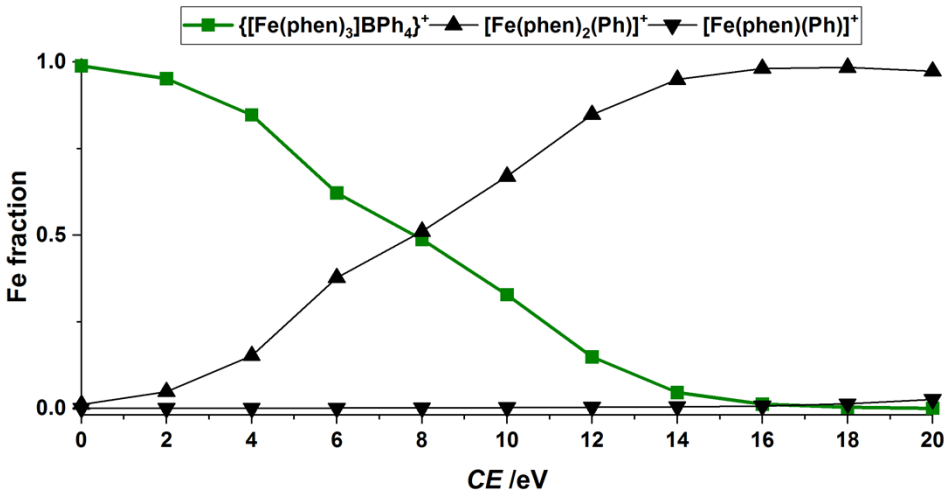

Figure S30. Breakdown curve for $\{[Fe(phen)_3]BPh_4\}^+$.

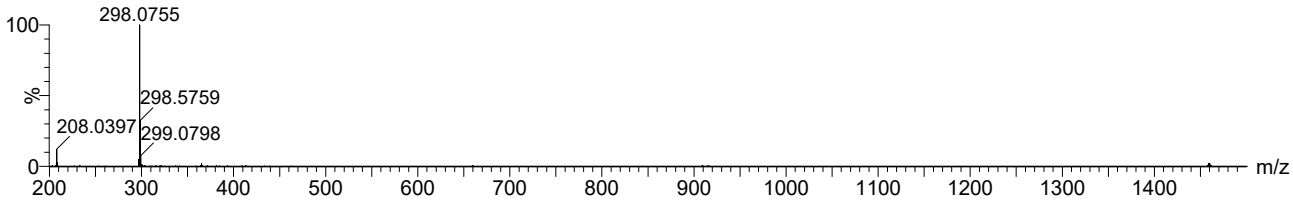

Figure S31. Positive-ion ESI-MS data for $[Fe(phen)_3]Cl_2$ (50 μM) + $2NaBAr^F{}_4$ (100 μM) acquired at a capillary voltage of 1.51 kV. Major species: *m*/*z* 1459 $\{[Fe(phen)_3]BAr^F{}_4\}^+$, 298 $[Fe(phen)_3]^{2+}$ and 208 $[Fe(phen)_2]^{2+}$.

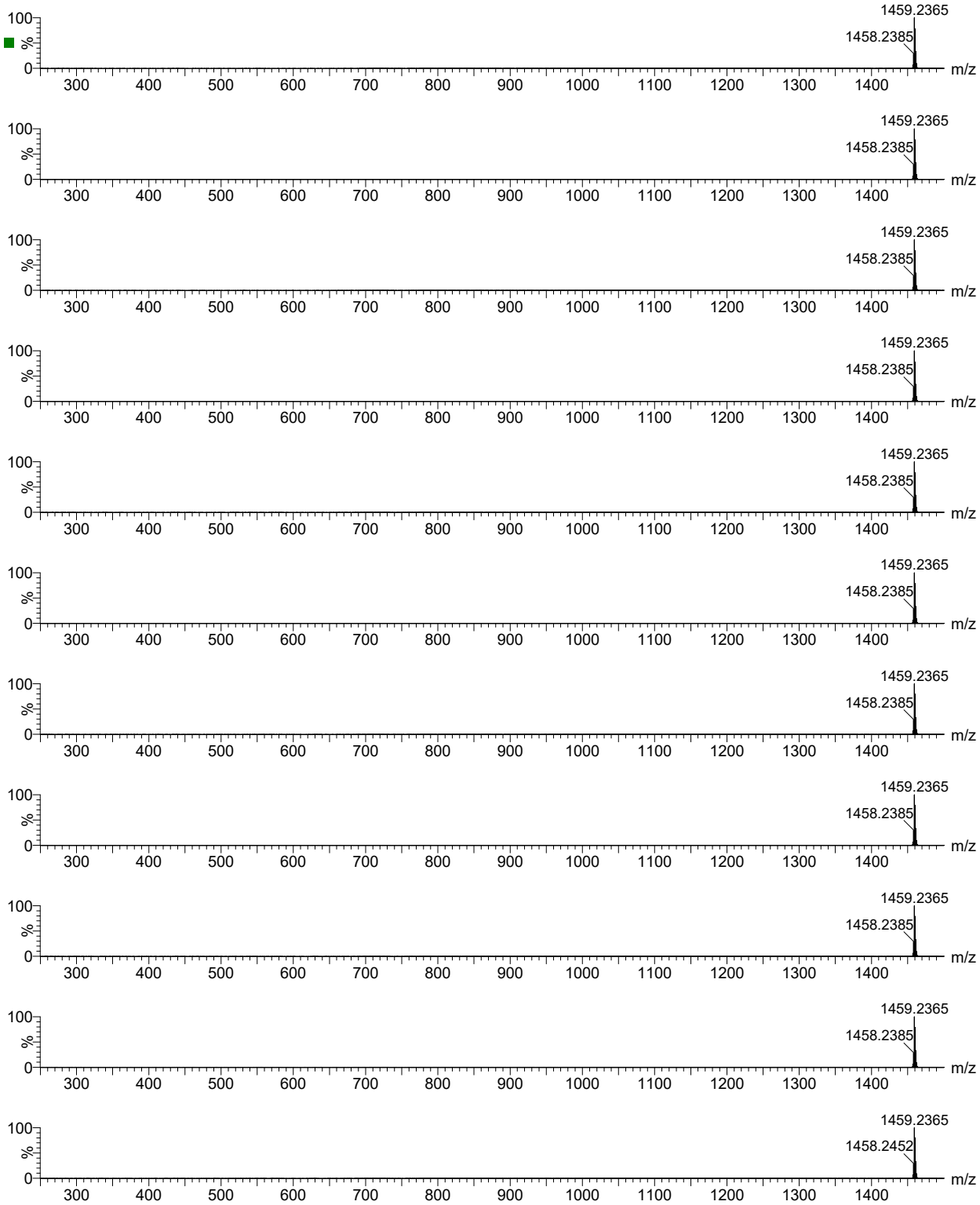

Figure S32. Positive-ion ESI-MS^2 data for the $\{[Fe(phen)_3]BAr^F{}_4\}^+$ parent ion generated from $[Fe(phen)_3]Cl_2$ (50 μM) and $NaBAr^F{}_4$ (100 μM). Data were acquired at low-mass resolution of 4.0 and transfer collision energies of 0, 2, 4, 6, 8, 10, 12, 14, 16, 18 and 20 eV (top to bottom). Major species: *m*/*z* 1459 $\{[Fe(phen)_3]BAr^F{}_4\}^+$, 629 $[Fe(phen)_2(Ar^F)]^+$, 435 $[Fe(phen)_2F]^+$ and 255 $[Fe(phen)F]^+$.

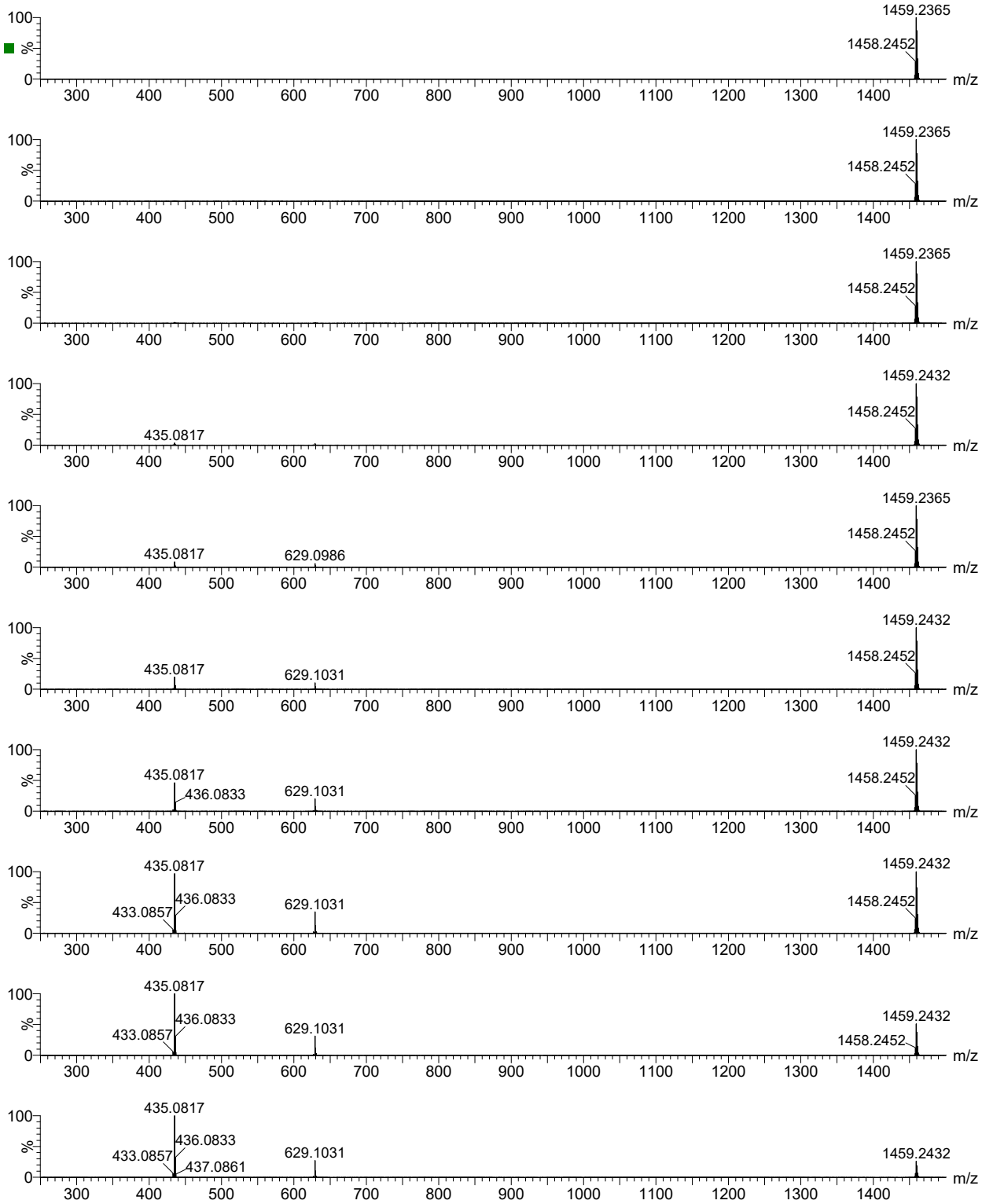

Figure S33. Positive-ion ESI-MS^2 data for the $\{[Fe(phen)_3]BAr^F{}_4\}^+$ parent ion generated from $[Fe(phen)_3]Cl_2$ (50 μM) and $NaBAr^F{}_4$ (100 μM). Data were acquired at low-mass resolution of 4.0 and transfer collision energies of 22, 24, 26, 28, 30, 32, 34, 36, 38 and 40 eV (top to bottom). Major species: *m/z* 1459 $\{[Fe(phen)_3]BAr^F{}_4\}^+$, 629 $[Fe(phen)_2(Ar^F)]^+$, 435 $[Fe(phen)_2F]^+$ and 255 $[Fe(phen)F]^+$.

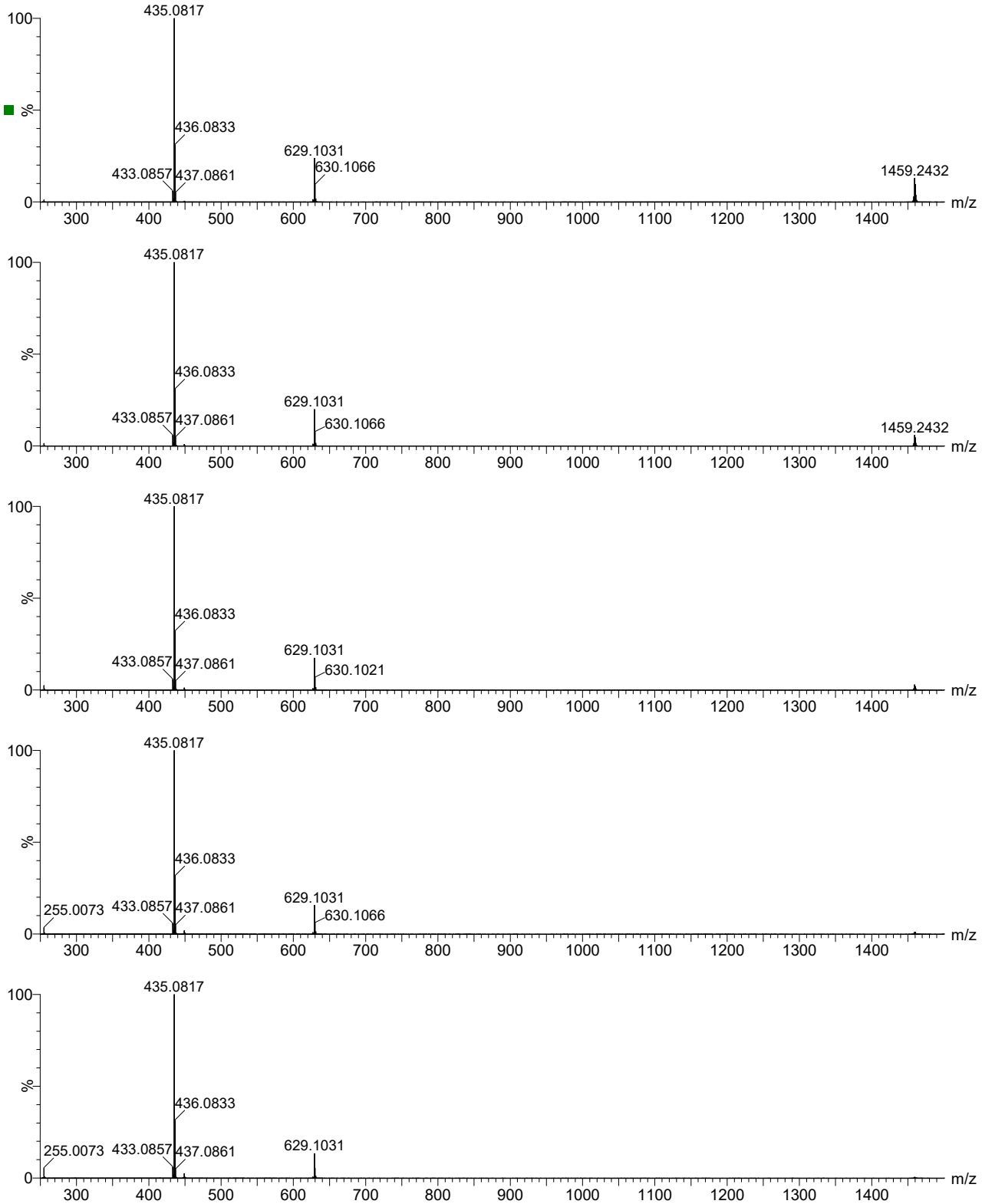

Figure S34. Positive-ion ESI-MS^2 data for the $\{[Fe(phen)_3]BAr^F{}_4\}^+$ parent ion generated from $[Fe(phen)_3]Cl_2$ (50 μM) and $NaBAr^F{}_4$ (100 μM). Data were acquired at low-mass resolution of 4.0 and transfer collision energies of 42, 44, 46, 48 and 50 eV (top to bottom). Major species: *m*/*z* 1459 $\{[Fe(phen)_3]BAr^F{}_4\}^+$, 629 $[Fe(phen)_2(Ar^F)]^+$, 435 $[Fe(phen)_2F]^+$ and 255 $[Fe(phen)F]^+$.

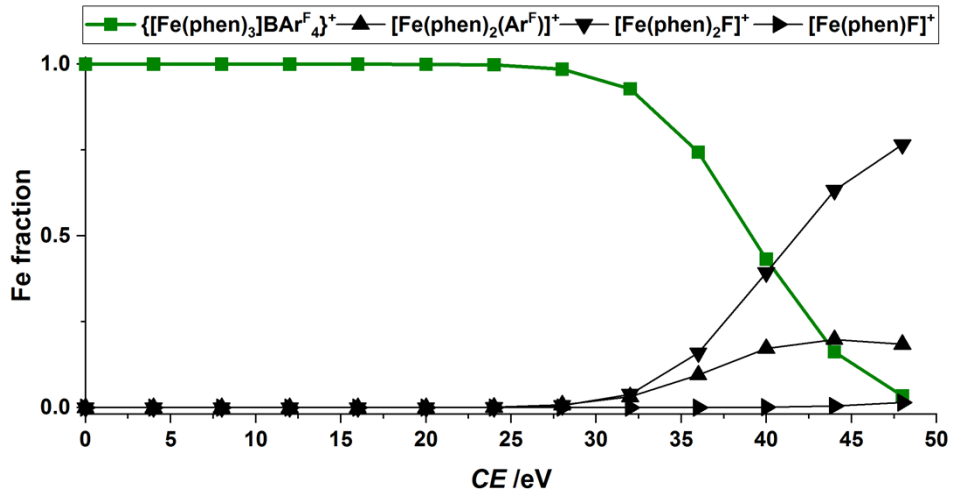

Figure S35. Breakdown curve for $\{[Fe(phen)_3]BAr^F{}_4\}^+$.

	BPh_4^-	$BAr^F{}_4^-$
$[Fe(bipy)_3]^{2+}$	1.00	0.71
$[Fe(phen)_3]^{2+}$	0.72	0.90

Table S2. Intensity ratio $\{[Fe(N^\wedge N)_3]BAr_4\}^+$ / $[Fe(N^\wedge N)_3]^{2+}$ for ions generated from $[Fe(N^\wedge N)_3]Cl_2$ (50 μM) and $NaBAr_4$ (100 μM) at a capillary voltage of 0.69 kV. Higher voltages afford overly high intensities that cannot be measured accurately.

Ions derived from $[Fe(bipy)_2(phen)]^{2+}$ and $[Fe(bipy)(phen)_2]^{2+}$

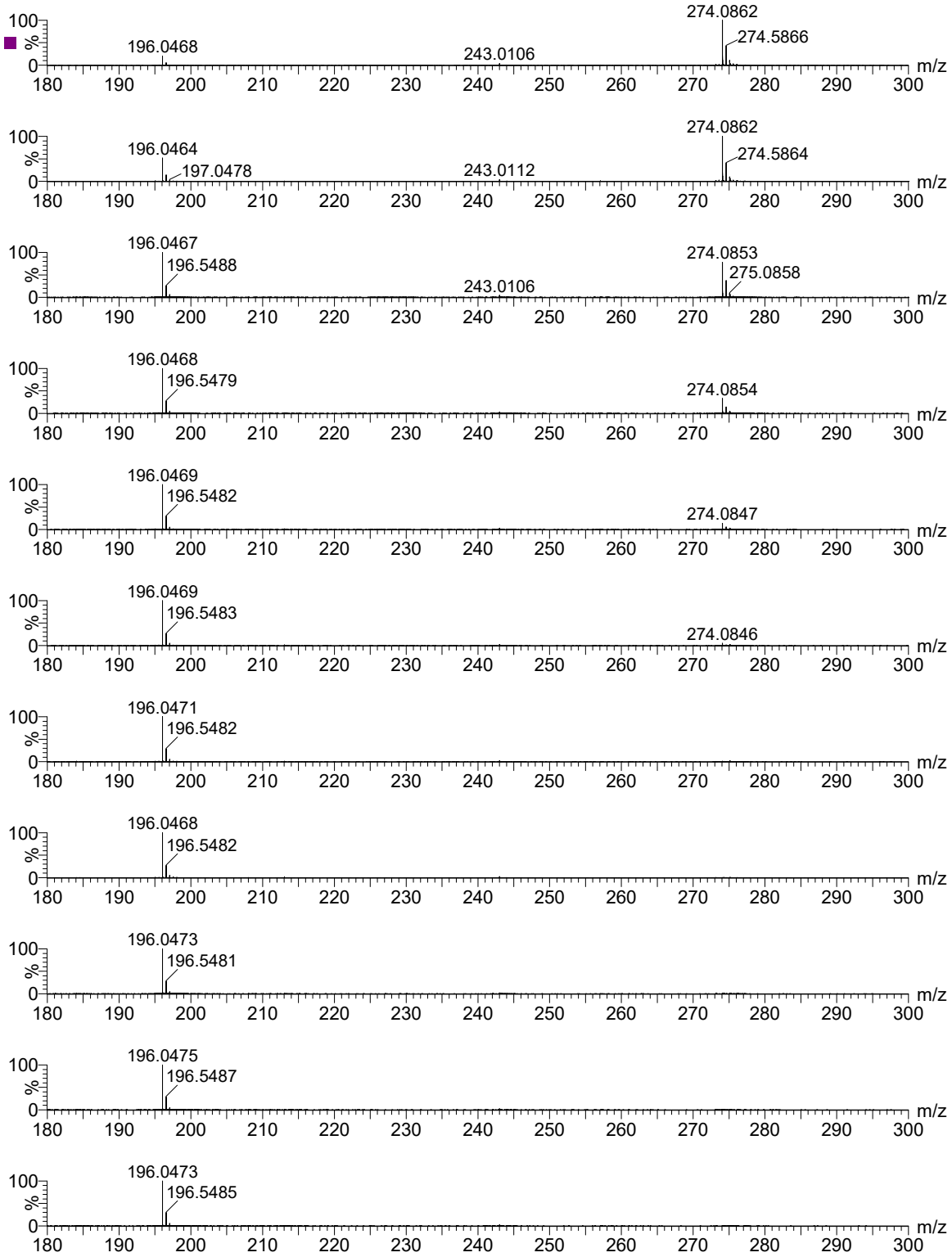

Figure S36. Positive-ion ESI-MS^2 data for the $[Fe(bipy)_2(phen)]^{2+}$ parent ion generated from $[Fe(bipy)_3]Cl_2$ (2.5 μM) and $[Fe(phen)_3]Cl_2$ (2.5 μM). Data were acquired at low-mass resolution of 5.0

and transfer collision energies of 0, 2, 4, 6, 8, 10, 12, 14, 16, 18, 20 eV (top to bottom). Major species: *m/z* 274 $[Fe(bipy)_2(phen)]^{2+}$ and 196 $[Fe(bipy)(phen)]^{2+}$.

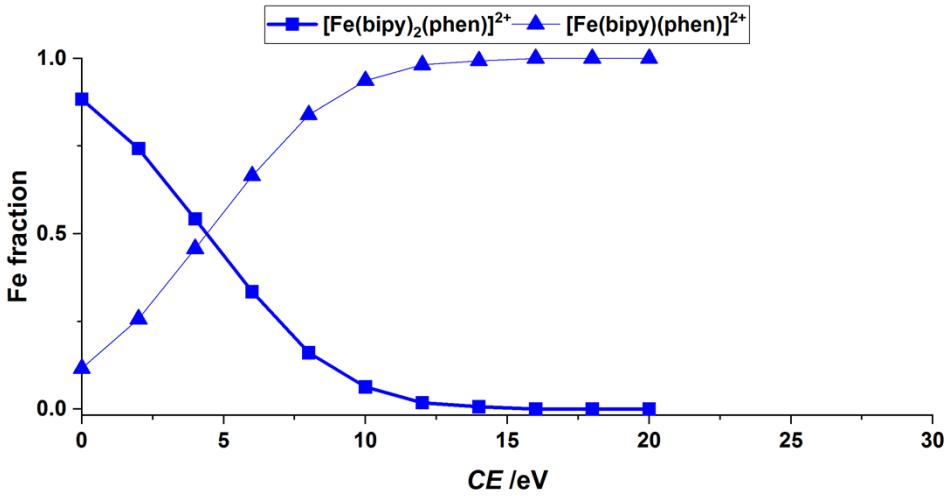

Figure S37. Breakdown curve for $[Fe(bipy)_2(phen)]^{2+}$.

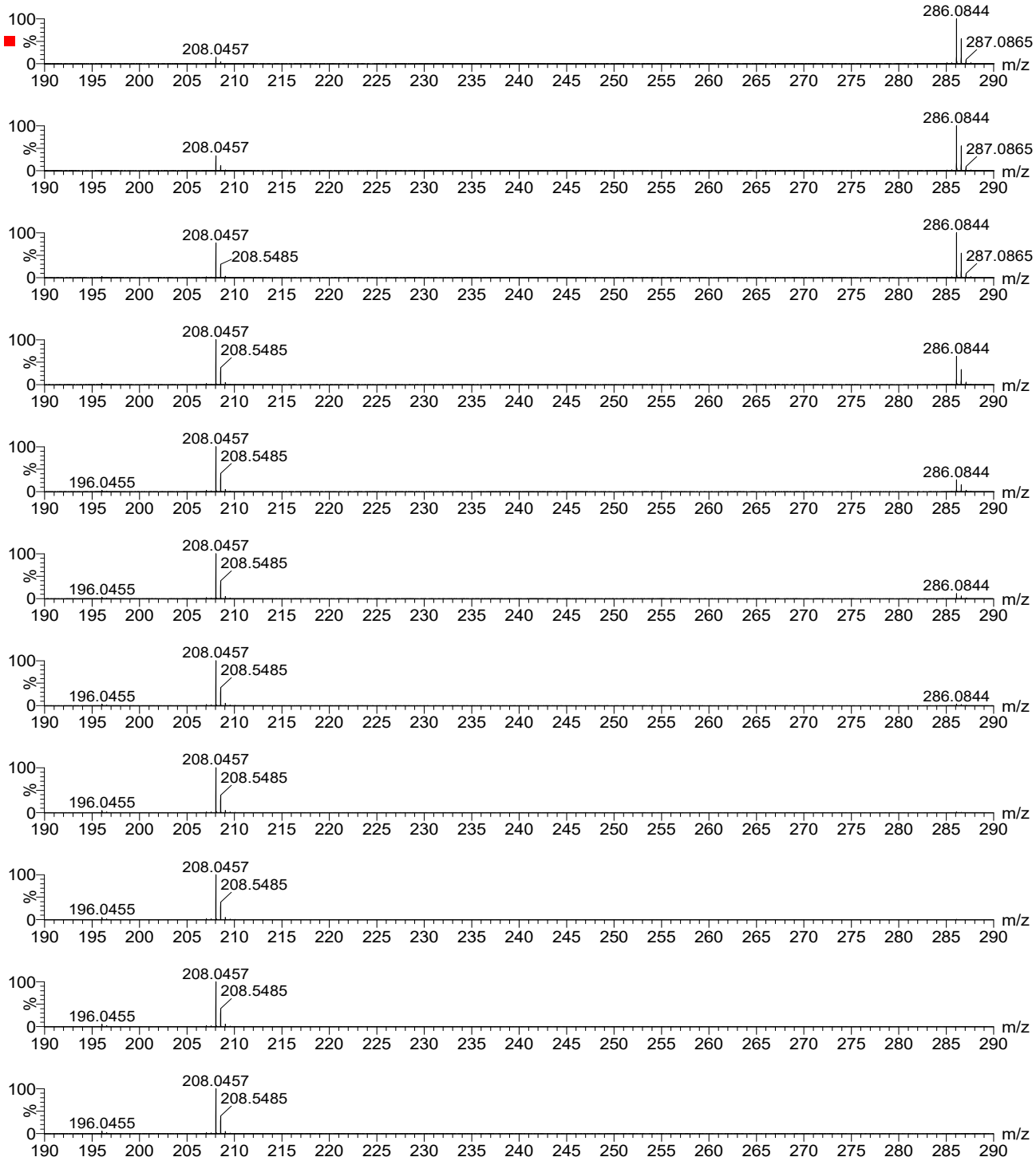

Figure S38. Positive-ion ESI-MS^2 data for the $[Fe(bipy)(phen)_2]^{2+}$ parent ion generated from $[Fe(bipy)_3]Cl_2$ (2.5 µM) and $[Fe(phen)_3]Cl_2$ (2.5 µM). Data were acquired at low-mass resolution of 5.0 and transfer collision energies of 0, 2, 4, 6, 8, 10, 12, 14, 16, 18, 20 eV (top to bottom). Major species: *m/z* 286 $[Fe(bipy)(phen)_2]^{2+}$, 208 $[Fe(phen)_2]^{2+}$ and 196 $[Fe(bipy)(phen)]^{2+}$.

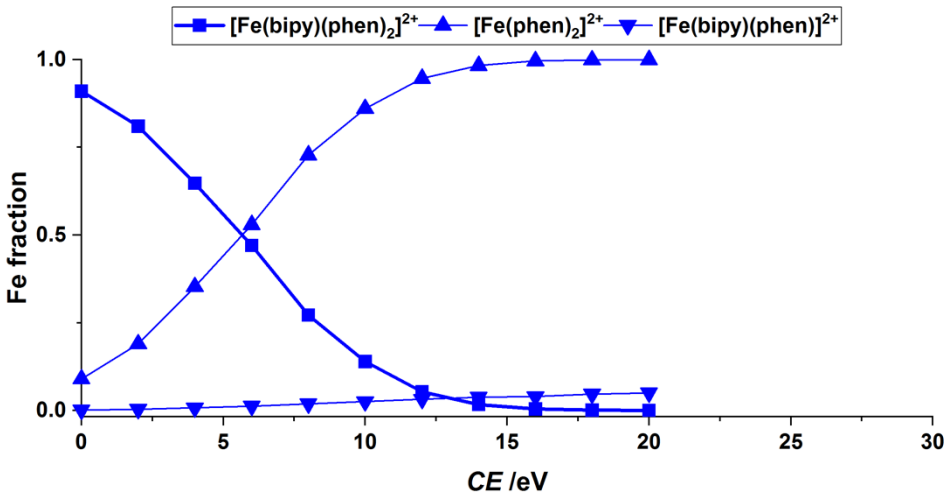

Figure S39. Breakdown curve for $[Fe(bipy)(phen)_2]^{2+}$.

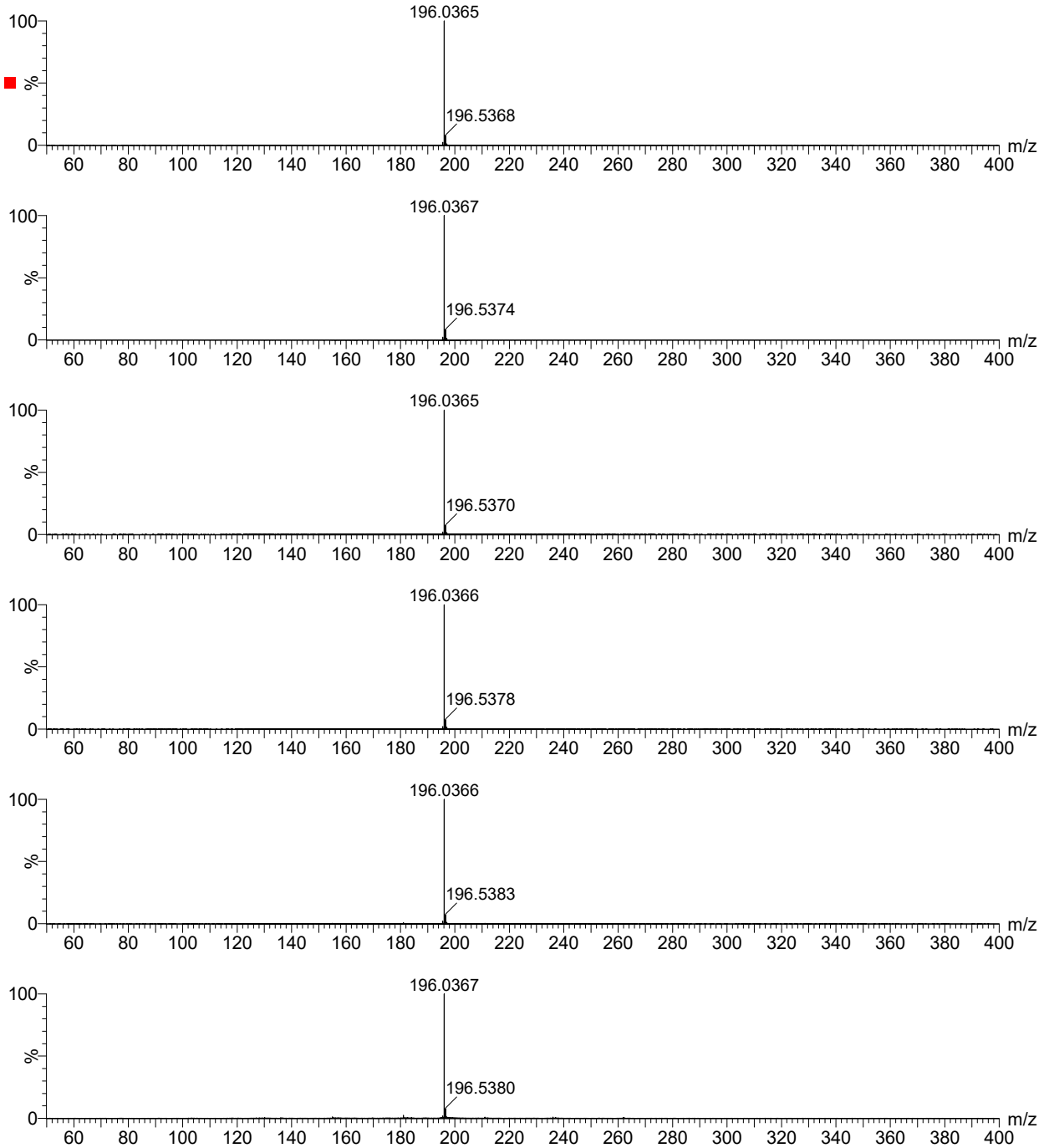

Figure S40. Positive-ion ESI-MS^2 data for the $[Fe(bipy)(phen)]^{2+}$ parent ion generated from $[Fe(bipy)_3]Cl_2$ (5 μM) and $[Fe(phen)_3]Cl_2$ (5 μM). Data were acquired at low-mass resolution of 15 and transfer collision energies of 0, 4, 8, 12, 16 and 20 eV (top to bottom, 30 scans per spectrum). Major species: *m/z* 262 unknown fragment, 236 $[Fe(phen)]^+$, 196 $[Fe(bipy)(phen)]^{2+}$, 181 $[phenH]^+$, 155 $[bipy-H]^+$, 136 $[FeH(py)]^+$, 128 $[bipy-NCH_2]^+$, 102 $[NC_7H_4]^+$ and 78 $[C_5H_3N]^+$.

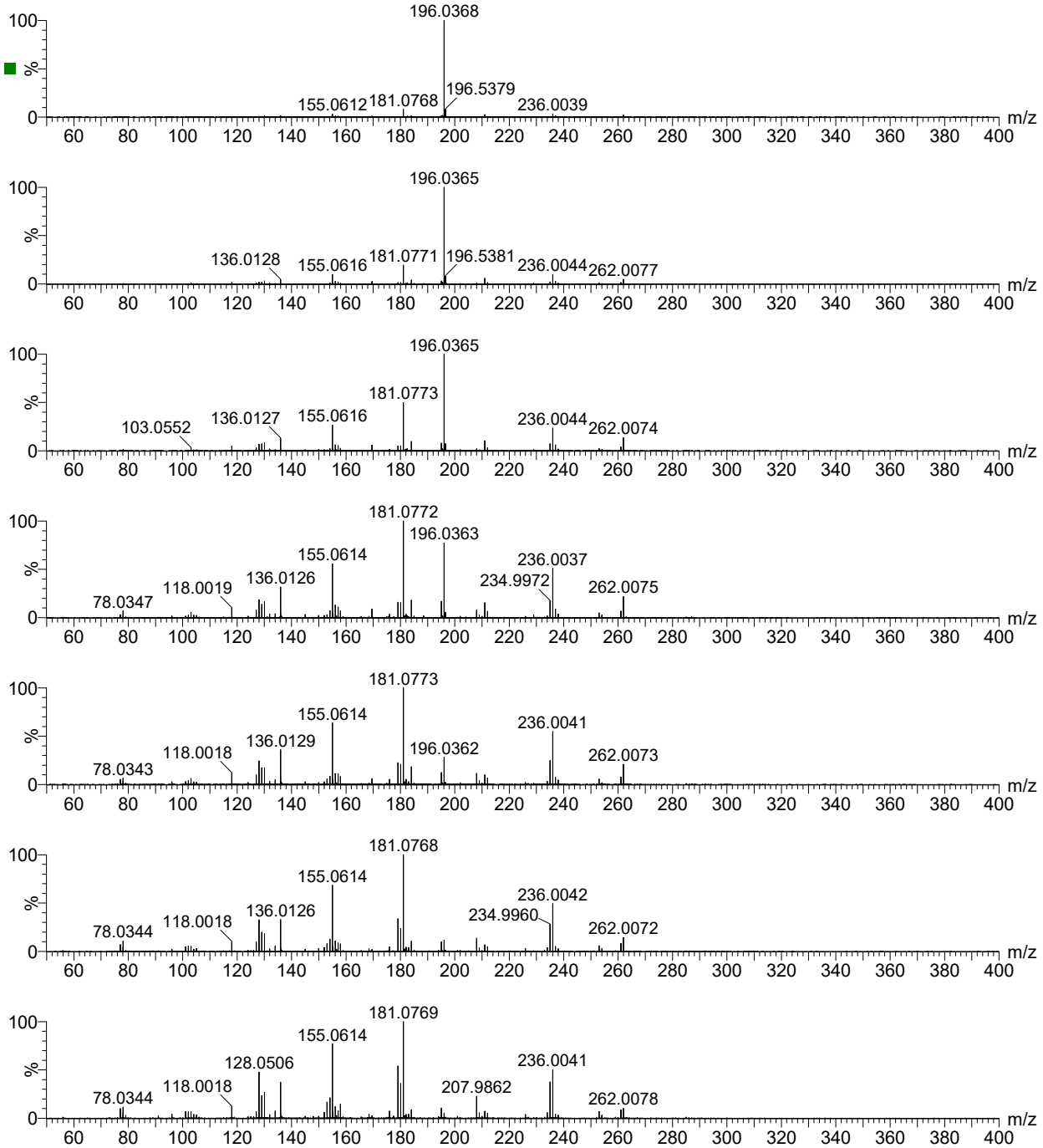

Figure S41. Positive-ion ESI-MS^2 data for the $[Fe(bipy)(phen)]^{2+}$ parent ion generated from $[Fe(bipy)_3]Cl_2$ (5 μM) and $[Fe(phen)_3]Cl_2$ (5 μM). Data were acquired at low-mass resolution of 15 and transfer collision energies of 24, 28, 32, 36, 40, 44 and 48 eV (top to bottom). Major species: *m*/*z* 262 unknown fragment, 236 $[Fe(phen)]^+$, 196 $[Fe(bipy)(phen)]^{2+}$, 181 $[phenH]^+$, 155 $[bipy-H]^+$, 136 $[FeH(py)]^+$, 128 $[bipy-NCH_2]^+$, 102 $[NC_7H_4]^+$ and 78 $[C_5H_3N]^+$.

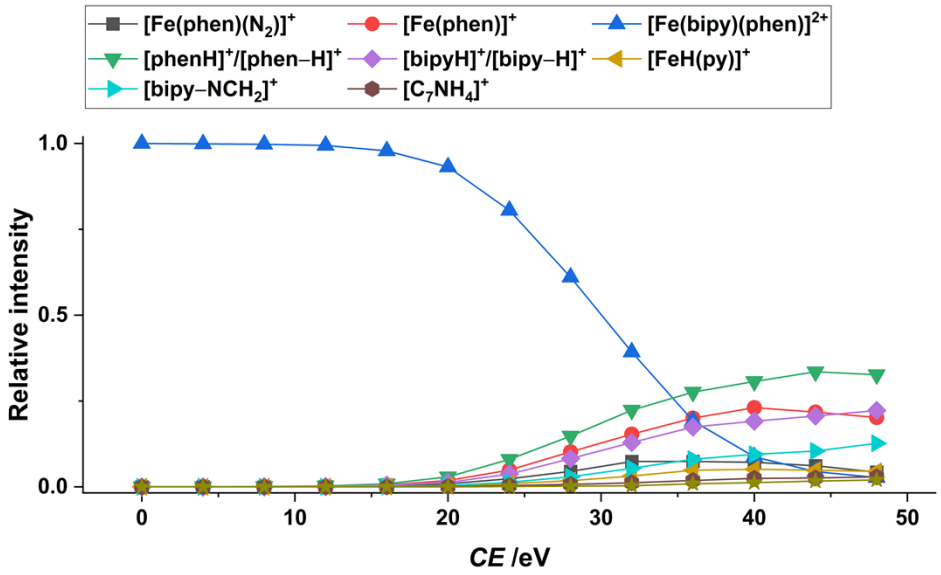

Figure S42. Breakdown curve for $[Fe(bipy)(phen)]^{2+}$.

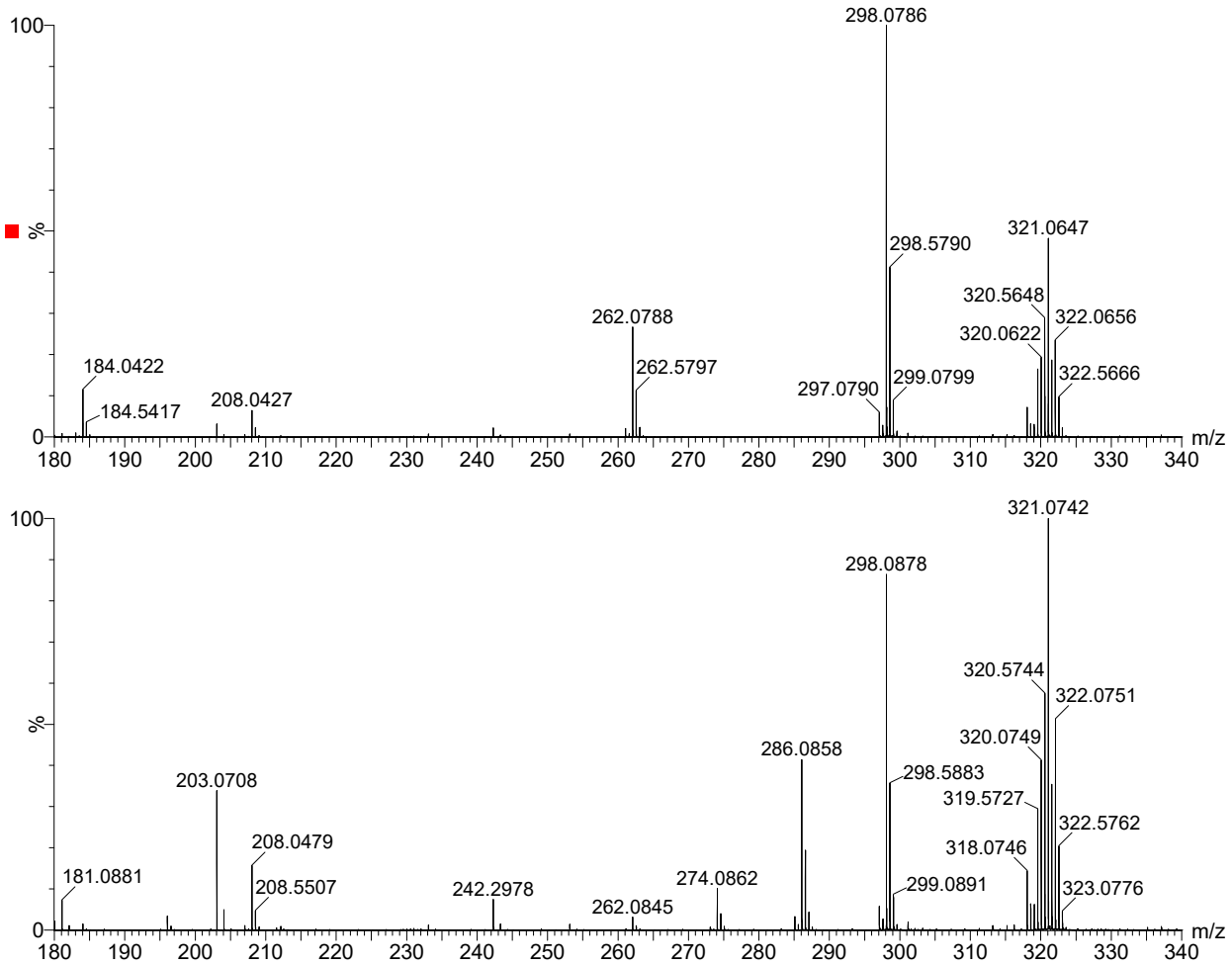

Figure S43. Positive-ion ESI-MS data for a $[Fe(bipy)_3]Cl_2$ (2.0 μM) and $[Fe(phen)_3]Cl_2$ (2.0 μM) mixture after 1 minute (top) and 241 minutes (bottom) at capillary voltage 1.25 kV. Major species: *m/z* 298 $[Fe(phen)_3]^{2+}$, 286 $[Fe(bipy)(phen)_2]^{2+}$, 274 $[Fe(bipy)_2(phen)]^{2+}$, 262 $[Fe(bipy)_3]^{2+}$, 208 $[Fe(phen)_2]^{2+}$ and 184 $[Fe(bipy)_2]^{2+}$. Note: *m/z* 321 $[Ru(phen)_3]^{2+}$ (2.0 μM internal standard), 242 $[^nBu_4N]^+$ (trace amount present from previous sample). The *m/z* ranges 180–190 and 250–330 are magnified 40× for clarity.

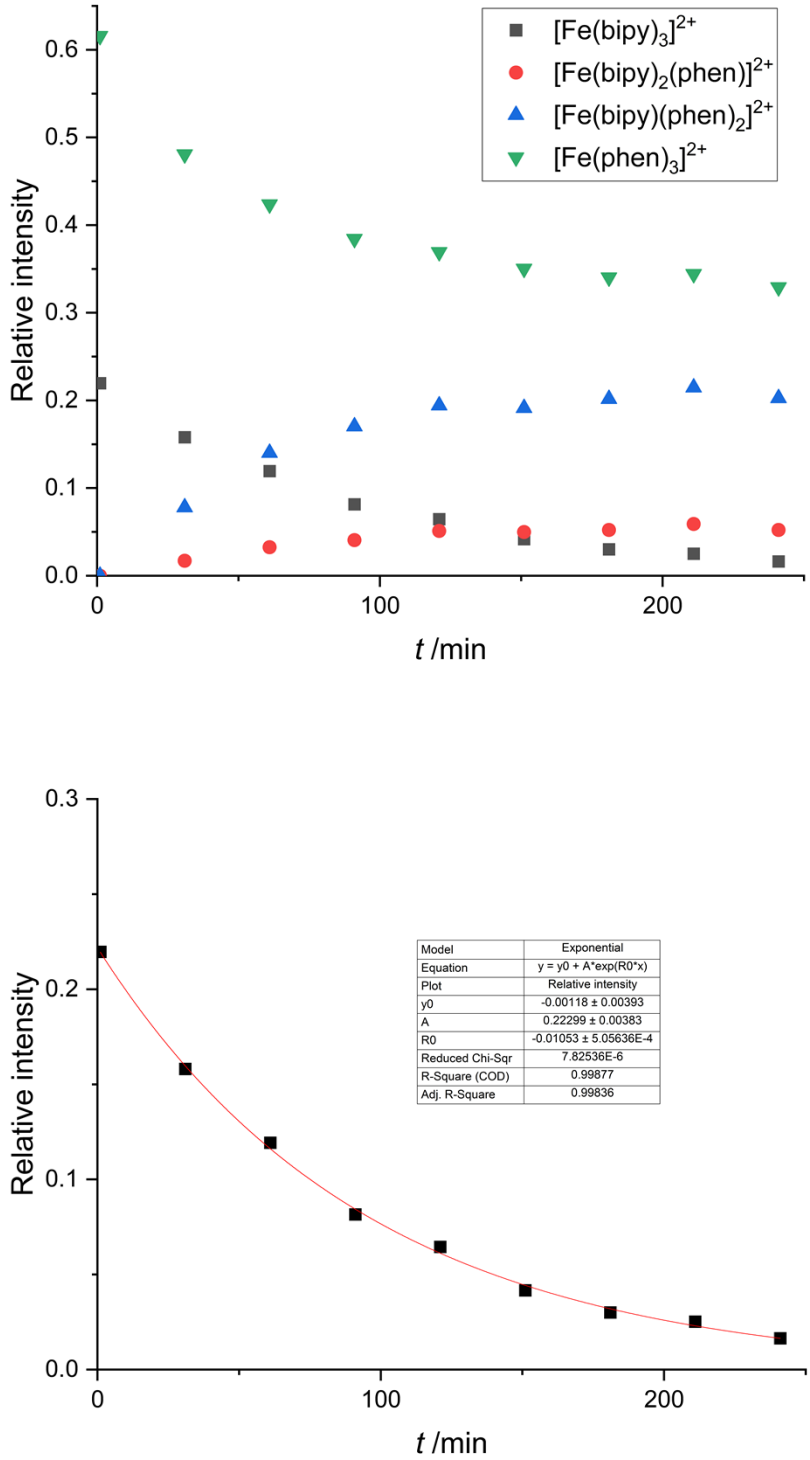

Figure S44. Time course of relative intensities of dicationic complexes relative to $[Ru(phen)_3]^{2+}$ (no added salt, top). Exponential fit of relative $[Fe(bipy)_3]^{2+}$ intensity (bottom).

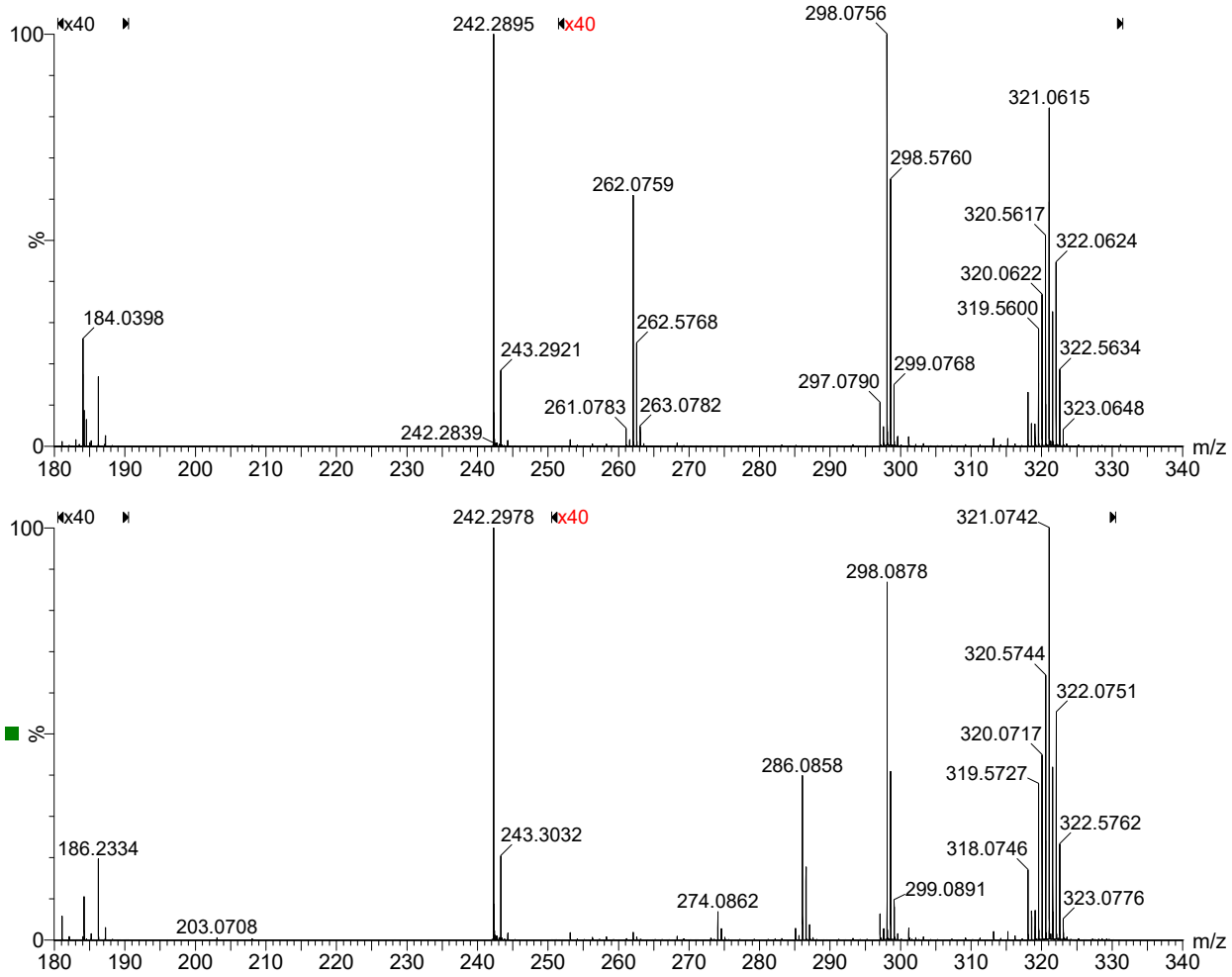

Figure S45. Positive-ion ESI-MS data for a $[Fe(bipy)_3]Cl_2$ (2.0 μM) and $[Fe(phen)_3]Cl_2$ (2.0 μM) mixture with added $[^nBu_4N]Cl$ (20 μM) after 1 minute (top) and 241 minutes (bottom) at capillary voltage 1.25 kV. Major species: *m/z* 298 $[Fe(phen)_3]^{2+}$, 286 $[Fe(bipy)(phen)_2]^{2+}$, 274 $[Fe(bipy)_2(phen)]^{2+}$, 262 $[Fe(bipy)_3]^{2+}$, 208 $[Fe(phen)_2]^{2+}$ and 184 $[Fe(bipy)_2]^{2+}$. Note: *m/z* 321 $[Ru(phen)_3]^{2+}$ (2.0 μM internal standard). The *m/z* ranges 180–190 and 250–330 are magnified 40× for clarity.

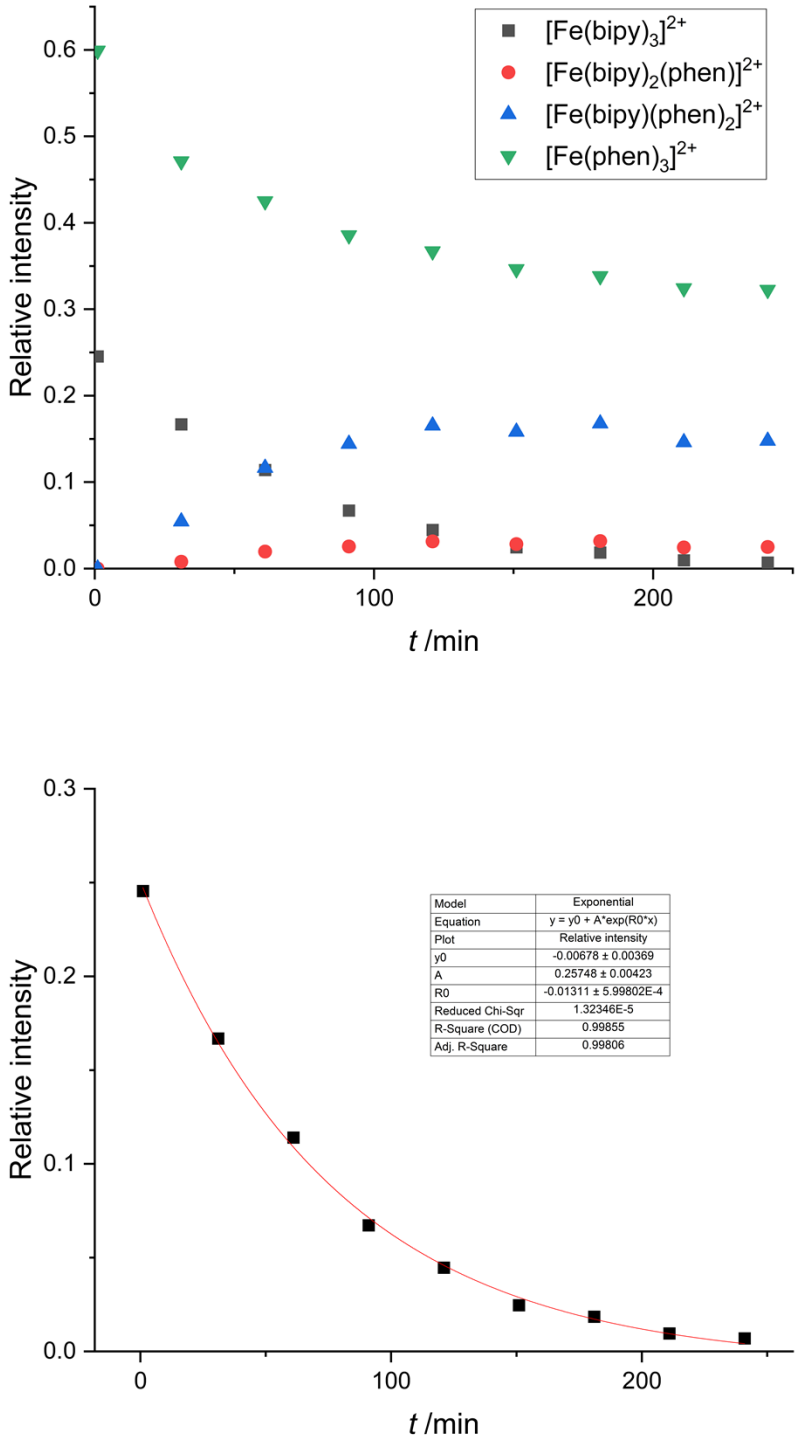

Figure S46. Time course of relative intensities of dicationic complexes relative to $[Ru(phen)_3]^{2+}$ (added added $[^nBu_4N]Cl$, top). Exponential fit of relative $[Fe(bipy)_3]^{2+}$ intensity (bottom).

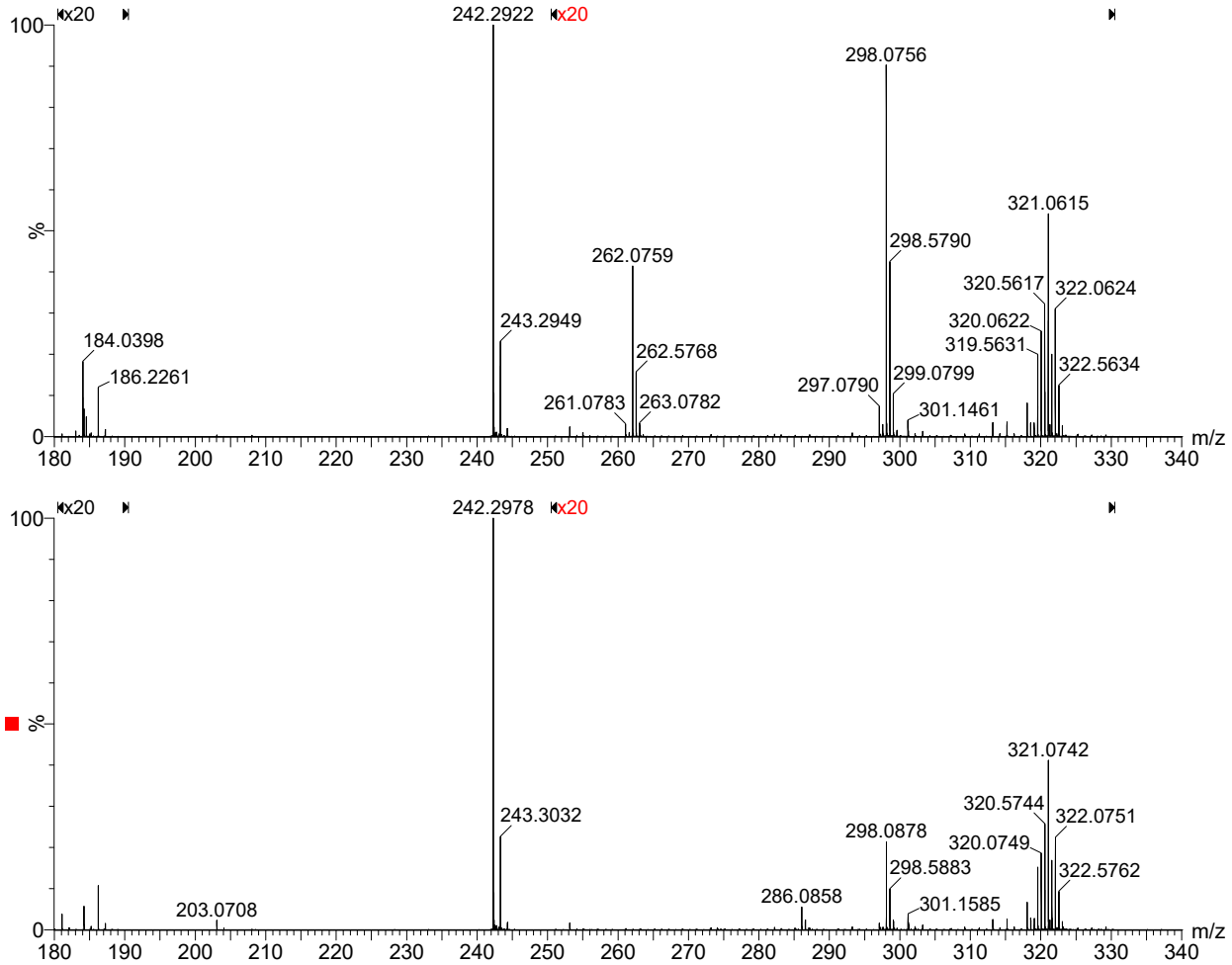

Figure S47. Positive-ion ESI-MS data for a $[Fe(bipy)_3]Cl_2$ (2.0 μM) and $[Fe(phen)_3]Cl_2$ (2.0 μM) mixture with added $[^nBu_4N]PF_6$ (20 μM) after 1 minute (top) and 241 minutes (bottom) at capillary voltage 1.25 kV. Major species: *m/z* 298 $[Fe(phen)_3]^{2+}$, 286 $[Fe(bipy)(phen)_2]^{2+}$, 274 $[Fe(bipy)_2(phen)]^{2+}$, 262 $[Fe(bipy)_3]^{2+}$, 208 $[Fe(phen)_2]^{2+}$ and 184 $[Fe(bipy)_2]^{2+}$. Note: *m/z* 321 $[Ru(phen)_3]^{2+}$ (2.0 μM internal standard). The *m/z* ranges 180–190 and 250–330 are magnified 40× for clarity.

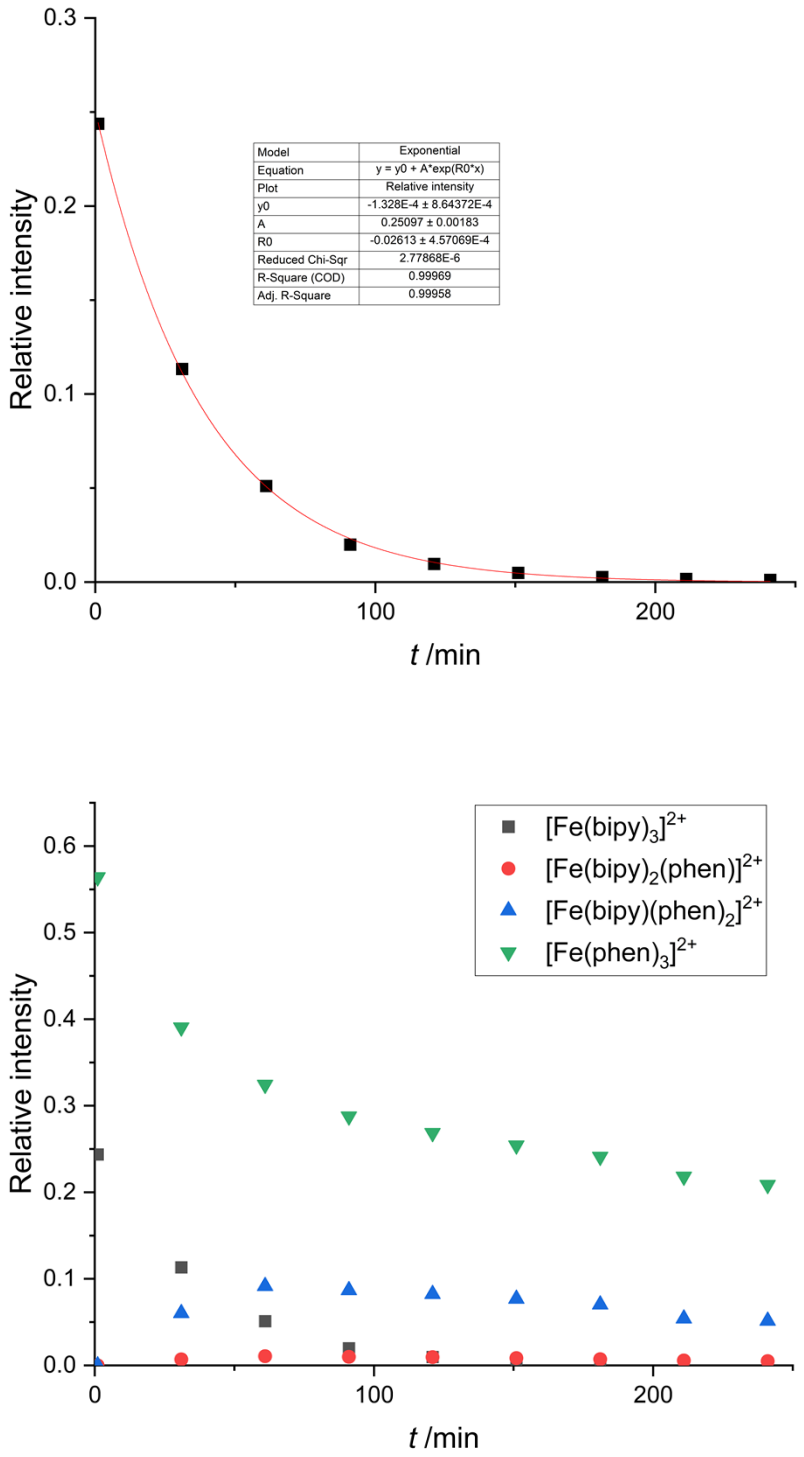

Figure S48. Time course of relative intensities of dicationic complexes relative to $[Ru(phen)_3]^{2+}$ (added added $[^nBu_4N]PF_6$, top). Exponential fit of relative $[Fe(bipy)_3]^{2+}$ intensity (bottom).

Ions derived from $[Fe(bipy^{Br})_3]^{2+}$

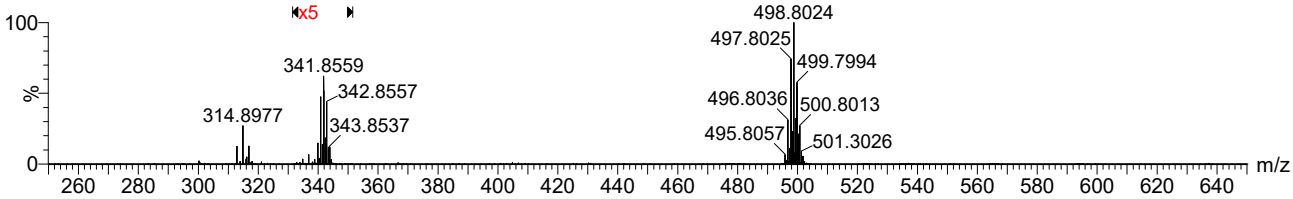

Figure S49. Positive-ion ESI-MS data for $[Fe(bipy^{Br})_3]Cl_2$ (10 μM) acquired at a capillary voltage of 1.52 kV. Major species: *m*/*z* 498 $[Fe(bipy^{Br})_3]^{2+}$ and 341 $[Fe(bipy^{Br})_2]^{2+}$.

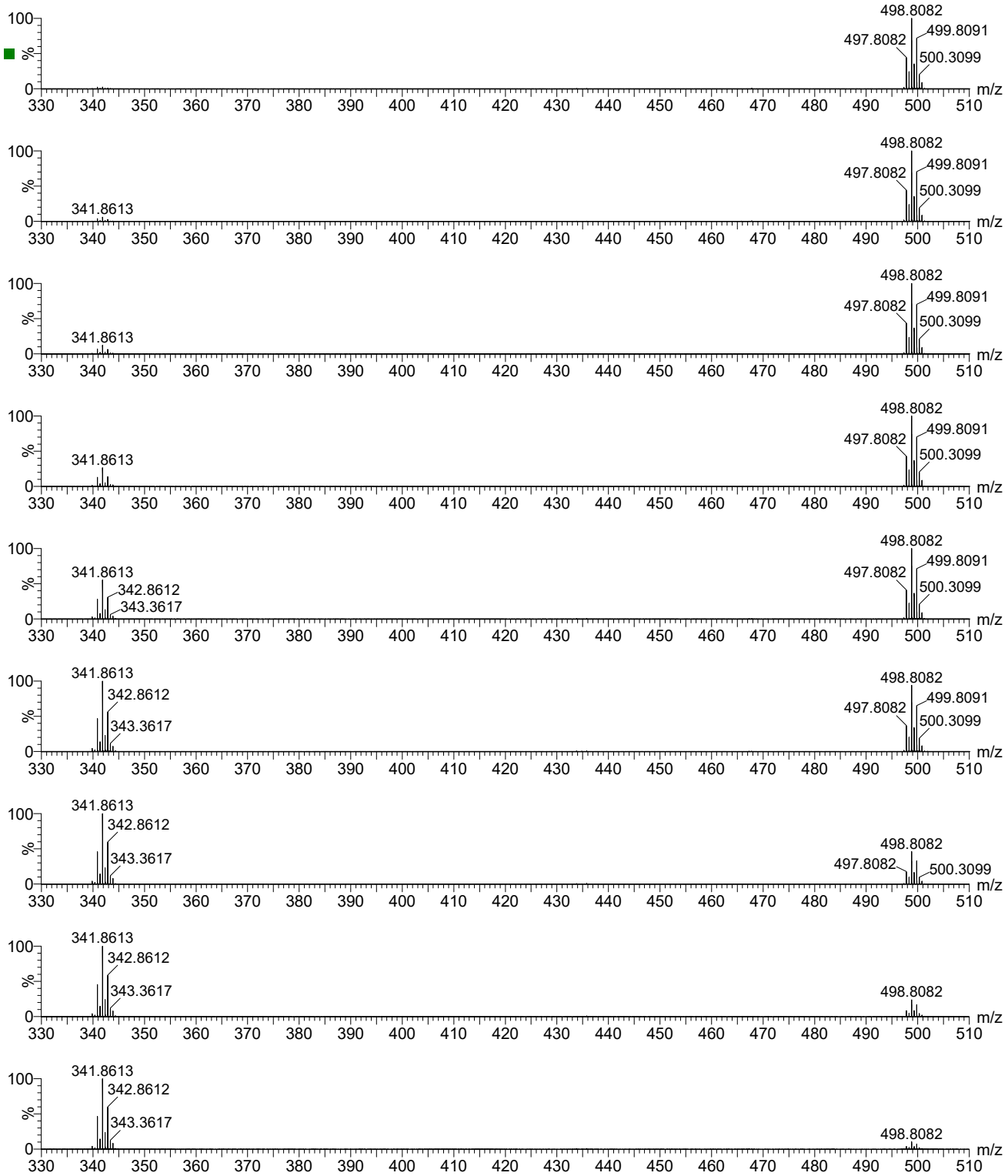

Figure S50. Positive-ion ESI-MS^2 data for the $[Fe(bipy^{Br})_3]^{2+}$ parent ion generated from $[Fe(bipy^{Br})_3]Cl_2$ (10 µM). Data were acquired at low-mass resolution of 4.5 and transfer collision energies of 0, 2, 4, 6, 8, 10, 12, 14 and 16 eV (top to bottom). Major species: *m*/*z* 498 $[Fe(bipy^{Br})_3]^{2+}$ and 341 $[Fe(bipy^{Br})_2]^{2+}$.

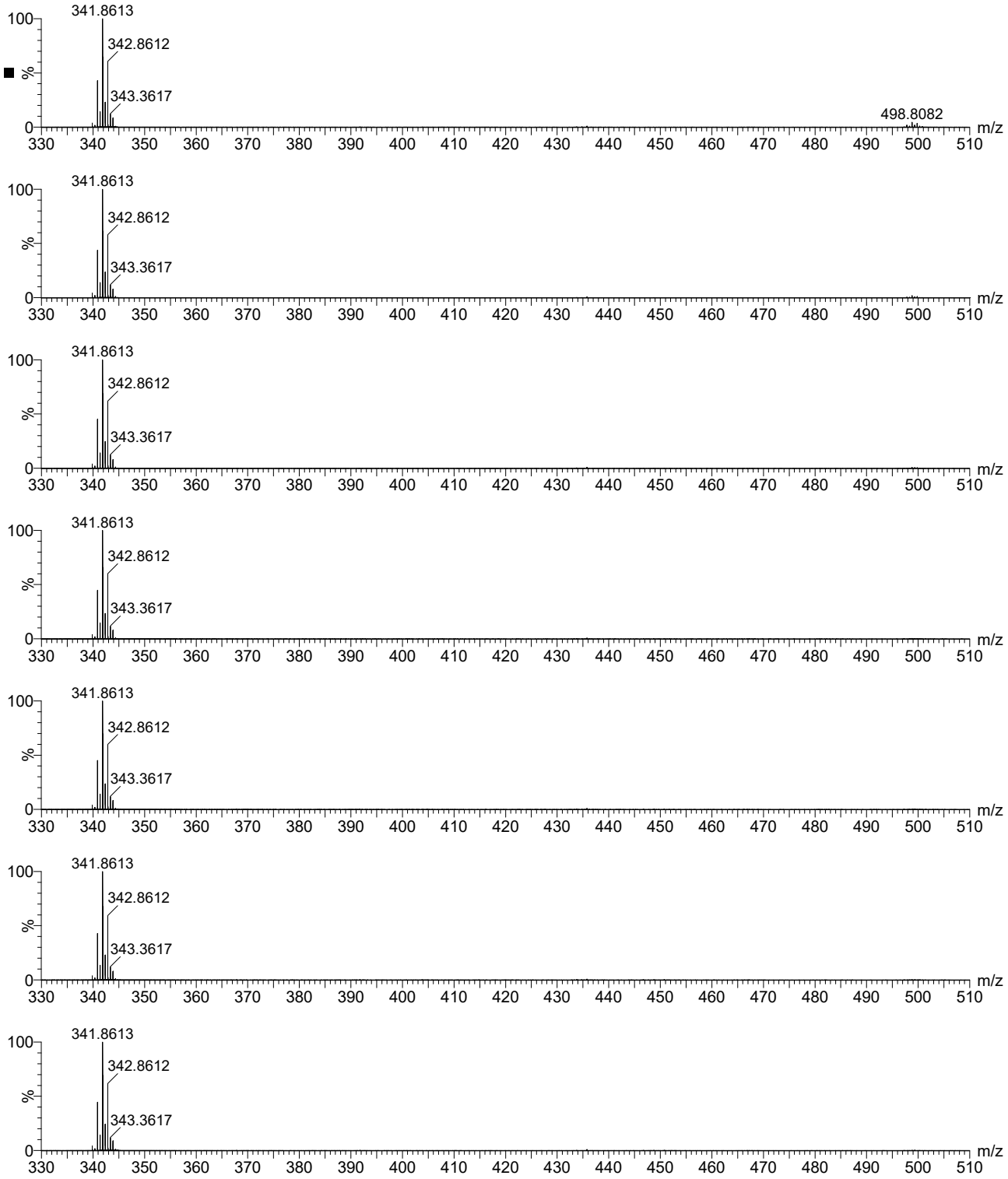

Figure S51. Positive-ion ESI-MS^2 data for the $[Fe(bipy^{Br})_3]^{2+}$ parent ion generated from $[Fe(bipy^{Br})_3]Cl_2$ (10 μM). Data were acquired at low-mass resolution of 4.5 and transfer collision energies of 18, 20, 22, 24, 26, 28, 30 eV (top to bottom). Major species: *m/z* 498 $[Fe(bipy^{Br})_3]^{2+}$ and 341 $[Fe(bipy^{Br})_2]^{2+}$.

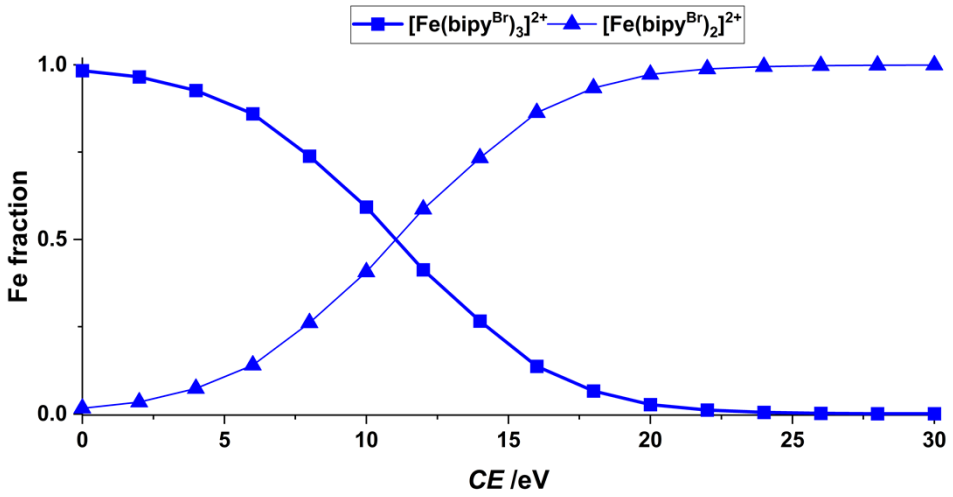

Figure S52. Breakdown curve for $[Fe(bipy^{Br})_3]^{2+}$.

Ions derived from $[Fe(bipy^{t\text{-}Bu})_3]^{2+}$

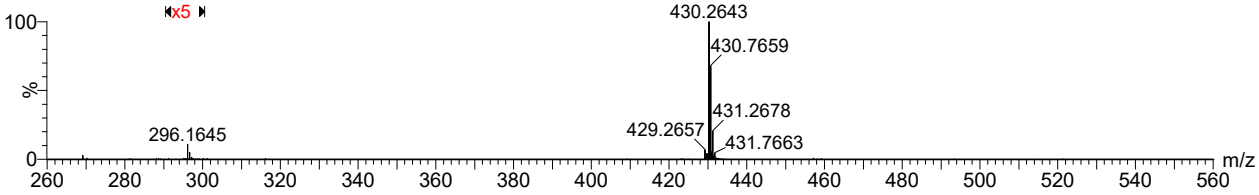

Figure S53. Positive-ion ESI-MS data for $[Fe(bipy^{t\text{-}Bu})_3]Cl_2$ (10 μM) acquired at a capillary voltage of 1.52 kV. Major species: *m*/*z* 430 $[Fe(bipy^{t\text{-}Bu})_3]^{2+}$ and 296 $[Fe(bipy^{t\text{-}Bu})_2]^{2+}$.

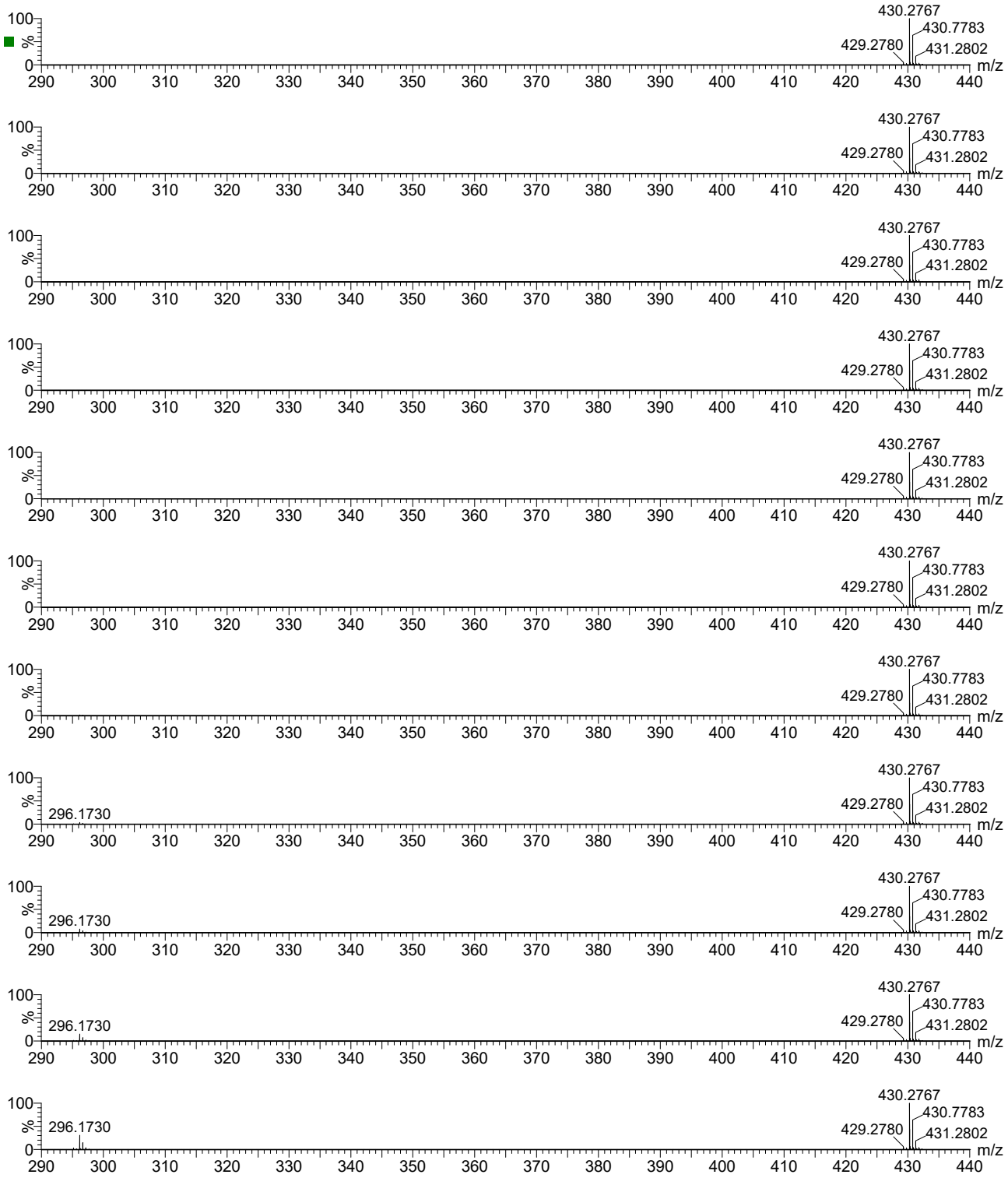

Figure S54. Positive-ion ESI-MS^2 data for the $[Fe(bipy^{t\text{-}Bu})_3]^{2+}$ parent ion generated from $[Fe(bipy^{t\text{-}Bu})_3]Cl_2$ (10 μM). Data were acquired at low-mass resolution of 4.5 and transfer collision energies of 0, 2, 4, 6, 8, 10, 12, 14, 16, 18, 20 eV (top to bottom). Major species: *m/z* 430 $[Fe(bipy^{t\text{-}Bu})_3]^{2+}$ and 296 $[Fe(bipy^{t\text{-}Bu})_2]^{2+}$.

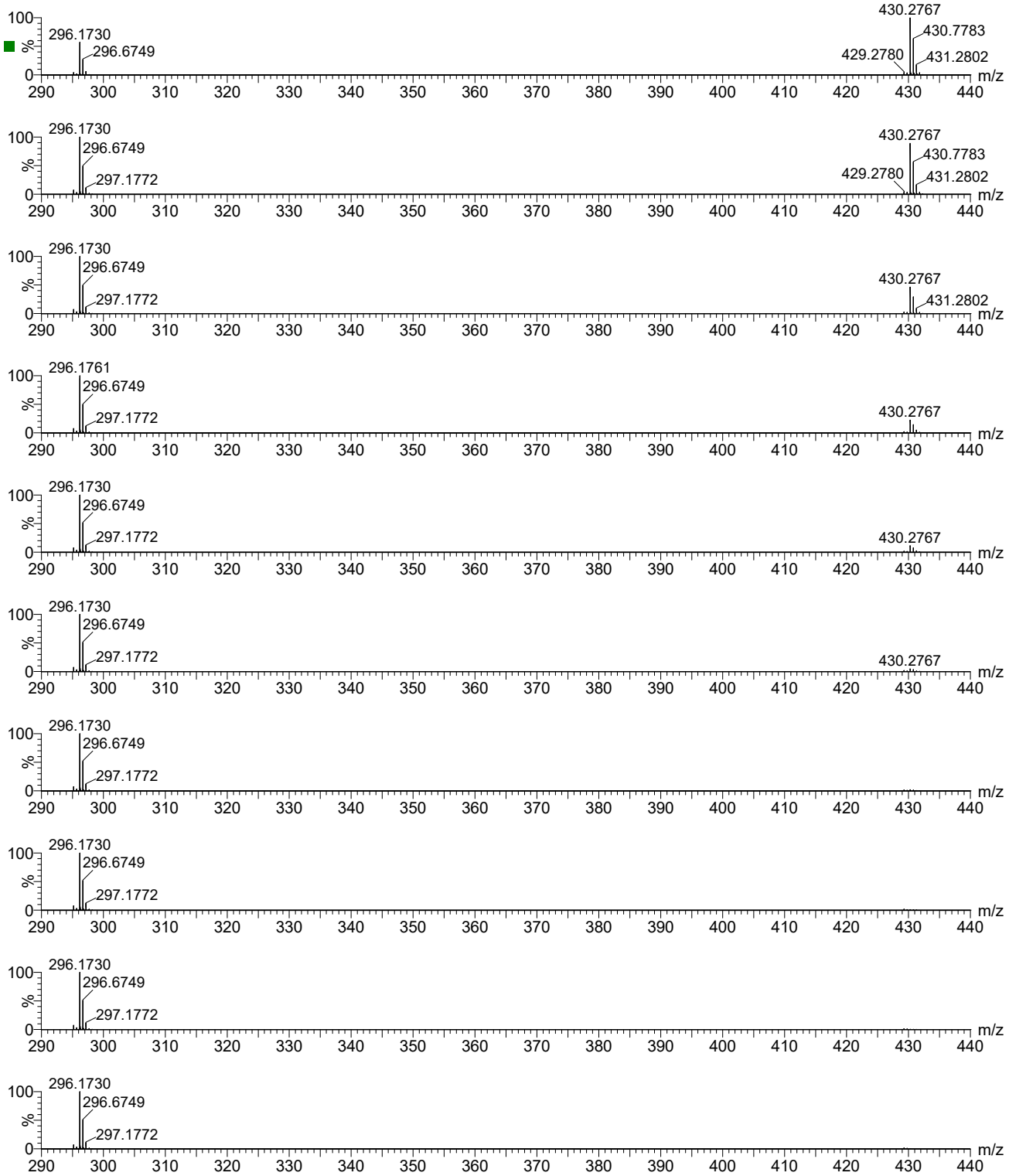

Figure S55. Positive-ion ESI-MS^2 data for the $[Fe(bipy^{t\text{-}Bu})_3]^{2+}$ parent ion generated from $[Fe(bipy^{t\text{-}Bu})_3]Cl_2$ (10 μM). Data were acquired at low-mass resolution of 4.5 and transfer collision energies of 22, 24, 26, 28, 30, 32, 34, 36, 38, 40 eV (top to bottom). Major species: *m/z* 430 $[Fe(bipy^{t\text{-}Bu})_3]^{2+}$ and 296 $[Fe(bipy^{t\text{-}Bu})_2]^{2+}$.

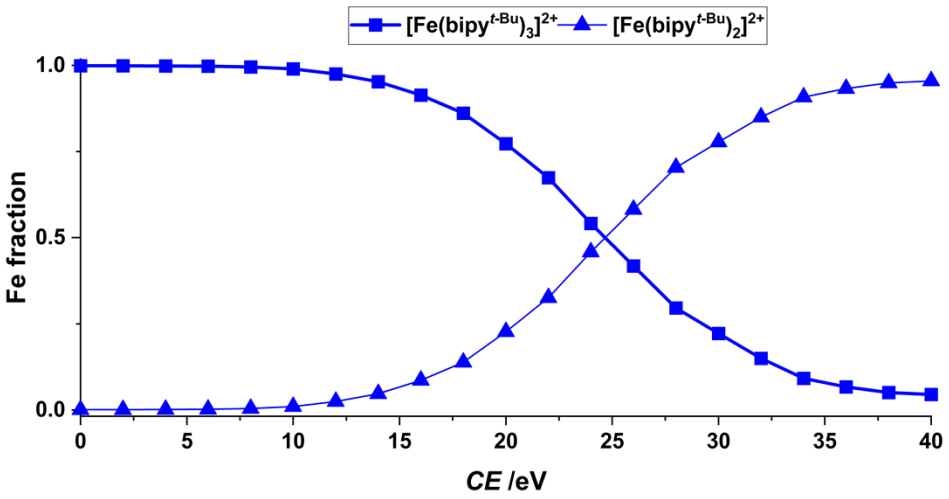

Figure S56. Breakdown curve for [Fe(bipy$^{t\text{-Bu}}$)$_3$]$^{2+}$.

Ions derived from $[Co(bipy)_3]^{2+}$

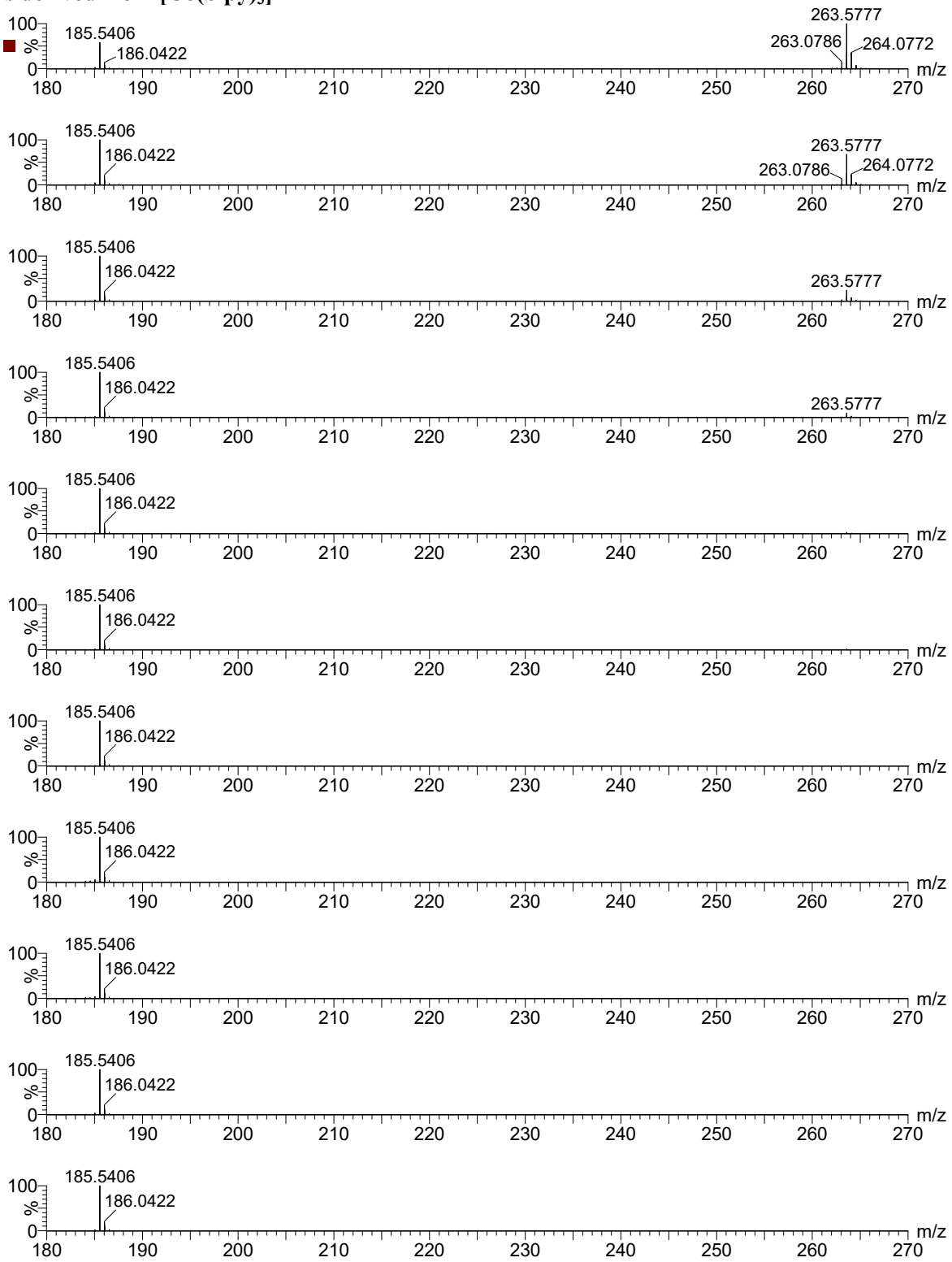

Figure S57. Positive-ion ESI-MS^2 data for the $[Co(bipy)_3]^{2+}$ parent ion generated from $[Co(bipy)_3](PF_6)_2$ (2.5 µM). Data were acquired at low-mass resolution of 5.5 and transfer collision energies of 0, 2, 4, 6, 8, 10, 12, 14, 16, 18 and 20 eV (top to bottom). Major Co species: *m/z* 263 $[Co(bipy)_3]^{2+}$ and 185 $[Co(bipy)_2]^{2+}$.

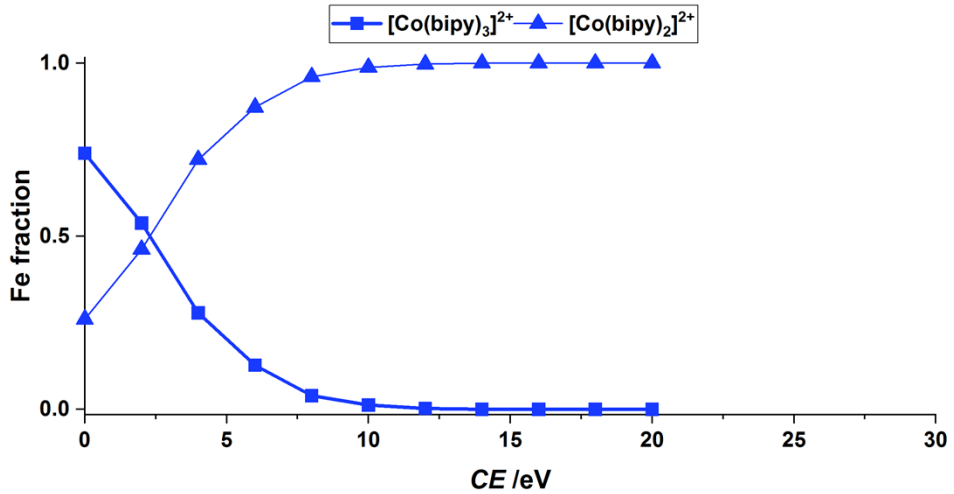

Figure S58. Breakdown curve for $[Co(bipy)_3]^{2+}$.

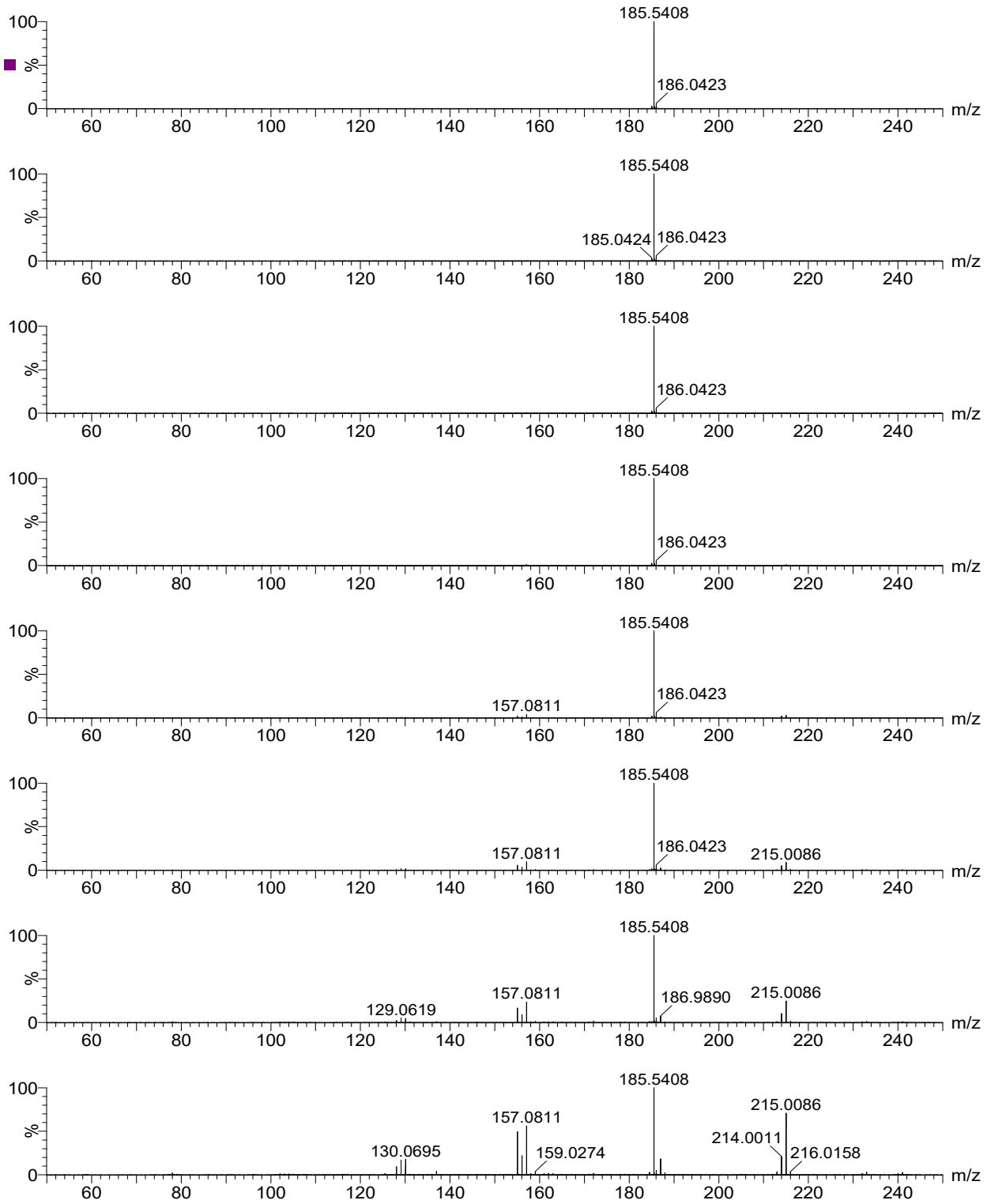

Figure S59. Positive-ion ESI-MS^2 data for the $[Co(bipy)_2]^{2+}$ parent ion generated from $[Co(bipy)_2]Cl_2$ (10 μM). Data were acquired at low-mass resolution of 15 and transfer collision energies of 0, 4, 8, 12, 16, 20, 24, 28 eV (top to bottom). Major species: *m/z* 215 $[Co(bipy)]^+$, 185 $[Co(bipy)_2]^{2+}$, 162 unknown fragment, 157 $[Hbipy]^+$, 155 $[bipy–H]^+$, 137 $[Co(C_5H_3N)]^+$, 128 $[bipy–NCH_2]^+$, 102 $[NC_7H_4]^+$ and 78 $[C_5H_3N]^+$.

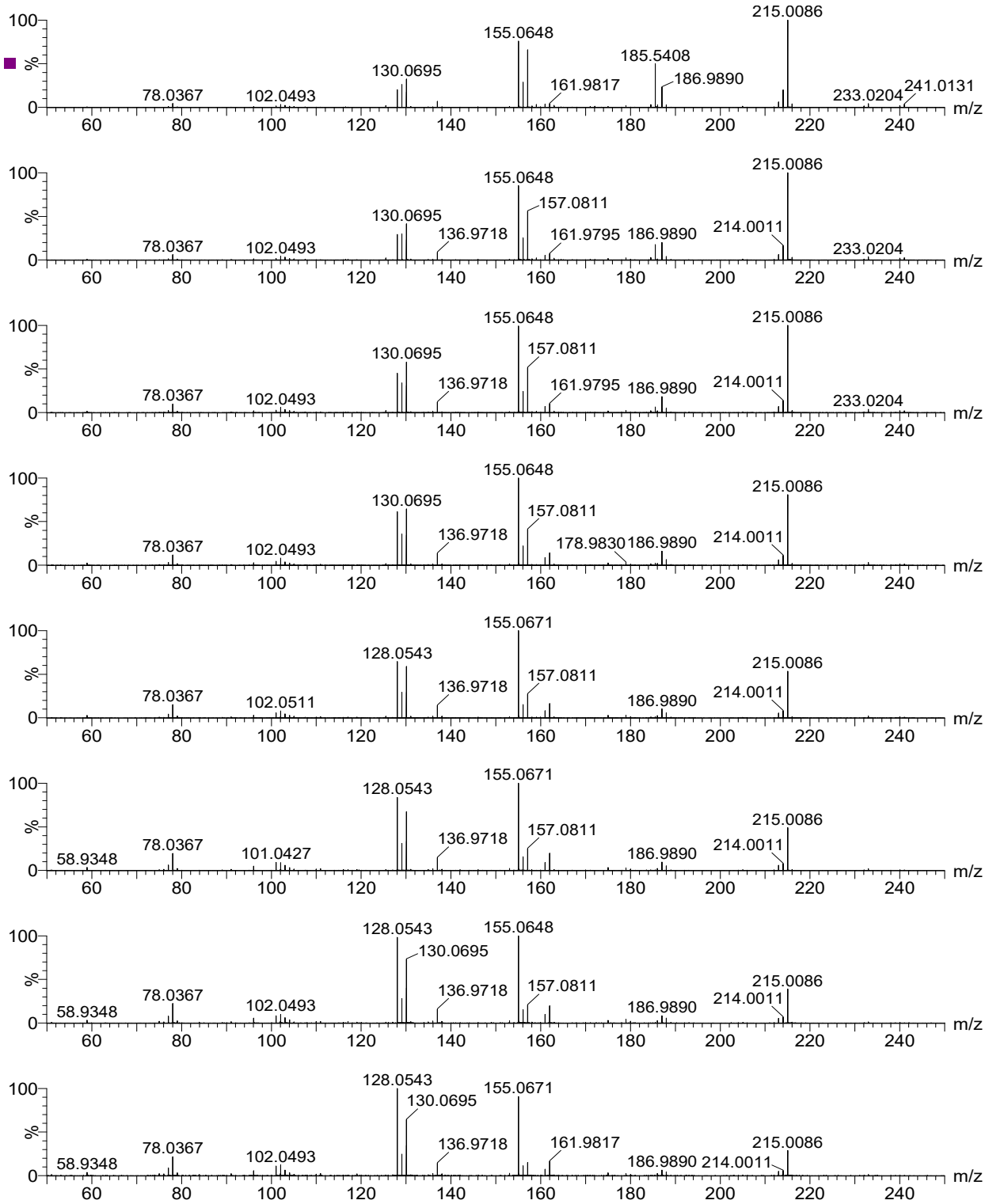

Figure S60. Positive-ion ESI-MS^2 data for the $[Co(bipy)_2]^{2+}$ parent ion generated from $[Co(bipy)_2]Cl_2$ (10 μM) acquired at low-mass resolution of 15 and transfer collision energies of 32, 36, 40, 44, 48, 52, 56, 60 eV (top to bottom). Major species: *m/z* 215 $[Co(bipy)]^+$, 185 $[Co(bipy)_2]^{2+}$, 162 unknown fragment, 157 $[Hbipy]^+$, 155 $[bipy–H]^+$, 137 $[Co(C_5H_3N)]^+$, 128 $[bipy–NCH_2]^+$, 102 $[NC_7H_4]^+$ and 78 $[C_5H_3N]^+$.

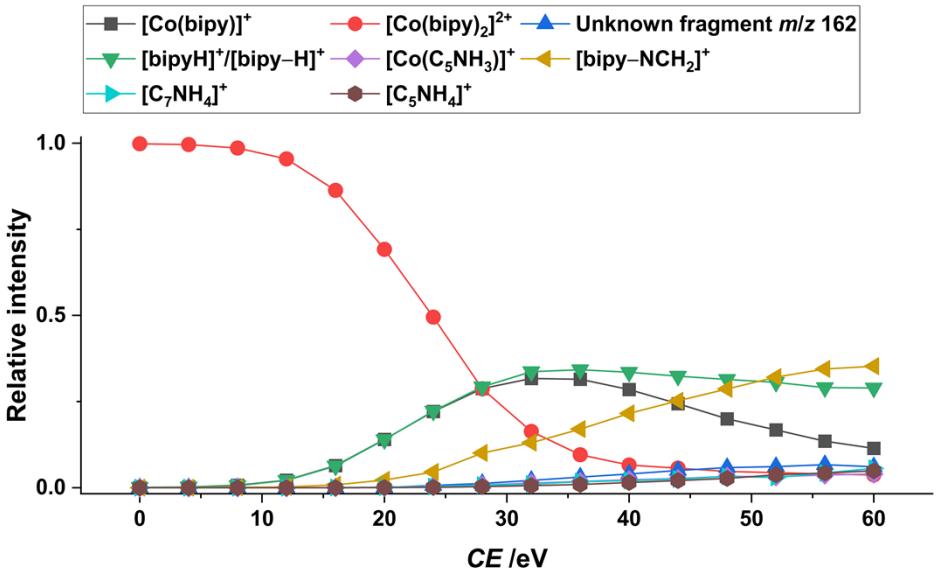

Figure S61. Breakdown curve for $[Co(bipy)_2]^{2+}$.

Ion-mobility data for diimine complexes

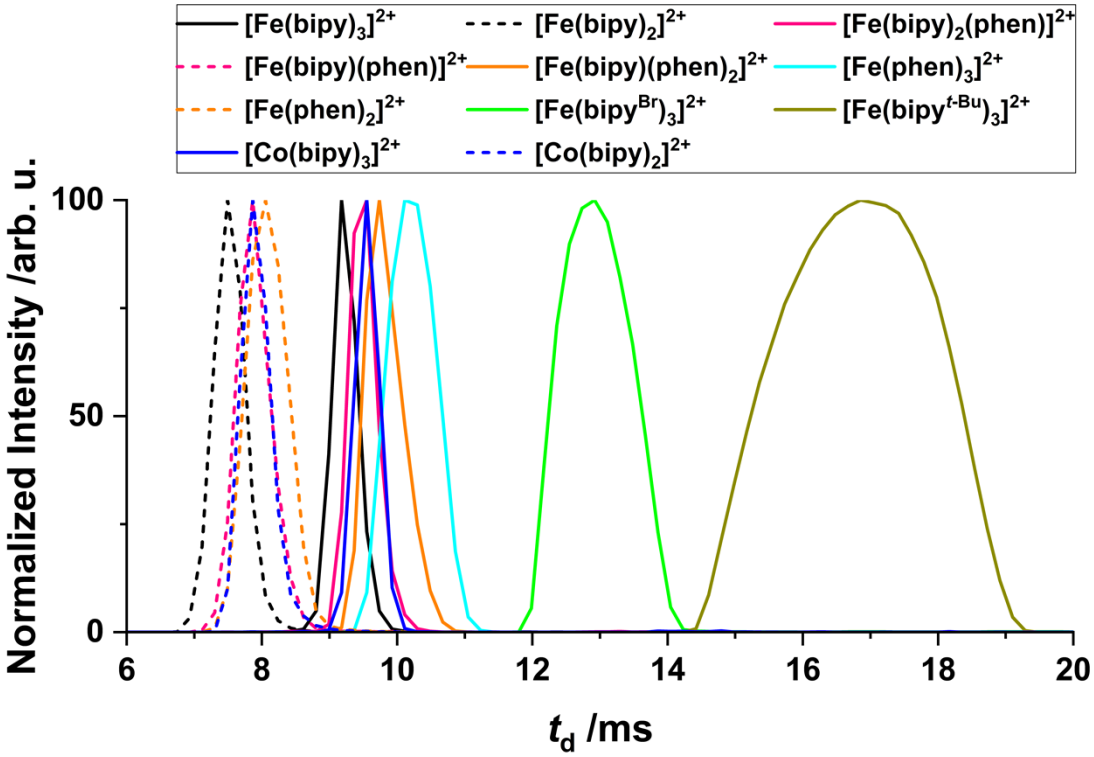

Figure S62. Mobilograms of diimine complexes.

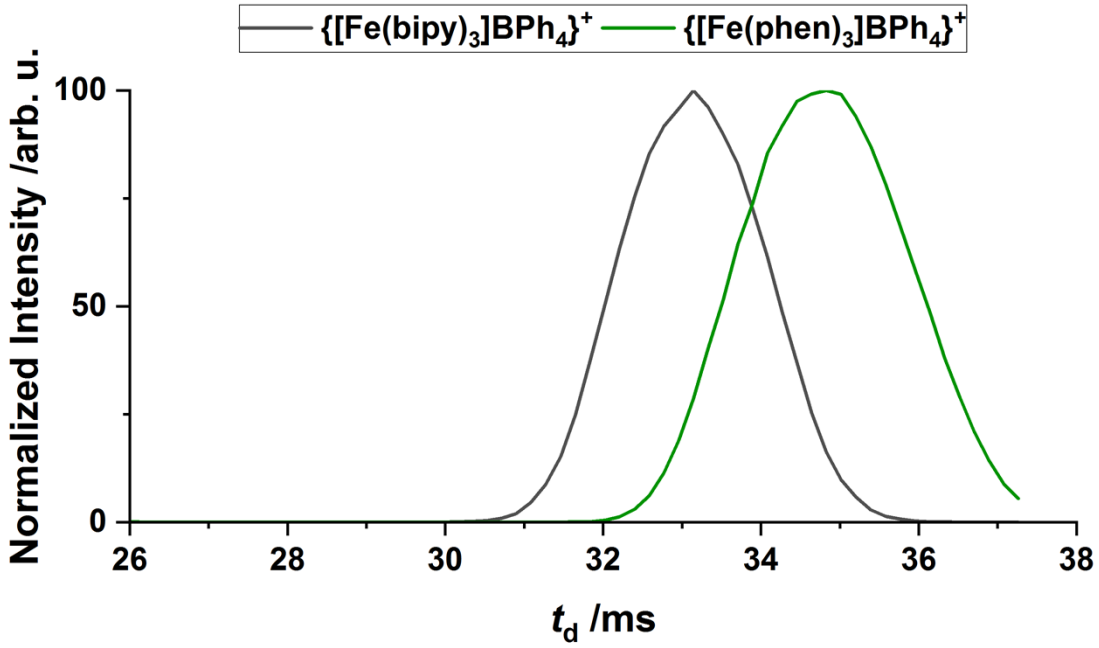

Figure S63. Mobilograms of ion pairs.

DFT calculations

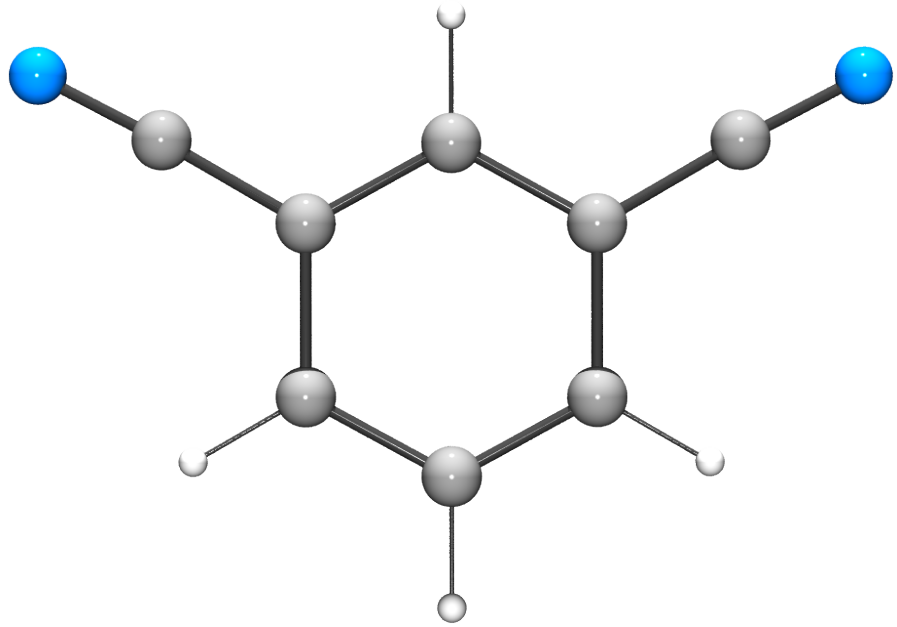

Figure S64. Optimized structure of [1,3-dicycanobenzene]$^{-}$.

Table S3. Atomic coordinates for [1,3-dicycanobenzene]$^{-}$.

Atom	*x*	*y*	*z*
N	-3.50024	-1.29808	0.000182
N	3.500333	-1.29798	0.000114
C	-1.23017	-0.04328	0.000247
C	1.230323	-0.04322	0.000161
C	-4.5E-05	-0.72507	0.000489
C	-1.22474	1.416246	-0.00011
C	1.224427	1.416481	-0.00035
C	-3.9E-05	2.08178	-0.00045
C	-2.44916	-0.75028	0.000292
C	2.449442	-0.75001	0.000218
H	8.11E-05	-1.81634	0.001023
H	-2.16806	1.960451	-0.00017
H	2.167848	1.960736	-0.00087
H	-2.7E-05	3.175883	-0.00092

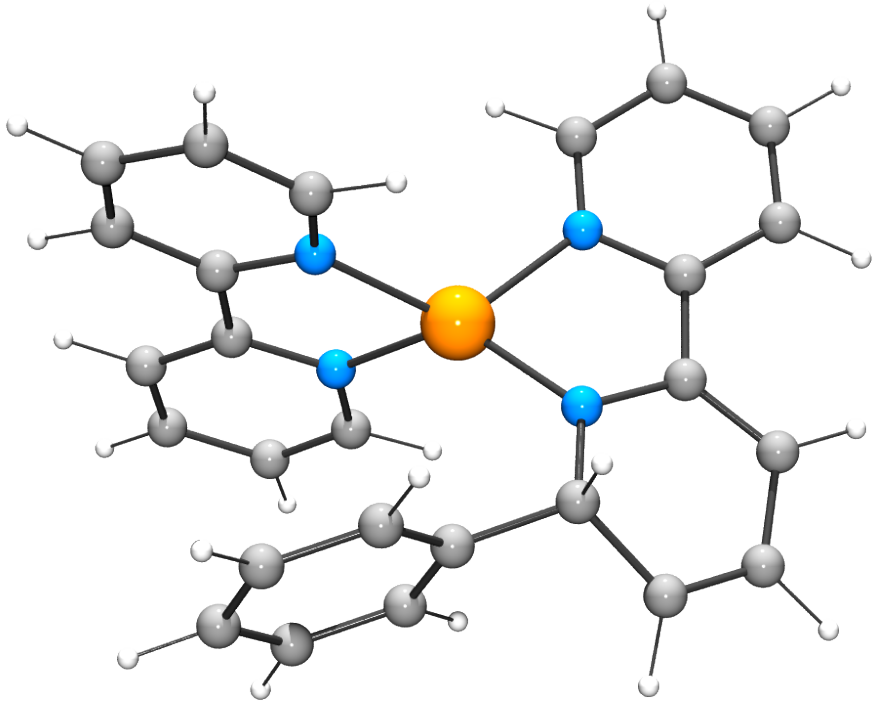

Figure S65. Optimized structure of high-spin $[Fe(bipy)(bipyPh)]^{+}$.

Table S4. Atomic coordinates for high-spin $[Fe(bipy)(bipyPh)]^+$.

Atom	*x*	*y*	*z*
Fe	-0.09365	0.465842	-0.92291
N	1.642007	0.916361	-1.94691
N	0.936475	-1.0118	-0.29541
C	2.576912	-0.07126	-1.76343
C	1.971625	2.020532	-2.65803
C	2.135213	-1.2105	-0.94178
C	0.558357	-1.97287	0.767434
C	3.860833	0.061496	-2.31011
C	3.235179	2.212839	-3.19667
H	1.180286	2.759692	-2.78859
C	2.806608	-2.41911	-0.89942
C	1.032215	-3.37062	0.445872
H	1.065828	-1.6475	1.703734
C	4.195794	1.209284	-3.01828
H	4.598196	-0.72361	-2.15431
H	3.460382	3.124897	-3.74661
C	2.155263	-3.54283	-0.2915
H	3.748955	-2.55431	-1.42467
H	0.489563	-4.21294	0.875326
H	5.200903	1.327757	-3.42287
H	2.555542	-4.54279	-0.46358
N	-1.19646	1.840931	0.165841
C	-2.42263	2.142224	-0.35547
C	-3.25649	3.072674	0.27761
C	-2.84131	3.681706	1.458563
C	-1.59398	3.349502	1.995636
C	-0.8064	2.42855	1.317826
H	-4.22707	3.322449	-0.14709
H	-3.48436	4.40624	1.956657
H	-1.23343	3.797849	2.920444
H	0.177211	2.140354	1.691339
N	-1.82723	0.551207	-2.05147
C	-2.78695	1.404055	-1.57889
C	-2.11119	-0.19865	-3.14241
C	-4.02868	1.520696	-2.21585
C	-3.33193	-0.14418	-3.80175
H	-1.31358	-0.8573	-3.48802
C	-4.30869	0.740231	-3.33374
H	-4.78029	2.209922	-1.83573
H	-3.50668	-0.77541	-4.67185

H	-5.27352	0.819883	-3.83317
C	-0.93638	-1.87238	1.023125
C	-1.41891	-1.30593	2.209291
C	-1.85586	-2.33981	0.070978
C	-2.79308	-1.1995	2.439141
C	-3.22963	-2.23503	0.2975
H	-0.70949	-0.95866	2.963846
C	-3.70103	-1.6612	1.482544
H	-3.15538	-0.7693	3.373382
H	-3.93397	-2.62026	-0.44107
H	-4.77363	-1.59248	1.667996
H	-1.48702	-2.80548	-0.84508

Table S5. Atomic coordinates for high-spin $[Fe(bipy)(BPh_4)]^+$ with two η^1-Ph rings.

Atom	*x*	*y*	*z*
Fe	3.425452	-0.55564	0.186274
N	4.929543	-1.02092	-1.21037
N	5.17668	-0.65282	1.38199
C	6.201713	-1.11157	-0.73428
C	4.718423	-1.17071	-2.53352
C	6.337856	-0.92258	0.726743
C	5.204711	-0.4785	2.717567
C	7.280941	-1.3606	-1.58938
C	5.746722	-1.40456	-3.44004
H	3.682797	-1.09413	-2.86461
C	7.555091	-1.00664	1.412029
C	6.379575	-0.55174	3.460101
H	4.245019	-0.27228	3.191884
C	7.051724	-1.50298	-2.95633
H	8.294136	-1.43597	-1.19932
H	5.522686	-1.50487	-4.50126
C	7.575888	-0.81588	2.791564
H	8.480817	-1.21745	0.880086
H	6.351738	-0.40259	4.53874
H	7.883634	-1.68744	-3.63624
H	8.516661	-0.87261	3.339121
B	0.794036	-0.10218	0.196033
C	2.040896	1.026445	0.120973
C	-0.17918	0.1886	1.47759
C	-0.12839	-0.07996	-1.14863
C	1.59521	-1.57182	0.378237
C	2.590473	1.633398	1.292755
C	-0.51897	1.503858	1.855392
C	-0.39274	1.110468	-1.85731
C	2.041617	-2.0162	1.662404
C	2.661531	1.392687	-1.11465
C	-0.85908	-0.84776	2.148019
C	-0.84932	-1.22036	-1.56083
C	1.93487	-2.41626	-0.72302
C	3.613196	2.586845	1.225695
C	-1.46047	1.771721	2.852961
C	-1.29031	1.155617	-2.92828
C	2.693907	-3.2446	1.838615
C	3.690292	2.345347	-1.17731
C	-1.80453	-0.59232	3.145864

C	-1.74826	-1.18931	-2.6298
C	2.591413	-3.64073	-0.54381
C	4.163629	2.949486	-0.00906
C	-2.10547	0.721921	3.510375
C	-1.96535	0.000627	-3.32875
C	2.966134	-4.06202	0.737325
H	2.140073	1.395734	2.258159
H	-0.05705	2.350308	1.341276
H	0.089522	2.041758	-1.55067
H	1.778542	-1.41715	2.536557
H	2.251681	0.986665	-2.0412
H	-0.67132	-1.88781	1.870248
H	-0.73409	-2.15962	-1.01438
H	1.600355	-2.12631	-1.72065
H	3.971075	3.062375	2.140402
H	-1.69884	2.805877	3.108359
H	-1.47222	2.100353	-3.44336
H	2.972942	-3.57112	2.841584
H	4.104376	2.632973	-2.14516
H	-2.31376	-1.42485	3.634819
H	-2.29129	-2.09388	-2.90891
H	2.79732	-4.27802	-1.40541
H	4.94716	3.706181	-0.06022
H	-2.84393	0.926055	4.286635
H	-2.66619	0.031071	-4.16361
H	3.461466	-5.02352	0.876828

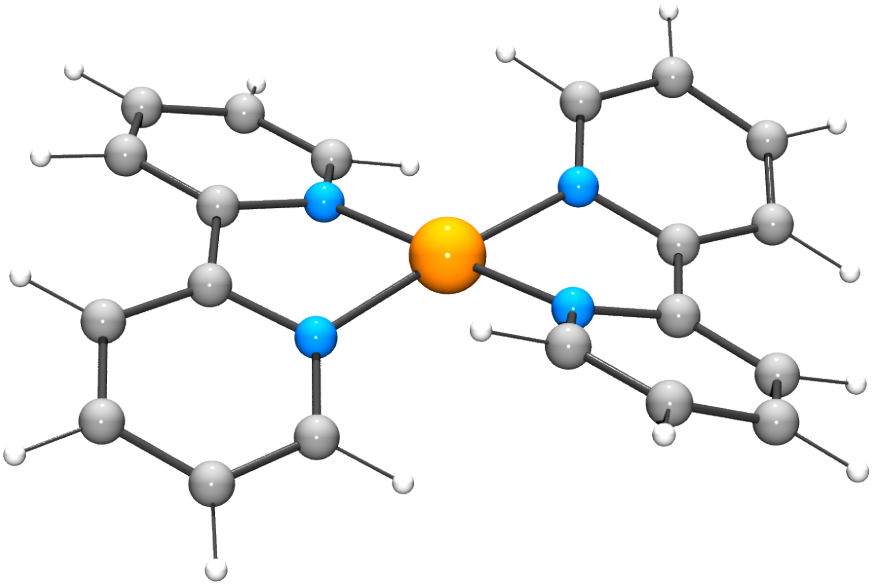

Figure S66. Optimized structure of low-spin distorted-square-planar $[Fe(bipy)_2]^{2+}$.

Table S6. Atomic coordinates for low-spin distorted-square-planar $[Fe(bipy)_2]^{2+}$.

Atom	*x*	*y*	*z*
Fe	0.000207	0.278454	-0.09015
N	1.55312	-0.01076	1.096713
N	0.746045	-1.31201	-0.94064
C	2.549421	-0.73102	0.478531
C	1.78739	0.4571	2.345693
C	2.082216	-1.49358	-0.67957
C	0.127315	-2.19386	-1.76652
C	3.820548	-0.84379	1.041816
C	3.020966	0.335838	2.97379
H	0.946912	0.918654	2.857314
C	2.829695	-2.4553	-1.36398
C	0.811538	-3.20324	-2.4317
H	-0.94808	-2.0836	-1.88223
C	4.068228	-0.28929	2.295711
H	4.603406	-1.39353	0.523114
H	3.147976	0.721597	3.984068
C	2.193291	-3.31147	-2.26055
H	3.896019	-2.56129	-1.17315
H	0.261491	-3.88805	-3.07656
H	5.051949	-0.38165	2.754993
H	2.759608	-4.07667	-2.79194
N	-0.85783	1.801859	0.805178
C	-2.20139	1.87418	0.509698
C	-3.05449	2.722358	1.218236
C	-2.52197	3.585377	2.174617
C	-1.14019	3.605377	2.375544
C	-0.3482	2.699501	1.682124
H	-4.12092	2.740148	0.997751
H	-3.17217	4.265218	2.724306
H	-0.67298	4.313265	3.058664
H	0.731877	2.698444	1.80461
N	-1.4798	0.566389	-1.32441
C	-2.56048	1.160534	-0.71855
C	-1.58936	0.197489	-2.62471
C	-3.80423	1.208958	-1.3511
C	-2.78429	0.291262	-3.3273
H	-0.68556	-0.17273	-3.10483
C	-3.92283	0.75449	-2.66359
H	-4.66747	1.627887	-0.83663
H	-2.8178	-0.00325	-4.37519
H	-4.88498	0.79763	-3.17378

Table S7. Atomic coordinates for high-spin tetrahedral $[Fe(bipy)_2]^{2+}$.

Atom	*x*	*y*	*z*
Fe	-7.1E-05	0.647337	-0.36807
N	1.85595	1.018143	-1.11683
N	0.943123	-1.10331	0.186126
C	2.769128	0.020375	-0.91379
C	2.22895	2.144958	-1.76403
C	2.258494	-1.16659	-0.18855
C	0.395722	-2.14226	0.856539
C	4.082228	0.159066	-1.36869
C	3.522397	2.335723	-2.23652
H	1.459101	2.905382	-1.90113
C	3.037121	-2.28528	0.117575
C	1.124925	-3.27877	1.193158
H	-0.65451	-2.04719	1.134097
C	4.462706	1.324896	-2.03427
H	4.811954	-0.63183	-1.20694
H	3.781893	3.261445	-2.74849
C	2.467922	-3.34799	0.820126
H	4.083282	-2.33363	-0.18007
H	0.645087	-4.08958	1.74006
H	5.488025	1.44313	-2.38562
H	3.068837	-4.2227	1.069227
N	-1.05913	1.948538	0.810592
C	-2.32768	2.198096	0.360791
C	-3.16104	3.086118	1.042893
C	-2.69594	3.724761	2.193496
C	-1.40125	3.466207	2.643083
C	-0.61466	2.571377	1.925482
H	-4.17035	3.284221	0.68753
H	-3.34092	4.419758	2.730971
H	-1.00086	3.9457	3.535268
H	0.402755	2.337963	2.240229
N	-1.7641	0.647465	-1.39248
C	-2.72428	1.467365	-0.86707
C	-2.03229	-0.06584	-2.50948
C	-3.97563	1.575536	-1.47899
C	-3.25855	0.005759	-3.16052
H	-1.23146	-0.70508	-2.88317
C	-4.24481	0.841839	-2.63549
H	-4.74201	2.228174	-1.06513
H	-3.42921	-0.58156	-4.06182
H	-5.21506	0.927143	-3.12424

Table S8. Atomic coordinates for high-spin trigonal-bipyramidal $[Fe(bipy)_2Cl]^+$.

Atom	*x*	*y*	*z*
Fe	0.000583	0.648954	-0.37056
N	-1.10863	2.135114	0.647586
C	-2.41892	2.21867	0.280811
C	-3.32909	2.975216	1.029971
C	-2.88492	3.672365	2.149981
C	-1.53883	3.591859	2.512235
C	-0.69164	2.805155	1.740844
H	-4.37727	3.028727	0.742085
H	-3.58232	4.269665	2.736816
H	-1.15101	4.118844	3.382701
H	0.36298	2.697766	1.99732
N	-1.7628	0.833973	-1.57261
C	-2.78339	1.490536	-0.95538
C	-2.00123	0.181802	-2.72471
C	-4.07734	1.473933	-1.49127
C	-3.25754	0.145559	-3.32246
H	-1.14766	-0.33343	-3.16674
C	-4.3149	0.79551	-2.68457
H	-4.89729	1.981576	-0.98731
H	-3.40195	-0.39103	-4.25869
H	-5.31731	0.772145	-3.11198
Cl	-0.70882	-1.14081	0.726221
N	1.019037	2.225777	-1.57197
N	1.958501	-0.10689	-0.83073
C	2.3212	2.00707	-1.89569
C	0.443352	3.380705	-1.96272
C	2.857292	0.706404	-1.45694
C	2.383198	-1.31552	-0.39323
C	3.067444	2.961607	-2.60125
C	1.116691	4.360692	-2.68228
H	-0.60093	3.513867	-1.67915
C	4.185625	0.310593	-1.65632
C	3.689776	-1.76285	-0.55673
H	1.624218	-1.91944	0.104343
C	2.461844	4.149295	-2.99774
H	4.112714	2.779066	-2.84369
H	0.600934	5.273484	-2.97765
C	4.609781	-0.93424	-1.20111
H	4.889571	0.971191	-2.15881
H	3.973193	-2.74408	-0.17792

H	3.031331	4.899911	-3.54621
H	5.642988	-1.24999	-1.34377

Table S9. Atomic coordinates for low-spin *cis*-[Fe(bipy)$_2$Cl$_2$].

Atom	*x*	*y*	*z*
Fe	-0.18282	-0.18367	-0.00085
N	-0.75181	1.646158	1.131942
C	-0.41294	2.88044	0.662683
C	-0.90483	4.049799	1.26592
C	-1.75794	3.955701	2.358904
C	-2.11051	2.685753	2.830108
C	-1.59238	1.5678	2.187607
H	-0.6295	5.026912	0.87285
H	-2.14993	4.856429	2.83154
H	-2.77594	2.557522	3.683464
H	-1.82871	0.548144	2.501871
N	1.845293	-0.25965	1.032876
Cl	-0.99344	-1.60653	1.598776
N	0.741709	1.655893	-1.02818
Cl	-1.81071	-0.16583	-1.60276
N	1.107498	-1.57845	-1.11176
C	0.453864	2.884138	-0.52526
C	2.788347	-1.09439	0.523007
C	2.136077	0.430316	2.150462
C	1.459853	1.579202	-2.16226
C	2.357606	-1.87005	-0.64445
C	0.627736	-2.30585	-2.14587
C	0.928754	4.055545	-1.14023
C	4.060161	-1.2074	1.113124
C	3.361165	0.350955	2.800998
H	1.337192	1.066924	2.530916
C	1.942157	2.693842	-2.83944
H	1.644184	0.570601	-2.53374
C	3.141718	-2.87679	-1.23055
C	1.355069	-3.31146	-2.77038
H	-0.38099	-2.02941	-2.45971
C	1.679565	3.96137	-2.30546
H	0.708636	5.033649	-0.71483
C	4.350363	-0.47982	2.259633
H	4.814077	-1.86528	0.683324
H	3.534359	0.923917	3.711522
H	2.51198	2.569892	-3.75997
C	2.643624	-3.602	-2.30529
H	4.132362	-3.09893	-0.83719

H	0.915434	-3.85382	-3.60668
H	2.053425	4.860885	-2.7949
H	5.32889	-0.56305	2.732733
H	3.243524	-4.38512	-2.7692

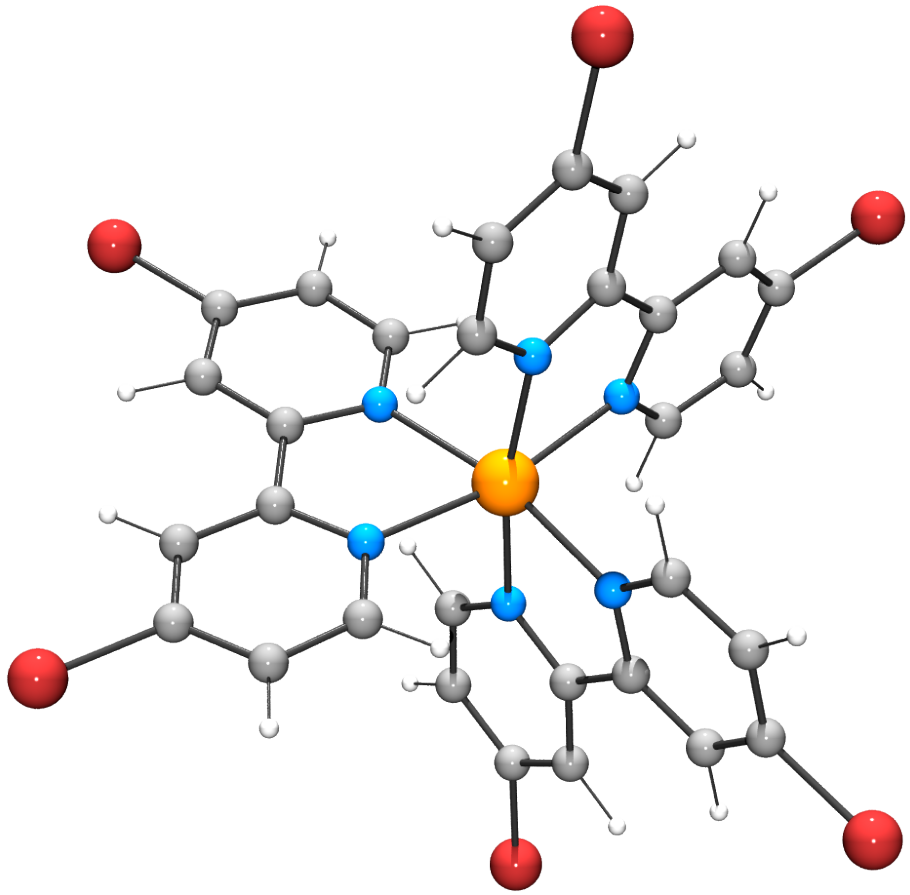

Figure S67. Optimized structure of high-spin $[Fe(bipy^{Br})_3]^{2+}$.

Table S10. Atomic coordinates for high-spin $[Fe(bipy^{Br})_3]^{2+}$.

Atom	*x*	*y*	*z*
Fe	8.18E-05	0.001563	6.82E-05
N	-0.73713	1.753559	1.116386
C	-0.44274	2.977661	0.598431
C	-0.93702	4.152759	1.173729
C	-1.73956	4.06981	2.3154
C	-2.03715	2.813843	2.854419
C	-1.51992	1.694293	2.214535
H	-0.71485	5.12765	0.746696
Br	-2.40929	5.639179	3.115256
H	-2.65602	2.708115	3.743777
H	-1.73585	0.696212	2.595943
N	1.847758	-0.19325	1.114155
N	-1.11143	-1.48298	1.103207
N	0.737143	1.754743	-1.11719
N	-1.84747	-0.19516	-1.11394
N	1.111188	-1.48175	-1.10119
C	0.42839	2.978593	-0.60742
C	2.758219	-1.07783	0.613189
C	2.199089	0.549151	2.188509
C	-2.32185	-1.84122	0.582103
C	-0.67545	-2.13836	2.203345
C	1.526546	1.696976	-2.21067
C	-2.75797	-1.07896	-0.6113
C	-2.19725	0.542889	-2.19161
C	2.320881	-1.84117	-0.57907
C	0.672598	-2.13908	-2.19881
C	0.910046	4.155397	-1.18932
C	4.02205	-1.22757	1.194646
C	3.429642	0.453575	2.820727
H	1.446789	1.247019	2.555253
C	-3.09102	-2.86144	1.15125
C	-1.39004	-3.14674	2.835663
H	0.298686	-1.83501	2.587363
C	2.03183	2.818497	-2.85673
H	1.756929	0.69863	-2.58342
C	-4.02306	-1.22697	-1.19097
C	-3.42781	0.446342	-2.82453
H	-1.44406	1.238964	-2.56015
C	3.088176	-2.86416	-1.14597
C	1.384003	-3.15168	-2.82699

H	-0.30065	-1.8328	-2.58347
C	1.714015	4.074431	-2.32978
H	0.674557	5.13061	-0.77057
C	4.358368	-0.46227	2.313108
H	4.74991	-1.92537	0.787584
H	3.655842	1.0732	3.686463
C	-2.62368	-3.51932	2.290725
H	-4.04448	-3.15413	0.71819
H	-0.98901	-3.63548	3.72197
H	2.654944	2.713912	-3.7431
C	-4.35864	-0.46393	-2.31117
H	-4.75229	-1.92069	-0.7796
H	-3.65229	1.061083	-3.6944
C	2.617805	-3.52435	-2.28257
H	4.041523	-3.15636	-0.71255
H	0.980566	-3.64394	-3.7101
Br	2.362598	5.646593	-3.14175
Br	6.046874	-0.66017	3.127625
Br	-3.64113	-4.90036	3.075692
Br	3.629667	-4.90945	-3.06601
Br	-6.0497	-0.65986	-3.12112

Table S11. Atomic coordinates for high-spin $[Fe(bipy)_3]^{2+}$.

Atom	*x*	*y*	*z*
Fe	-0.0001	0.001387	5.59E-06
N	-0.73993	1.754937	1.118182
C	-0.43541	2.977018	0.602843
C	-0.90978	4.152527	1.199822
C	-1.69524	4.074126	2.347657
C	-2.00348	2.819081	2.873163
C	-1.5116	1.691043	2.222909
H	-0.67349	5.127207	0.778069
H	-2.06341	4.983158	2.823392
H	-2.61453	2.711732	3.768495
H	-1.73516	0.690694	2.593296
N	1.850781	-0.20348	1.113983
N	-1.10302	-1.48504	1.10985
N	0.736908	1.756149	-1.11915
N	-1.8501	-0.20219	-1.11266
N	1.104432	-1.48478	-1.10991
C	0.420863	2.977705	-0.6094
C	2.745758	-1.10293	0.612027
C	2.202457	0.53033	2.192999
C	-2.30846	-1.85136	0.585187
C	-0.66174	-2.12548	2.216794
C	1.517206	1.692846	-2.21799
C	-2.74515	-1.10215	-0.61034
C	-2.20076	0.524543	-2.19759
C	2.307749	-1.85441	-0.58306
C	0.663853	-2.12186	-2.21836
C	0.890875	4.153889	-1.20786
C	4.005964	-1.2688	1.201646
C	3.433454	0.4074	2.825537
H	1.454916	1.235973	2.555134
C	-3.06811	-2.87635	1.164761
C	-1.37737	-3.13538	2.849593
H	0.308221	-1.80738	2.598176
C	2.007697	2.821804	-2.86772
H	1.748166	0.692515	-2.58375
C	-4.00328	-1.27329	-1.20307
C	-3.42885	0.394124	-2.83422
H	-1.45508	1.231855	-2.55981
C	3.065625	-2.88135	-1.16092
C	1.379235	-3.13144	-2.85227

H	-0.305	-1.80078	-2.60069
C	1.685805	4.076288	-2.34953
H	0.644392	5.128697	-0.79247
C	4.353317	-0.51162	2.316577
H	4.722114	-1.97632	0.788861
H	3.66242	1.01958	3.696686
C	-2.60255	-3.52435	2.305029
H	-4.01823	-3.17496	0.726943
H	-0.9748	-3.61063	3.743229
H	2.626185	2.715553	-3.75834
C	-4.34921	-0.52333	-2.32306
H	-4.71833	-1.98059	-0.78935
H	-3.65563	1.00141	-3.70923
C	2.601762	-3.52496	-2.30483
H	4.012981	-3.18559	-0.71997
H	0.97859	-3.60222	-3.74929
H	2.050961	4.986235	-2.82585
H	5.332507	-0.63362	2.779417
H	-3.18681	-4.32433	2.758733
H	3.185123	-4.32521	-2.75936
H	-5.32661	-0.64957	-2.7883

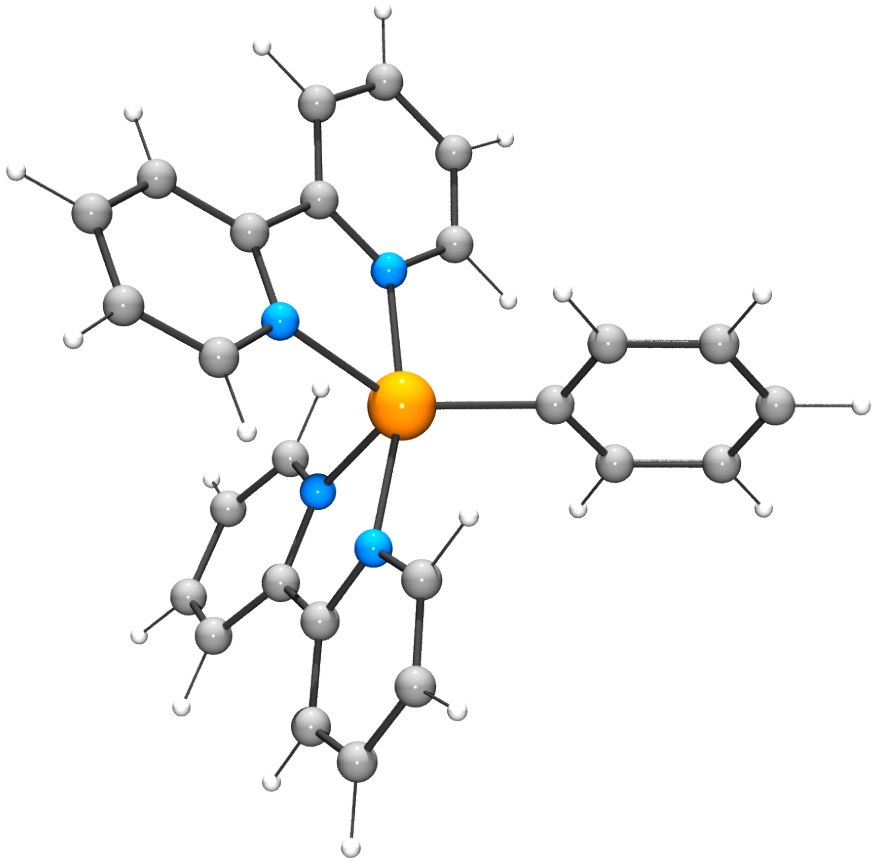

Figure S68. Optimized structure of high-spin trigonal-bipyramidal $[Fe(bipy)_2Ph]^+$.

Table S12. Atomic coordinates for high-spin trigonal-bipyramidal $[Fe(bipy)_2Ph]^+$.

Atom	*x*	*y*	*z*
Fe	0.00098	-0.00041	-0.00121
N	-0.56305	1.661682	1.218881
C	-0.37793	2.892141	0.651912
C	-0.93461	4.047895	1.218696
C	-1.65548	3.953792	2.403334
C	-1.81423	2.69802	3.000419
C	-1.26545	1.588498	2.372615
H	-0.81785	5.011296	0.724863
H	-2.09215	4.843967	2.855439
H	-2.36395	2.576893	3.932753
H	-1.38683	0.590187	2.790883
N	-1.11611	-1.38947	1.111912
N	0.654354	1.668658	-1.12056
N	-1.75345	-0.27997	-1.1981
C	1.685633	-1.05468	-0.07372
C	0.446809	2.89791	-0.56215
C	-2.30701	-1.79063	0.57469
C	-0.62574	-2.06973	2.175582
C	1.466229	1.583526	-2.20198
C	-2.72272	-1.05805	-0.62919
C	-2.04075	0.368938	-2.34749
C	2.759294	-0.80072	0.802614
C	1.833335	-2.09081	-1.0175
C	1.034248	4.054203	-1.09608
C	-3.02212	-2.86912	1.114563
C	-1.29413	-3.13342	2.764839
H	0.344652	-1.73507	2.544427
C	2.061657	2.692103	-2.78699
H	1.631486	0.578458	-2.59172
C	-4.00339	-1.1471	-1.19228
C	-3.27736	0.29295	-2.97326
H	-1.23729	0.975295	-2.76343
C	3.934703	-1.55806	0.742772
C	3.011422	-2.84265	-1.08773
H	1.02188	-2.3298	-1.71144
C	1.837798	3.955906	-2.22607
H	0.883099	5.019081	-0.61423
H	2.69322	0.000528	1.544558
C	-2.5195	-3.54038	2.223935
H	-3.95081	-3.19933	0.652349

H	-0.85803	-3.63588	3.627113
H	2.693084	2.565788	-3.66561
C	-4.28468	-0.46903	-2.37262
H	-4.77757	-1.73509	-0.70185
H	-3.44997	0.831447	-3.90398
C	4.061935	-2.57891	-0.20353
H	4.752749	-1.34764	1.433818
H	3.107201	-3.637	-1.82988
H	2.297374	4.845801	-2.65547
H	-3.06583	-4.37912	2.654408
H	4.97833	-3.16754	-0.2522
H	-5.27801	-0.52811	-2.81722